

DISSERTATIONES PHYSICAE UNIVERSITATIS TARTUENSIS

17



INITIATION OF CORONA PULSES

by

Peeter Paris

TARTU 1994



INITIATION OF CORONA PULSES

by

Peeter Paris

TARTU 1994

The study has been carried out at the Institute of Experimental
Physics and Technology of University of Tartu, Estonia

Supervisor:

Assoc. prof. M. Laan

Official opponents:

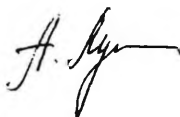
Prof. R. S. Sigmond (Trondheim)

Prof. M. Elango (Tartu)

Cand. Sci. A. Treshchalov (Tartu)

The thesis will be defended on June 8, 1994 at 2 p.m. in the Council
Hall of Tartu University, Ülikooli 18, EE2400 Tartu, Estonia.

Secretary of the Council:



A. Lushchik, Dr. Sci.

Peeter Paris was born in 1953 in Tartu. In 1976 he graduated from
Tartu University as a physicist. At present he is research associate of
the Institute of Experimental Physics and Technology of the same
university.

The author's permanent address:

Institute of Experimental Physics and Technology, University
of Tartu, Tähe 4, EE2400 Tartu, Estonia

Contents

Introduction	4
1 General	
1.1 Corona discharges	6
1.1.1 Positive point-to-plane corona	8
1.1.2 Negative point-to-plane corona	17
1.2. Initiation of discharge	24
1.2.1 Optical breakdown of gases	25
1.2.2 Ionisation of gases by laser radiation	29
1.2.3 Laser triggered spark switches	33
2. Experimental	
2.1. Experimental set-up and apparatuses	
2.1.1. Experimental set-up	39
2.1.2. The x-ray generator	42
2.1.3 The excimer laser	44
2.1.4. Gases	46
2.2. Experiment	
2.2.1. Positive point	46
2.2.2. Negative point	61
3. Discussion	
3.1. Main results and open problems	63
Conclusion	71
Acknowledgements	71
Publications	72
References	72
Kokkuvõte	79
Articles	
A1. Laser action on corona pulses	81
A2. Streamer initiation by x-ray pulse	88
A3. The multiavalanche nature of streamer formation in inhomogeneous field	97
A4. Formation of corona pulses	123
A5. On the formation of negative coronas	139

Introduction

The aim of the present work is the experimental study of formation times of corona discharges and to clear up some probable formation mechanisms of corona discharges on the basis of these measurements. The experiments are performed at high pressures (near atmospheric pressure) in inhomogeneous point-to-plane discharge gap.

This study is of significance as the formative processes of high pressure coronas are not sufficiently investigated yet and there are still several open and unsolved problems in understanding and explaining of the formation processes of corona discharges at high pressures.

Besides to the general understanding of the fundamental processes of the formation of discharge, there are at least two subjects of a great practical value in this field:

- a) High pressure bulk discharges, which are often used as an active medium of gas lasers. It has been observed in a number of situations that the cathode region of a high pressure glow discharge plays a central role in the development of instabilities, formation of hot spots, which give rise to filaments. As it is established, there are striking similarities between corona formation and development of these instabilities [1, 2]. In a point-to-plane gap in molecular gases the discharge is localised near the point electrode and the influence of the processes on the opposite electrode as well as in the gap is considerably suppressed. It gives an opportunity to study separately the processes near the cathode and anode. Thus the corona discharge can be consider a good model for studies of instabilities in the case of high pressure bulk discharges.
- b) High pressure gas spark gaps that are used for rapid commutation of a powerful electrical systems. The study of initiating and triggering corona discharges enables us to model similarly the initial processes in spark switches, and thus clarify the processes responsible for triggering them. It is also very actual to minimise the jitter of

triggering and increase the reliability of spark switches. Optical triggering of switches has a special relevance in this sphere.

The thesis consists of:

- 1) the introductory part where a short review of the literature about the problems under observation is given;
- 2) the experimental part, where the descriptions of experimental apparatuses, of those experimental results which are not included into the five papers in the last chapter of the thesis, and main results are presented;
- 3) five most essential articles, where the main results, discussions and conclusions of the thesis have been published.

In the chapters 1.1 - 1.2 of the main part a short survey of the forms of gas discharges in inhomogeneous discharge gap is represented, and the models for describing coronas are discussed. The most attention is focused on the initiating methods and difficulties of the triggering of corona discharges as well as to the common problems like triggering of spark gaps. A short overview of methods of optical triggering spark switches are given as supplementary, the methods of adequate initiating of gas discharge in the case of homogeneous field are quite well elaborated. The purpose of such an accent is to collect all recent available results dealing with the problems of initiation of gas discharge.

In the chapter 2 the experimental conditions, used apparatuses and gas mediums are described. In this chapter these details of experimental technique and results of measurements that have not been reflected in the papers included into the thesis are brought forward.

In the chapter 3 are represented the results of measurements, more details are given about these results that have not been reported in the included papers.

In the chapter 4 the main conclusions are given and the supposed models of corona formation are discussed. Moreover, the further possible directions for corona formation studies in the light of present work are proposed.

The results which are in conjunction with the subject matter of the thesis have been published in the following papers [A1 - A11] (see publications in page 72 of the thesis).

1. General

1.1 Corona discharges

The first studies of corona discharge were performed in the beginning of this century by Townsend. The discussions of physical processes of corona discharges were started by Loeb and his school in thirties. Reviews of corona discharge have been published by Loeb [7], Nasser [8] and Sigmond [9 - 11]. The present thesis is concentrated on the initial stages of negative and positive DC coronas. Corona events will be observed and discussed on the example of point-to-plane discharge gap.

Corona occurs in strongly inhomogeneous fields. The definition of corona given in [10] is: A corona is a self-sustained electrical gas discharge where the geometrically determined (Laplacian) electrical field confines the primary ionisation processes to region close to high-field electrodes.

Consequently, the corona is possible when one or both electrodes have considerable curvature, and ionisation processes can occur near the electrode at much lower voltages than is needed for the breakdown of the whole gap. Thus a corona discharge system must have a high-field active electrode which is surrounded by ionisation region where ionisation processes take place. A low field passive electrode is insulated from the active electrode by the drift region of low conductivity. In low-field drift region charged particles drift and can react. A DC corona is called positive or negative according to the polarity of active electrode.

We will very briefly discuss some most important processes in gas discharges. Significant role in gas discharges is played by electron avalanches, which were first studied by Townsend and are often called Townsend processes after him.

If N_{e0} electrons are released in a gas in an electric field $E(r)$, they will drift with velocity $v = -\mu_e E$ up the electric field line (μ_e is the

mobility of electrons), each producing α new electron-ion pairs and suffering η attachment per unit drift length. So we can write

$$dN_e = N_e \cdot (\alpha - \eta) \cdot dr = N_e \cdot \alpha' \cdot dr, \quad (1)$$

where α is the first Townsend ionisation coefficient and $\alpha' \equiv \alpha - \eta$ is the net primary ionisation coefficient. After integrating we get :

$$N_e(r) = N_{eo} \exp \int_{r_0}^r \alpha' ds. \quad (2)$$

The exponential in the equation ($M \equiv \exp \int_{r_0}^r \alpha' ds$ is the electron

multiplication of the gap neglecting all electrons liberated by detachment process) can easily reach the values 10^3 - 10^8 across the ionisation region [10]. The self-sustained discharge needs feedback process to maintain the number of initial electrons. Secondary processes are summarised by secondary ionisation coefficient γ , which is the number of replacement electrons produced by an ionisation collision in the ionisation region. (γ_p -feedback to cathode by photons, γ_i - by positive ions, γ_m - by metastables,

γ_{pg} - feedback to the gas by photons). The Townsend's criterion for self-sustained discharge is

$$\mu_r = \gamma \int_0^d \alpha' dx \exp \int_0^x \alpha' ds = 1 \quad (3),$$

where μ_r is the reproduction factor. The integral $\int_0^x \alpha' ds$ is known as

ionisation integral. The values of γ , α and η depend quite strongly on the electric field.

In the case of positive corona the cathode is separated from the ionisation region by the drift region, which delays and often even blocks

the cathode processes according to attaching-detaching properties of the gas. In negative coronas the cathode is surrounded by the active zone and the negative coronas become self-sustained by the Townsend cathode feedback mechanism, while photon feedback (γ_{pg}) to the gas bordering on the ionisation region often predominates in positive coronas. In negative coronas in even weakly electron attaching gases, the current pulsations known as "Trichel pulses" are usually observed, which at higher currents transit to the continuous corona. Positive point-to-plane corona may typically pass through the following stages as the gap voltage is increased: dark current, burst pulse and onset streamer corona (this phase probably exist only in electron-attaching gases), positive glow and pre-breakdown streamers, transition to spark and spark breakdown [9]. The burst pulses may join together at higher voltages, becoming a positive glow (Hermstein glow) that covers the active electrode. Bursts that occur in non-self-sustained positive coronas in gases that have some electronegative constituents, seem to be trains of avalanches connected by photon feedback to the gas just outside the ionisation region. At slightly higher voltages than the onset of burst pulses may occur streamers that develop far into the discharge gap. Burst pulses are also formed between the succeeding streamers. The studies by Miyoshi and Hosokawa [12] show that there has to be time interval $\tau \geq 50 \mu s$ between the streamer start and the preceding burst pulse. It is supposed to be due to the space charge field influence. The influence of previous corona pulse to the propagation of subsequent discharge is experimentally confirmed in works [13, 14].

If the corona current density causes sufficient thermal ionisation across the gap, its differential resistance turns negative, which results in a breakdown of the gap.

1.1.1 Positive point-to-plane corona.

In the case of hemispherically capped rod-plane gap it has been established that the positive corona in air starts always with burst pulses, followed at slightly higher applied voltage, by onset streamer pulses [9, 15 - 18]. The positive streamer formation and propagation in non-uniform field have been investigated experimentally and theoretically in

[6, 19 - 23]. Mathematical-physical models for calculating the onset streamer pulses have been presented by the authors of [25 - 30]

Above threshold, self-sustained discharges maintain themselves but it is impossible to start them without initial or triggering electrons in the gap to start the primary multiplication. Time lag is defined as the time delay between the corona voltage turn on and establishment of a specified corona form. It can be divided into the statistical time lag before the appearance of the first seed electron, and the formative time lag. Several sources of initial electrons might be active in atmospheric air:

1. Natural production of electron ion pairs by natural radioactivity or cosmic rays (≈ 20 ion electron pairs /cm³ per second [7])
2. Electron detachment from negative ions under the influence of applied electric field. In [9] the detachment process is considered to be not a secondary ionisation mechanism, but a rapid release mechanism for stored secondary electrons.
3. Field emission of electrons from the cathode
4. Field emission electrons through the oxide films on the cathode.

Drift velocities, diffusion coefficients, photon absorption, electron attachment might be affected by impurities of gas [31]. The production of significant amount of metastables in the streamer channel is supposed by Hartmann [32]. The energy storage by metastables, negative ions and the electric field will contribute to streamer formation and propagation. In gases with a metastable energy level U_m , a 10^{-8} - 10^{-4} admixture of impurities with ionisation potentials $U_i < U_m$ will have remarkable effects on the effective ionisation coefficient [4]. The influence of previous discharge to subsequent is explained by metastables in [13], but in [14] negative ions are found to be responsible for this influence.

The first explanations to positive coronas have been given by Loeb [7]. The field at any locus is composed of the field components caused by the electrodes (Laplacian field), and by the electrons and ions space charge. At the ionisation zone boundary at the distance of r_0 from the point electrode the ionisation coefficient α equals to the attachment coefficient η . The avalanches increase in size as the applied voltage V on the positive point is raised. An electron moving from r_0 to a in the

gap creates $\exp \int_{r_0}^a \alpha(x) \cdot dx$ new electrons. The primary avalanche proceeds towards the point electrode and ends at its surface. During this

motion $f \exp \int_{r_0}^a \alpha \cdot dr$ photons are emitted in all directions. The photons

are absorbed by the gas and some of them lead to photoionization. Photoelectrons produced too far (outside of a sphere r_0) from the centre, suffer attachment in electronegative gases, inside this sphere they will produce auxiliary avalanches. The magnitude of r_0 is dictated by the field intensity. The positive space charge, as it accumulated after several avalanche generations, will soon extinguish the corona. Loeb has set the condition for the onset of positive burst pulse corona as [7,p.55],

$$0.5 f f_1 \exp \left(\int_0^{r_0} \alpha \cdot dr - 1.86 \mu r_0 \right) = 1, \quad (4)$$

where f is the ratio of the number of ionising photons to the number of ions in the electron avalanche, f_1 is the chance for the photons to ionise the molecules, when they are absorbed, r - the distance from the tip of the positive point along the axis, r_0 - the optimum distance within which the most ionisation occur (the radius of ionisation zone) and μ - the absorption coefficient of ionising radiation.

The electrons suffer diffusion because of the high random velocity of the electrons, having a diffusion coefficient D during the avalanche. The diffusion radius will be $\bar{r} = \sqrt{6Dt}$. In order to estimate the electric field of the space charge is assumed that the space charge at the head of the avalanche is contained in a sphere of radius ρ . The radius of the

avalanche head ρ is determined by the diffusion and can be calculated

$$\rho^2 = 4 \int_0^L \frac{D}{\mu_e} \cdot \frac{1}{E(z)} dz; \quad (5)$$

(the ratio of D/μ is usually known) [33].

The field produced by this charge at the head of an avalanche is :

$$E_\rho = \frac{e}{3\pi\epsilon_0} \cdot \frac{\alpha'(z)}{\rho} \exp \int \alpha'(z) dz. \quad (6)$$

This field parallels and adds to the Laplacian field $E(z)$.

Amin [15, 16] has investigated the positive point-to-plane corona in air in the same electrode configuration as ours ($r = 0.5$ mm, $d = 4$ cm). Corona discharge at the threshold appeared in the form of burst pulses. In all cases the sequence of pulses began with a larger pulse followed by a number of secondary pulses. At slightly higher voltage streamers occurred, burst pulses were active simultaneously. Streamer was generally followed by a burst pulse. In this case the initial large pulse was absent, and the burst pulse consisted of many small pulses following the streamer. The repetition rate of the onset streamers increases with the voltage up to a certain critical value at which the negative space charge develops that chokes off this form of discharge. Amin explained such an occurrence by the following model.

As soon as the field conditions are proper, an electron appearing into the gap forms an avalanche according to $\int \alpha \cdot dx$ law. Air is a good photoabsorbent of its own photons, and this helps the initial pulse to spread over the point by photoionization. Once the initial pulse has spread over the point, it is choked off by its own space charge. Due to the nonuniformity of the field the point will be partially cleared and a second pulse, triggered by the photons, is permitted to form and spread. Because of the presence of the space charge of the initial pulse, the second pulse is not permitted to spread very far, and is quickly quenched, i.e. has a smaller amplitude. This process is repeated until the space charge accumulated in the relatively lower field region of the

gap will choke the whole pulse. No other pulse can take place until this space charge is cleared sufficiently. When the space charge has moved far enough across the gap to the cathode, another burst can occur. This qualitative model has generally been accepted up to now.

The steady glow is formed when the density of the space charge becomes high enough to completely suppress the onset streamers. The glow forms an ionised layer adhering to the electrode surface. The resulting corona current at higher voltages is a direct current with some ripples. With increasing voltage the breakdown streamers originate from spots of higher activity on the ionised Hermstein layer. Breakdown streamers resemble the onset streamers but they are deviated from the axial position by the space charge, they start from the periferic part of the glow. Their amplitude is of the same order as the amplitude of the onset streamers. The length, amplitude and repetition rate of these streamer pulses grow with the voltage and further increase in voltage leads to breakdown.

Weissler in his early experiments in pure gases and gas mixtures [34] found that the onset potential is usually higher for positive corona than for negative corona in the same electrode configuration. It was assumed to be probably due to the more efficient cathode secondary ionisation processes in case of negative corona. He found that the lowering of the positive corona onset potentials by small additions of O_2 to N_2 could be the indication of the importance photoionization feedback. Neither preonset streamers nor burst pulses were observed in pure N_2 . Adding traces of O_2 to N_2 instantly produced weak preonset streamers and at higher concentration produced also burst pulses. Fully developed burst pulses were found only in the O_2 N_2 mixtures (not in other gas mixtures used by Weissler). The whole basic behaviour of discharge in pure nitrogen observed by Weissler has been confirmed by Korge [35, 36]. In pure nitrogen the threshold is considerably higher than for the same electrode configuration in air. At the onset establishes a steady discharge presenting a channel bridging the discharge gap, this steady discharge is usually formed after the streamer has passed [36]. Increasing the potential resulted in a brighter corona that extended further towards the cathode in form of a continuous luminous channel. Further increase in gap voltage caused the appearance of

streamers. They could go across the gap at relatively low potentials without causing the breakdown of the gap. At higher potentials the number of streamers increased considerably until they became strong enough to initiate the spark breakdown. Evidently the efficiency of photoionisation as a secondary mechanism is considerably lower in nitrogen, which is proved by the absence of burst pulses at voltages that exceed the threshold of burst pulses in the air more than 2 kV; and by a considerable increase in the streamer threshold compared with air. Raether has predicted the possibility of avalanche development up to amplification 10^8 and more in N_2 [37].

The streamer mechanism was first proposed by Raether [37] to explain the electrical breakdown of strongly overvolted spark gaps at near atmospheric pressure. He has suggested that a streamer can start when the electron avalanche grows to a size that it is capable of partially shielding itself from the applied field that is estimated to occur when the avalanche reaches about 10^8 electrons.

A large avalanche will leave a positive space charge near the point electrode. The field outside of this spike is increased because of the geometry, leading to the formation of still larger avalanches in front and leaving weakly conducting plasma filament behind, forming a positive streamer. This streamer might propagate straight through positive glow drift region, make contact with the cathode, and then turn on active γ processes on the cathode, resulting in the background current [9]. For the formation of the streamer the secondary electron liberation near the ionisation region boundary must take place. One must always take additionally into account the possible effects of stepwise ionisation in streamer propagation [38]. If the external field is sufficient the growth continues and a streamer forms. If not, a localised or laterally spreading burst will form, depending on the mean free path of the gas ionising radiation. The burst is quickly quenched by its own space charge, and a new burst or streamer, will not form until this space-charge has drifted away sufficiently.

The electric field everywhere is the sum of the applied Laplacian field and the field from the space charge created by discharge. Approximation often used assumes that a Laplacian field distribution across the ionisation region of a strength is determined by the geometry

and the applied voltage, and the cross effect of the space charges with Laplacian field in the drift region. Raether's estimation gives that when the number of electrons in a single avalanche exceeds 10^6 - 10^8 , the space charge of an avalanche equals to the applied electric field and the previous approximation would be invalid.

In their calculations Ibrahim and Singer [25, 26] have assumed one electron to start the first avalanche at the initial boundary of the ionisation zone. According to the calculation, they found that the distortion of the field strength starts with the beginning of rapid current rise. After about 2.5 ns the field strength decreases quickly. Through this drop of field values, the secondary avalanches will be broken for some time, and therefore the current will drop. In this way a step at the beginning of the leading part of the corona pulse that was observed in experiments will be built up. In their simulations a superposition of several generations of electron [26] avalanches is assumed.

In their streamer breakdown criterion Pedersen et al [22] have presumed that the streamer breakdown is caused by a single avalanche of critical size initiated by one or more electrons. They suggested that the streamer breakdown would occur when the ionisation integral attained a certain value K (usually $K \approx 18$, which is consistent with the Raether criterion for homogeneous field gap). At the same time they have stressed that one must always take into account the variation of E and α with z . In the earlier work by McAllister [39] it has been suggested that this criterion requires the use of measured values of the variation of $\bar{\alpha}(z)$ with field strength and gas pressure p , the data which are not always available for inhomogeneous discharge gap. In contrast to Pedersen, McAllister et al in [6] have affirmed that in the streamer formation the basic feature was the multiple avalanche process. In this work it was supposed (as the ionisation created by the first avalanche is low) that the subsequent avalanches space charge would overlap the primary space charge. They have got a "clear evidence that at onset the corona discharge (streamers) does not result from the formation of a single critical avalanche, but from the accumulative effects of multiple avalanche process". The net positive charge 10^8 required at the streamer onset is not realistic. For preonset streamers in point-to-plane inhomogeneous field, however, there are only 10^5 electrons in a single

avalanche, $r_0 \approx 0.2$ mm [8]. As point potential increases, r_0 also increases and avalanche size increases exponentially. It does not advance as a streamer until successive avalanches have fed into the space charge field of the initiating avalanche head at the anode. Moreover, in [23] it is found that at corona onset the number of carriers associated with the accumulation of space-charge is $\approx 4 \times 10^7$. They have drawn a conclusion that the general form of the avalanche pulse (burst pulse) leading to streamer formation was similar to that recorded in uniform field studies. As a result of this study McAllister et al concluded that nevertheless the critical avalanche carrier number suggested by Raether was in consistent with the streamer inception criterion, the concept of a critical charge density had more physical relevance and the ionising radiation was the mechanism responsible for the generation of streamer. This statement is in consistence with Raether assumption that the streamer formation is determined rather by the critical density of charged particles than by the size of a single avalanche [37]. As it was determined by the field probe measurements by McAllister [6], the streamer development suppressed the field strength at the point electrode, and field changes were to be associated with the motion of ionic charges. Crichton and Williams [3] confirm the concept of critical charge density for streamer criterion. Unfortunately the papers cited here have not reported a number of essential parameters and experiment conditions as gap voltage, field probe construction and method of field measurements, experimental set-up.

After the streamer is initiated, its active head is normally the only visible part with optical radius measured by Bastien and Marode to about 20 μm . at 40 kPa [40]. At 1 atm the radius is probably 10 μm after Marode [21]. At the same time Dawson and Winn have given a theoretical estimation of 60 μm [9], Kunhard and Tzeng have found the diameter of cathode directed streamer to be of 50 μm in plane-plane gap [41]. In recent studies of Gibert and Bastien [42] have been measured as large diameter as 170 μm for point-to-plane gap ($d = 2.1$ cm, $r = 50$ μm).

An explanation of formation of steady glow bases on the movement of space charge of positive ions left by avalanches. As long as the space charge has not sufficiently cleared away after preliminary ava-

lanches, burst pulse or streamer, the appearance of new streamers is restricted. The excited atoms from primary avalanches radiate photons causing so secondary avalanches. The formation of avalanches will continue until the high field region near the point electrode is occupied by positive ions. Electrons from avalanches are drawn rapidly into the anode, positive ions drift slowly to the cathode, restricting the formation of larger

In another model given by Loeb [7] negative ions are found be responsible for the establishment of steady glow. Before reaching the high field region, the electrons form O_2^- ions by attachment to O_2 molecules. Other O^- ions are created by dissociative attachment in the streamer. Between the positive ion cloud and the point a rapidly increasing and nearly equal cloud of slowly moving negative ions is created. The negative ion cloud increases the field near the anode and slows the movement of positive ions. The increased field near the anode is, however, of shorter length than the original high field region which started the streamer. Thus once a negative space charge of adequate size can form, the avalanches diminish in length. They cause a number of avalanches simultaneously in different places and the net field will decrease. The discharge spreads over the cathode surface.

The simplest set of equations containing the basic physics necessary for describing streamer formation and propagation is the set of continuity equations for electrons and ions coupled with Poisson's equation for electric field. Several analytical solutions of these equations based on the following well-accepted physical processes have been reported.

Most of these models have been essentially one dimensional, Dhali and Williams [27 - 30] have recently published a series of papers where the two-dimensional approach for streamer modelling is used. Their method allows to solve numerically transport equation under strongly dominating space-charge conditions. It can be considered the first application of two-dimensional model.

Dawson and Winn [43] state that a positive streamer head may propagate into zero Laplacian field region, without any streamer channel connection to the anode. The propagation of streamer is possible on the account of energy stored in the streamer head. In an inhomogeneous field a streamer tip consists of a limited volume of plasma with

about 10^8 - 10^9 positive ions in a limited volume of the order of $3 \cdot 10^{-3}$ cm in radius which propagates by its own space charge field and photoionization in advance of it, guided only slightly in the low gap field region by the Laplacian field. It gradually loses energy by ionisation and excitation as well as by branching. Its initial energy is gained in the high field region of the anode from the field which determines its charge. Their model does not take into account the conductivity of the streamer channel. The calculation based on the ideas of this model have been made by Gallimberti [19, 20]. He improved the previous model proposing that if the streamer head was like an insulated sphere of space charge, where α was corrected for the self retarding field of the avalanche.

Badaloni and Gallimberti [44] simulated the corona streamer branching, taking into account the probability of the developing of two equivalent avalanches simultaneously. The model proposed by Fernsler [45] confirmed that the advance of the streamer was largely controlled by its self-fields with little guiding effects from the electrodes. The main goal of this model was to determine the streamer velocity v as a function of applied potential and initial electron conductivity.

Different approach was made by Wright [46]. It was assumed in this work that the streamer filament is conducting with almost equal densities of positive ions and electrons and with negligible attachment rate. This model allows to calculate the streamer tip potential as a function of the anode potential. Marode [21, 22] has interpreted the positive streamer development in terms of glow discharge. He describes the streamer as a filamentary track of transient glow discharge positive column with a moving active head. The gas plays the feeding role of the cathode in the formative phase. A true cathode region is formed when the primary streamer arrives the plane. The arrival of the streamer on the cathode marks a turning point in the discharge development. The differences in potential are then redistributed along the streamer filament through the rapid propagation of a potential wave from the cathode towards the anode: the return wave, which is observed [47] at low pressures.

1.1.2. Negative point-to-plane corona

In the electronegative gases the corona current consists of series of pulses which are very regular in air and in some other electron attaching gases over a wide range of applied voltages, and are called Trichel pulses after G.W. Trichel, who carried out the first systematic study of negative corona [49]. An important characteristic of these Trichel pulses is very short rise time of order 1.4-1.5 ns at atmospheric pressure in air, and is fairly independent of cathode material and tip radius [30]. Although much experimental and theoretical work has been done on this subject, a basic physical description of the fast pulse rise is far from complete. The phenomena causing such a regular sequence and shape of Trichel pulses have not been explained satisfactorily yet. In non-attaching gases under the same electrode configuration only a continuous glow corona occurs. Sigmond has drawn attention [51] to the fact that in free electron gases an external circuit can cause pulses that are almost indistinguishable from genuine Trichel pulses.

After Trichel the studies of negative corona were continued by Loeb and his school [52 - 57]. The first survey of the effects of gas type and impurities on short point-to-plane gap coronas was presented by Weissler [58]. Weissler recorded the appearance of Trichel pulses whenever the free electron gas (N_2) contained even the faintest traces of electronegative gases. The smallest percentage (0.1%) of O_2 in N_2 resulted immediately in Trichel pulses. Exhaustive surveys of coronas have been published by Loeb [7] and Sigmond [9,10].

The semiquantitative explanation for the discharge type is given by Loeb. In recent years Morrow and his colleagues have been developed the theory of negative corona and proposed the computing model for Trichel corona. Cernak and Hosokawa have further developed this theory and for higher pressures have pulled forward the assumption of negative streamer-like mechanism responsible for the rapid initial current rise of negative corona.

When a negative DC voltage is applied to the point electrode in an electronegative gas like air, the corona current at the threshold increases abruptly from $\approx 10^{-12}$ to $\approx 10^{-6}$ A [59, 61]. The Trichel pulse corona is preceded by a low-current ($i < 10^{-9}$ A) quasi-steady discharge

as it was described by Loeb et al [52], later the low-current discharge was observed by Weissler [58] in pure nitrogen, and recently studied by Korge [35,36] also in pure nitrogen.

The pulse repetition frequency of Trichel corona is nearly proportional to the average discharge current and extends from some kHz up to some MHz at atmospheric pressure. At a point electrode the discharge originates at the point tip, but it continuously changes its position. At a hemispherical electrode the discharge may be yielded simultaneously at several spots changing their position in the course of time. The constancy of pulse shape when varying the average current indicates that the pulses are formed and decay under conditions independent to the actual gap voltage [9].

When the current is raised, the time intervals between Trichel pulses are shortening, at the same time their plateau is lengthening. When they nearly touch each other, trains of pulses may join in long, steady plateau pulses with separate Trichel pulses between. A very small further increase in current makes all pulses join in one continuous plateau - the continuous glow. The transition is accompanied by the change of the visual appearance of the discharge. The wandering of the discharge ceases and it becomes fixed at one point. The entire luminous area shows a contraction. Physically, the pulsless corona shows the same characteristics as that of glow discharge. It has a small bright spot of negative glow adjacent to the point, a short but well-defined Faraday dark space, and a positive column. The negative pulsless corona is considered to be a kind of abnormal glow discharge under high pressure [61].

Loeb explained the occurrence of Trichel pulses as following. An electron emitted from the cathode under proper field conditions forms an avalanche. The photons created in this process strike the cathode and liberate secondary electrons by photoelectric action (γ_p). The secondary electrons form a number of successive avalanches that give rise to a very rapidly growing pulse. The positive ions formed by the avalanche are created in a dense cloud at some distance x_0 from the point electrode. They move slowly into the cathode. The moving electrons form via the dissociative attachment a space charge of negative ions (O^-) near the negative point. It will choke the pulse when the accumu-

lated space charge becomes sufficient. If after a certain time when positive ions reach the cathode the field is still reduced, the secondary electrons created by positive ion bombardment (γ_i) are not capable of forming any more excitation and ionisation. Thus, the discharge is completely choked until the space charge has cleared and another pulse can start. But if upon the arrival of positive ions at the point the reduced field has not developed because of insufficient density of electron attachment (lower pressure, higher field, weakly electron attaching gas), the liberated secondary electrons are capable of forming more avalanches, and the discharge continues via the liberation of secondary electrons by ions striking the cathode (γ_i), until enough space charge is formed to choke the discharge completely. The next pulse must wait for the drifting away of the negative ions, consequent rising of the gap voltage, and also wait for a new seed electron.

By their measurements Sigmond and Torsethaugen have found that the ionisation in the cathode region never ceases at all [62]. Current is still flowing from the cathode, exciting and ionising the ionisation region. They supposed that this weak decreasing electron current from the cathode during the interpulse period is caused by diffusing metastables formed by the pulse. When the negative ions are cleared away sufficiently to raise the ionisation region voltage to the self-sustaining value, a new negative glow pulse occurs immediately since the seed electron is always available. As a result, the Trichel pulse corona in air has a very regular, voltage dependent repetition frequency. In strongly electron attaching SF_6 on the other hand, pulses are randomly delayed and irregular in their appearance and in amplitude - that is due to the lack of initiatory electrons.

Amin first present the assumption that the tail of Trichel pulse is due to the ion motion across the gap [53]. The fact was confirmed by Gardiner [63]. He found that the Trichel pulse frequency near the threshold involved a full transit time of negative ion space-charge layer. O^- predominates in air particularly for high pressures. As the Loeb's avalanche mechanism was too low for the observed very short Trichel pulse rise times, Aleksandrov [64] extended Loeb's theory by multiple avalanche mechanism, presuming nearly parallel development

of many avalanches initiated by γ_p effect at the cathode. He succeeded in predicting much faster rise time for the main pulse.

The systematic study of the leading edge of negative corona current pulse was made by Zentner [65, 66]. He discovered that the current pulse had a complex structure - there was a step before the current reached its peak value.

Cernak and Hosokawa studied mainly the first pulses of negative corona and found the existence of hump or step on the leading edge of the current pulse.

Explanation for the complex rise of current pulse by only one secondary (γ) mechanism is impossible. On the bases of studies of double peaked corona pulses by [67 - 69], Morrow established a theory [71, 72] which described only the first pulse and like Loeb's assumption incorporates two processes that cause electron emission from the cathode: secondary emission due to photon impact on the cathode (γ_p) and secondary emission due to positive ion impact (γ_i). Morrow proposed that the initial current growth due to prompt photons and delayed current growth due to the arrival of slower ions at the cathode was responsible for the formation of the step on the leading edge of the corona current pulse. As the number of electrons created by positive ion impact is about three orders of magnitude larger than that produced by photons, a step on the leading edge of the current pulse will occur. After the initial rise in current due to the photoemission, space charge effects lead to a reduction in the electric field near the point and to the formation of a cathode sheath causing a fall in current. The discharge is then maintained by ion secondaries, and further current amplification occurs until the number of positive ions in the cathode-fall region begins to be depleted. This decline, and the consequent decrease in the electric field causes the current to reach the maximum and then decrease to the transient glow discharge stage, i.e. the current peak is generated.

The next current pulse occurs only after the space charge has drifted far enough from the point to allow the field increase to a value that allows the avalanche formation at the point. This theory has no explanation for the trailing edge.

Since the ionisation phenomena associated with negative corona current pulses are localised in the immediate vicinity of the cathode, any question of the actual mechanism for the rapid negative corona current pulses rise is immediately connected with the question of the role played by cathode secondary photoemission γ_p in the steep discharge current growth. On the basis of their experiments Cernak and Hosokawa [73 -75] concluded that Morrow's model was valid at lower pressures, but at higher pressures the observed waveforms were caused by a cathode-directed ionising wave. As it was observed, the glow corona formation was preceded by a peaked current signal, of conspicuous similarity to the Trichel pulse rise and its initial decay. They suggested that the two phenomena had a common mechanism. This opinion is in contrast to the conventional Trichel pulse model [7], which presumes, that the initial steep Trichel pulse decay is due to the fast electron attachment.

The measurements show that the steep pulse rise is not dependent on cathode secondary emission processes for pressures above 30 kPa. Considering the secondary emission at the cathode due to ionic impact too delayed to play any role in the time scale of interest here, it could be explained that the rapid pulse rise associated with the Townsend mechanism must be sustained by released γ_p electrons. The quenching properties of methane CH_4 molecules over the excited states of nitrogen are well-known [37] - the addition of CH_4 to N_2 greatly reduces the γ_p emission. Comparing the results of measurements in N_2 and $N_2 + Ar$ and $N_2 + CH_4$, the mixtures indicate that the γ_p emission does not play an important role in feeding the rapid Trichel pulse rise at higher pressures [76].

It is supposed that for higher pressures the feedback to the cathode mechanism is supplanted by a faster streamer-like mechanism. Experimental studies have shown that during the pulse current rise a luminous region of discharge moves towards the cathode with the velocity of the order of 10^6 cm/s at low pressures and $10^7 - 10^8$ cm/s at atmospheric pressure. Ikuta and Kondo [77, 78] suggested that the luminous region was related to the cathode-directed streamer. It seems to be confirmed by experiments [79, 80], which indicate that a transition from precorona avalanche to the Trichel pulse - i.e. negative corona

onset occur when space charge of positive ions created in the avalanches gives rise to a critical field for the formation of streamer. The initial current rise is due to the ionisation fed by γ_{ph} emission. The current rise is further enhanced by the formation of cathode - directed streamer -like ionising wave [73 - 75], which results in an observed step on the pulse leading edge. The pulse maximum is attained just as the wave reaches the cathode, and subsequently, the current begins to fall because of the rapid field decrease behind the wave. When the positive ions generated prior to the ionising wave ignition reach the cathode, the current being fed by γ_i emission rises temporarily again, and the hump on the pulse trail is generated.

The streamer is not initiated immediately after the critical space charge is formed. During some certain period, the critical space-charge partially shields itself from the external field, creating a quasi-neutral plasma region. The positive ion space charge that appears in front of the cathode-faced surface of the plasma region to shield the interior unavoidably enhances the field there and a cathode directed streamer head is formed.

All these proposed models do not explain the nature of prepulse steady discharge and its role in corona pulse formation as well as a step dependence on point electrode material.

The measurements by Korge [35, 36] indicate that two types of quasi-steady modes of point-to-plane discharge exist in nitrogen. Depending on voltage, it may be a low-current or a strong current discharge. We can also distinct a transient mode between low-current and strong current modes that proceeds very similarly to the Trichel pulse in air as it is described by Cernak and Hosokawa [81]. The low-current $i < 10^{-9}$ A steady discharge stage was at first studied by Loeb in air [52] and by Weissler in pure nitrogen [58]. Some Korge's results have been referred to here [35, 36]. The discharge in nitrogen arises as a diffuse glow covering the point tip, that is time dependent, its current and brightness decay in the course of time. When the current falls below 10^{-10} A, the discharge presents a little luminous spot wandering on the point tip, which is accompanied by current fluctuations. Analysis of the I-U curve indicates that the low current discharge is determined by the field emission. The field emission of electrode surfaces has been

studied in detail for pre-breakdown current in vacuum as well as in case of high pressure [1, 82 - 84]. After increasing the voltage over certain value, the current increases about three orders of magnitude and a steady strong current $i > 10^{-4}$ A discharge establishes. This current is controlled by circuitry resistance [36]. Visually the strong current has a cathode spot, a sting like bright glow region that gives origin to the diffuse channel bridging the gap.

At negative voltage the threshold of discharge is considerably lower than in air. The lowering of threshold is explicable by the greater value of the ionisation coefficient in nitrogen compared with the air as well as by enhancement of secondary processes on the cathode. If to consider the emissivity of the cathode as a secondary mechanism γ , the low-current discharge is a self-sustained discharge.

The time-spatial distributions of both the light and the current pulse during the first ten nanoseconds of this transition are very similar to that of Trichel pulses in air [36]. The difference lies in the fact that in pure nitrogen this transition ends with the establishment of a steady state strong - current discharge controlled by circuitry resistance, while in air the discharge is pulsing. Korge has suggested that the change of mechanisms of excitation and ionisation must take place in transient discharge. It can be supposed that the disbalance of generation and loss of charged particles in cathode layer here predetermines the type of discharge: if generation will prevail losses, the steady self-sustained discharge establishes as in pure nitrogen, if losses will prevail, the discharge can be only pulsative as in air. Considerable field reduction in this region, as presumed in [72], presumes the replacement of direct ionisation by another mechanism that supports the steady-state discharge.

1.2 The initiating of discharge.

Two conditions must be simultaneously satisfied in order to enable an electrical discharge can occur in gas. At first, at least one free electron must be available in a discharge gap in a suitable location. Secondly, the electric field must be of sufficient strength and duration to ensure the avalanche generation by this electron. It is confirmed that

gas discharges are always preceded by a waiting period that is known as the total time lag or simply delay time of discharge (Δt). It comprises of two well-defined parts - the initiatory or statistical time lag t_{st} and the formative time lag t_f , i.e. $\Delta t = t_{st} + t_f$ [85]. The statistical time lag is determined by the appearance of the first seed electron into the discharge gap after applying voltage. Naturally free electrons are produced by cosmic rays or natural radioactivity and t_{st} depends on the statistical nature of the electron liberating processes at cathode or in gas. The secondary ionisation processes responsible for avalanche initiating determine the duration of the formative time. In experimental studies the measured time lags are always the total time lags Δt . If the information concerning the formation process of discharge is required then the statistical time lag must be minimised. It is possible to do in homogeneous field gaps as the first electron that appears leads to breakdown there. It is achieved practically by the illumination of the cathode by strong ultraviolet or soft x-ray and α -radiation. In the case of inhomogeneous field this kind of initiation usually does not enable the reduction of statistical time lag or jitter of initiation. In electronegative gases as, for example, in air, electrons liberated in low field region suffer attachment to the electronegative molecules as O_2 , H_2O . The formed negative ions have a long drift time and the places and time moments of attachment and detachment in the gap is also unknown. Thus creating of initiating electrons at suitable time moment in suitable location of discharge gap is impossible using traditional initiating methods. Intense α -particle initiating could even suppress the formation of corona pulses as it was observed in several studies [7, 86].

For the described reasons the formative times of the formation of corona pulses are not well known and the initial stages of corona discharges have not been studied sufficiently. The discharge current during the formative time of discharge is not adequately detectable - only integrated current pulse waveforms can be detected. The formative time t_f can give us some information about the discharge before the visible discharge occurs. Due to the counted experimental difficulties the formative times of corona pulses have not been determined with sufficient precision and the adequate corona formation models have not been worked out as yet.

With the development of lasers it becomes possible to initiate discharge or breakdown by laser radiation and even to perform the optical breakdown of gas by a powerful laser flash. The first known perfect experiment with discharge initiating and then adequate discharge current measurement with nanosecond time resolution was performed by Verhaart and van der Laan [87].

1.2.1 Optical breakdown of gases by laser radiation

The gas breakdown by laser radiation became possible after developing the Q-switched lasers and using them in giant impulse regime. The first report of gaseous breakdown in the high intensity laser beam focus was made in 1963 by P. Makers and his colleagues. After that term the influences of laser radiation on the gas discharge and laser radiation interaction with matter have been the objects of permanent interest of many researchers.

The first experiments were made using giant pulses of Q-switched ruby lasers, the peak power of which was of tens of megawatts [88, 89]. The concentration of electrons produced in laser focus during the breakdown was of $10^{13} - 10^{15} \text{ cm}^{-3}$. Minck has achieved in his work [89] that the maximum light energy density that can be transmitted through the air without causing optical breakdown is $7 \times 10^{11} \text{ W/cm}^2$ at all pressures, for which the electron mean free path is small compared with the beam diameter.

Several discrepancies were found in optical breakdown with known breakdown mechanisms in static and microwave fields. The electric field strength (10^7 V/m) in the laser beam focus was less by an order of magnitude than that required for direct electric field to strip an electron from an atom [90,91]. At the same time the surprising fact is that the quantum of energy associated with ruby laser is only $h\nu = 1.78 \text{ eV}$, which is much lower than ionisation and excitation energies of investigated gases (24.6 eV and 15.8 eV for *He* and *Ar*, respectively), but which can be ionised by the action of light. The plasma with electron densities $>10^{13} \text{ cm}^{-3}$ was readily produced.

Experiments in comparison with theory have shown [88] that multiple photon absorption alone cannot be responsible for the breakdown.

When a high power laser beam of intensity I interacts with gas, electrons can be generated by two main mechanisms: direct multiphoton ionization (MPI) and electron impact ionisation. In the first process, an atom or molecule of ionization energy U_i absorbs simultaneously n photons of energy $h\nu$, subject to the condition $kh\nu \geq U_i$, and thereby becomes photoionised. The ionization rate varies as I^k and the electron density for a constant intensity pulse increases linearly with time. In the second process electrons gain energy from the laser field through inverse bremsstrahlung (IB) collisions with neutrals involving absorption of the laser beam photons by a free electron in the presence of third body (atom or ion). This latter process leads to avalanche growth of free electron and ion concentration in the same manner as under static and microwave fields applied to gases. A free electron is required in the lens focus when the flash occurs to initiate the cascade growth process.

The electrons can readily ionise gas when their energy exceeds E_i . At sufficiently high fields, ionising collisions will cause an electron cascade to occur with the electron density increasing exponentially with time. Cascade breakdown is the dominate mechanism at long wavelengths ($\lambda > 1 \mu\text{m}$). As the wavelength is shortened below $1 \mu\text{m}$, multiphoton effects are expected to play an increasingly important role in the breakdown process.

The initiatory process is assumed to be the multiphoton ionisation of the gas (or gas impurities) followed by an avalanche growth of ionization.

The optical breakdown threshold is defined as the power level at which a visible spark was obtained. The state of breakdown is defined in rather an arbitrary fashion [92]: as the attainment of the electron concentration of about 10^{17} cm^{-3} in the focal region at the pressure of 1 atm., which is common breakdown criterion found in literature [93], or as the ionisation of a fraction of $\delta \sim 10^{-3}$ [92] (or 10^{-2} in [93]) of the gas atoms in the focal region. In [94] the gas breakdown is defined as a sudden onset of high electrical conductivity in a normally non conducting gas. This, of course, occurs due to the appearance of free electrons in the medium and is generally accompanied by the emission of bright light and by a strong absorption of the incident laser light. In [93]

Rosen and Weyl have given an additional breakdown determination criterion: detectable (5%) absorption of incident laser beam energy in created plasma. As the actual threshold appears to be very sharp [89], the onset is normally very well defined and there is little ambiguity in the meaning of that term.

The appearance of laser produced plasma in gases can take many forms depending on laser and focusing optics. The appearance of plasma fireballs is often connected with the presence of microparticulate matter - dust or aerosols in the atmosphere [92].

After Morgan [95] the transformation from neutral gas into plasma can be divided into three distinct phases: firstly initiation, secondly formative growth and the onset of breakdown and thirdly plasma formation. We shall mainly be concerned with the physical processes involved in the first two stages.

The initiatory phase occupies a period of time during which the laser flash releases free electrons so initiating the growth of free electron concentration in gas. This phase is very brief, significant initiatory time lag has not been found there and the initiatory phase is completed at a very early stage of the flash [92, 95]. Recent theoretical and experimental studies of the initiating phase have shown that the initial ionization is achieved during at least the first two nanoseconds of the laser pulse [93, 96]. Rosen and Weyl assumed that the multiphoton ionisation alone was active during the development time of one cascade. Then, after initiating electrons have been created, a more effective inverse bremsstrahlung absorption could dominate.

As soon as the conditions for the onset of breakdown are satisfied the ionization growth will continue as long as the irradiation continues. Then follows the rapid plasma development stage. The gas will remain heated for substantially longer than the duration of the laser flash which created it; local thermodynamical equilibrium with the surrounding gas is re-established in times $>10^{-5}$ s.

The precise determination of the intensity of the laser radiation in the focus is not easy because of the difficulty in accurately defining the extent of the focal region. In many papers the laser beam intensity in focus is estimated using expression

$$I = 4P/\pi f^2 \theta^2, \quad (7)$$

where P is the beam power, f the focal length and θ the beam divergence. The formula has been derived on the basis of assumption that the beam can be focused to a diffraction limited spot of diameter $d = f\theta$ [92]. There is a need to determine the axial extent l and the volume V of the focal region. The length l is often taken as the distance between points along the beam axis at which the intensity is half of that at the focal plane

$$l = (\sqrt{2} - 1) f^2 \theta / D, \quad (8)$$

thus

$$V \approx \pi(\sqrt{2} - 1) f^4 \theta^3 / 2D, \quad (9)$$

where D is unfocused beam diameter. Important complications arise due to the effect of spherical aberration by focusing optics - phase changes cause interference of the monochromatic laser light in the focal region. This causes the substantial variation of intensity over quite large distance. The extent of lateral and radial energy distribution caused by spherical aberrations are proportional to fD^3 and f^2D^2 respectively, so the focal volume V increases sharply with increasing D . The extent of the focal region is also influenced by the homogeneity of the laser beam, and existence of hot spots. In practice it is possible to estimate the dimensions of focal region by the dimensions of hole burned into metal folio or pattern on the surface of photo-plate.

1.2.2. Ionization of gas by laser radiation

The surprising fact that gases with high ionization potentials U_i are readily ionised by intense laser beam implies that these atoms absorb simultaneously $k = U_i/h\nu$ quanta and ionization results in a process known as multiphoton ionization (MPI). An analyse shows that probability W_k for ionisation of atoms with ionisation potential U_i in the unit time is given by

$$W_k = \frac{\sigma_k F^k}{\nu^{k-1} (k-1)!} = A F^k = A' I^k, \quad (10)$$

where A and A' are constants for a given atomic species and radiation wavelength λ , σ - photon absorption cross section into a virtual state. F is photon flux of identical quanta of energy $h\nu$, I - corresponding beam intensity. Here k is the next integer larger to $U_i/h\nu$. If a volume V of gas at pressure p containing pN_0V atoms (N_0 = Loschmidt's number / 760) is illuminated for a time τ by a constant uniform photon flux F , the number of electrons and ions created by multiphoton ionization is $N_i = AF^k pN_0V \tau$, that can be rewritten for practical case as

$N_i = AF_0^k pN_0V_k \tau_k$, where V and τ are replaced with effective volume V_k and effective flash duration τ_k and F with peak flux F_0 , thus

$W = N_i / pN_0V_k \tau_k$. The rate of MPI depends on the photon statistics in the laser beam and in an incoherent beam it is $k!$ times larger than in a coherent beam. If the σ_k is the cross section for multiphoton ionisation

in a coherent beam, then the incoherent MPI rate is $W_k = k! \frac{\sigma_k}{(h\nu)^k}$. If

there are very many temporal modes in the laser output the fluctuations may approach to characteristics of a thermal light source so that $F^k = k! \langle F \rangle^k$ and W_k are increased in $k!$ -fold [92]. Thus experimental values of W can range between W_k and $k!W_k$ depending on whether single or multimode output is used.

On the other hand the number of electrons liberated by multiphoton absorption in a time τ is [92]

$$N_i = N_0 p V \tau F^k \sigma_k / \sqrt{k-1} (k-1)! \quad (11)$$

If a free electron in a gas undergoes scattering collisions with atoms during the period of laser irradiation it may gain sufficient energy to excite and ionise the atoms so that the plasma formation can proceed into an avalanche or cascade process. Gamal et al in the studies [97, 98] have developed the microwave breakdown theory considering additionally the collisional ionisation of excited atoms, the photo-ionisation of excited atoms and some other effects. In [98, 99] they developed the cascade model for molecular gases as N_2 and O_2 at a wide range of pressures. The rate of ionization growth and the plasma formation threshold intensity are sharply pressure dependent, in contrast to the

weak pressure dependence characteristics of multiphoton processes. A very rough rule of the thumb for the separation of multiphoton ionization from inverse bremsstrahlung absorption regimes is the following: multiphoton effects dominate for values $p\tau \leq 10^{-7}$ Torr-sec. If the condition for the onset of breakdown is the release of a certain number N_c of electrons in the time τ , then the breakdown threshold flux will

$$\text{be: } F_{th} = (v/\sigma) \left[\frac{N_c(k-1)!}{N_0 p V \tau v} \right]^{1/k} \quad \text{if } N_c \geq 10^{13} \text{ cm}^{-3}. \quad (12)$$

It depends weakly upon the gas pressure p as $p^{-1/k}$ and flash duration τ as $\tau^{-1/k}$.

When MPI dominates, the number density of electrons at the end of the pulse is

$$n_e = N \int_{-\infty}^{+\infty} W_m I^k(t) dt = N W_m \bar{I}^k g \tau_p, \quad (13)$$

where \bar{I} are the average intensity and g a numerical factor of order 1 that takes into account the particular temporal profile of the pulse. If the pulse had a constant intensity, the electron density would increase linearly with time. In the case of IB breakdown, however, the electron density grows exponentially with time. The diffusion effects are not important in MPI dominated breakdown since electrons are generated from neutral particles which remain in the focal volume. One must, however, consider the effects of the diffusion of electrons out of the focal volume for cascade dominated breakdown case. Diffusion losses are expected to be quite important at the small focal diameters ($<50 \mu\text{m}$).

Though many breakdown measurements have been carried out at the ruby laser wavelength ($\lambda = 0.69 \mu\text{m}$ and at longer wavelengths, there is much less data about shorter wavelengths. Threshold intensities $I_{th} > 10^{11} \text{ W/cm}^2$ are found for gases at atmospheric pressure, for flashes generated by Q-switched ruby or Nd glass lasers, or $I_{th} > 10^9 \text{ W/cm}^2$ for infrared flashes from gain switched carbon dioxide lasers [92]. Weyl and Rosen in their paper [93] have collected most of the available data for shorter wavelengths and have carried out the

theoretical calculation of laser induced breakdown thresholds as a function of pressure and pulse length. At visible and UV wavelengths, one must consider the fact that highly excited states can be readily photo-ionised over time much shorter than the laser pulse length. Rosen and Weyl used wavelengths 532 and 355 nm for gases like argon nitrogen and others. They assumed a diffraction limited focusing. For nitrogen they found extremely high threshold (10^{12} Wcm^2 for $\lambda = 0.35 \mu\text{m}$) if compared with other gases. It was higher than in neon, even though neon has the ionisation potentials 21.6 eV compared with 15.5 eV for nitrogen. Argon and nitrogen have similar ionisation potentials but the threshold intensity in nitrogen for $0.53 \mu\text{m}$ was about ten times higher than for argon in the same conditions. They studied the effect of pulse duration on the breakdown threshold in nitrogen. The threshold was seen to vary as $\tau_p^{-0.34}$. In [95] Gamal has developed the theoretical model for investigating the influence of the laser pulse length on the threshold of breakdown ($\lambda = 0.35 \mu\text{m}$). They found that for short laser pulse 0.4 ns electrons are mainly generated by multiphoton ionisation of ground state of atoms. This process builds up the electron density to a value 10^9 cm^{-3} in time of about 0.1 ns. Above this time up to the end of the laser pulse breakdown proceeds via cascade ionisation

In other case with medium duration laser of 15 ns, during the early time up to 2.5 ns the growth of ionisation proceeds via MPI, which produces the electron density of 10^4 . This higher electron density results in the increase in the rate of inelastic processes which lead to the catastrophic increase in electron density. As soon as sufficient electron density n is generated, cascade process starts to act effectively leading to exponential increase in n .

They found that stepwise ionisation process played an important role in explaining the observed threshold intensities.

A certain amount of the threshold intensities data as the function of the wavelength of irradiation are summarised in the book by Raizer [91]. Here it is shown that the optical breakdown intensity increases with decreasing the wavelength till the wavelength is about 550 nm. Further shortening of the laser wavelength causes the decrease in the threshold intensity. At longer wavelengths the breakdown threshold is

proportional to v^2 , that is in accordance with the classical microwave breakdown theory [91, 100], at shorter wavelengths multiphoton processes will dominate. In [100] it is shown that a nonmonotonic dependence of the optical breakdown threshold on the radiation frequency is related with the quantum character of electron energy variations in the wave field. A drastic reduction in the threshold in the UV region is explicable with quantum effects. In all reports available [93, 96, 101] the same tendency was found: the lowering of breakdown intensity with the shortening of the wavelength, especially for UV lasers.

Resonantly produced plasma

The efficient laser produced ionization could be generated if the laser quantum energy is in resonance with the energy differences between allowed atomic states. In this case the ionization can take place in two steps - firstly, multiphoton excitation to the relatively long-lived allowed state involving a large number k of photons and secondly, photoionisation from the allowed level involving only few photons. The first step would have an ionization rate W_1 and the second W_2 and $W_2 \gg W_1$. The ionization rate per atom is then approximately W_1 and will be much larger than W . Frost et al in [102] have generated a long ionised current carrying channel using KrF laser ($\lambda = 248$ nm) with energy of only 5 mJ. This plasma generation was induced by resonant two step photoionization of organic "seed" molecules, which were added in small amounts to buffer gas.

1.2.3 Laser triggered spark switches

Spark gaps are traditionally triggered by overvoltage or by internal auxiliary electrodes. The use of lasers as trigger sources has significant advantages. In laser triggered gaps the formative lag times and jitter can be minimised, and breakdown can be initiated at voltages significantly below the self break value.

Numerous investigations have been made by the means of pulse lasers to control the time lag of sparking of gas and vacuum discharge switches [85, 103, 104, 105]. Using lasers makes it possible to produce

controlled and very rapid breakdown in gaps even though the interelectrode voltage V may only be a small fraction of the static breakdown voltage V_s .

In [103] Williams discusses the laser triggering of gas filled gaps. The laser triggered gaps were first time reported by Pendleton and Guenther in 1965. In [105] Guenther and Bettis have described many configurations of laser triggered switches and discuss the physical processes in triggering of them. The laser triggered switches have a line of advantages as electrically uncoupled remote operation, short and variable delay with low jitter, low-voltage triggering of long gaps, etc. They are simple to construct and insensitive to electromagnetic interference. An exhaustive study by Kawada et al [106] shows that the breakdown characteristics in the uniform field are essentially different from those for point-to plane gap. Furthermore, the different characteristics for positive and negative polarities of the struck electrode in the homogeneous spark gaps have been shown.

In most of the models the initial stages of gap breakdown are explained in terms of Raether streamer mechanism.

In laser triggered gaps the charged particles are liberated by the laser irradiation. They propagate across the gap under the influence of the applied field. By the Townsend mechanism the particles make α collisions per centimetre of travel, the charge density increases across the gap until at some critical distance of propagation it achieves the critical value, forms a streamer that very rapidly crosses the remainder of the gap.

Delay is defined as the time difference between the first arrival of the laser beam at the spark gap until the rise of breakdown signal. That and jitter, which is a measure of the reproducibility of delay, are the characteristics of prime interest.

Two types of laser triggered gaps are commonly used. In most laser triggered gaps the laser beam enters the gap through a hole in the centre of one electrode and traverses the gap along the gap axis (convenient geometry). The laser beam is focused onto a surface of the opposite electrode where it produces a small plasma fireball. This fireball is found to be responsible for triggering the gap [104] (electrode surface triggering). In this case plasma production at electrodes is read-

ily achieved with beam intensities and energies some orders of magnitude less than the threshold for gas breakdown. In the other type the laser beam is focused on a point in the centre of the gap and may pass out the gap through the hole in the opposite electrode. In this case the laser induces the optical breakdown of the gap fill gas, which triggers the gap (longitudinal volume triggering). Spark gaps can be volume triggered by inducing the laser beam into the gap also transversely. This is called transverse volume triggering.

Significantly different values of formative time t_f , and consequent delay time can occur depending upon which conditions are used. If during the volume triggering the laser beam causes only the ionisation of the gas in the gap but does not create plasma, the electrons and ions produced by multiphoton absorption are amplified by inverse bremsstrahlung absorption, which simultaneously provides initiatory electrons in the gas, distort the electric field and as a result gives enhanced conductivity. This requires beam intensities just below the gas breakdown. In that case the time lag to breakdown is relatively long.

When a high intensity laser pulse causes the gas breakdown in the gap, then the laser beam creates a large concentration of ionization accompanied by the emission of the intense ultraviolet radiation capable of photoionization of the gas, thus distorting the applied electric field and enhancing the liberation of additional free electrons at the cathode and in the gas. The duration of the lags for fixed V depends on the position of the laser produced plasma in respect to the electrodes [85]. The lags are shorter than for previous conditions.

In the case of electrode surface triggering laser generates a plume of ionised metallic vapour which expands rapidly into the gap and leads to the breakdown in a very short time. In [107] the threshold of plasma formation on the metal target was studied. The threshold is defined as the intensity of laser beam at the moment when the rapid ionisation of created metal vapours begins. The experiments were performed with the $XeCl$ 0.5 J excimer 20 ns laser and threshold for Al was got 220 MW/cm^2 , for Cu and W this was value 390 MW/cm^2 .

It was first suggested by Guenther and Bettis [105] that the electrode surface triggering was due to the formation and propagation of a streamer across the gap and later they presented an evidence for the in-

teraction of the propagating streamer with the laser. Dougal and Williams have given a model for longitudinal striking electrode geometry breakdown.

The focused incident beam rapidly heats the surface of the struck electrode, explosively evaporating electrode material which is then further heated and serves as a seed for heating the fill gas, probably through the inverse bremsstrahlung, cascade ionisation process [90]. The result is a small protrusion of relatively dense plasma on the electrode surface which then shields itself from the applied field, thereby setting up a region of enhanced field at the tip. Electrons in this enhanced field region experience very high ionisation rates and rapidly extend the protrusion into the gap as a streamer. In regions of high laser intensity the velocity of streamer is enhanced by interaction with the laser. This interaction may take a form of a direct ionisation rate enhancement due to inverse bremsstrahlung heating near the streamer head, or an indirect rate enhancement due to vibrational or electronic excitation of the gas in front of the streamer. At some point the laser-streamer interaction will cease, either because the laser pulse ends or because the streamer reaches the vicinity of opposite electrode. After the streamer has crossed, the gap is bridged by a thin, weakly conducting filament which is rapidly heated by ohmic heating. Due to this heating the gap current rises rapidly until a spark forms.

The model proposed in [110] shows that the expansion of the spark column is primarily caused by the convection of the hot ionised core of an ionised channel. The convective expansion of this core is augmented by photo- and thermal ionisation of the neutral gas.

Bradeley have performed experiments [111] in which the velocity of streamer has been controlled over order of magnitude by introducing pulsed preionization ahead of an already propagating streamer. It has also pointed out that even very weak preionization of the order of 10^3 cm^{-3} is sufficient to affect radically streamer propagation.

Aleksandrov [112], Akmanov [113], Norinski [114], Greig et al [115] and others have shown in their experiments that laser beam can guide streamer propagation. In [115] it was found that the discharge was laser guided even when the laser beam was arranged to be approximately normal to the natural breakdown path. Dougal and Williams in their

experiments compared the laser triggered gap breakdowns with and without the laser assisted streamer with untriggered weakly overvolted gap [108, 109]. They did not find any qualitative differences between the breakdowns of untriggered gap and laser triggered gap where the streamer propagated without the assistance of the laser. Dougal and Williams have published evidence directly showing the interaction between the laser and streamer in laser triggered gaps. Preliminary estimations of the effect of the interaction between the laser beam and propagating streamer have been carried out by Dhali [94]. It is shown that laser increases the ionisation rate through an inverse brehmsstrahlung, cascade ionisation process. Dhali's calculation demonstrates that this interaction between the laser and propagating streamer has an important effect in aiding the propagation of undervolted streamers and supports the role of laser streamer interaction in laser triggering of the gaps.

In the case of volume triggering the physical mechanisms responsible for the initial optical breakdown have been only partially understood. A spark gap can be volume triggered by introducing the laser beam into the gap in either longitudinal or transverse geometry. Transverse mode is not very well developed.

Gap triggering results from the formation of relatively high conductivity channel in the middle of the gap. The physical mechanisms responsible for the initial optical breakdown are only partially understood. Several studies have reported very low jitters for UV laser triggered gaps [93, 96]. It has been determined that if the delay is less than the effective pulse width of the laser, the jitter will be a minimum and essentially constant. If the delay becomes longer than the laser pulse length, the jitter increases rapidly. It has been found that the importance of UV radiation provides the initial electrons needed for inverse brehmsstrahlung heating process.

All the available results indicate that the low jitter triggering in this geometry requires a two-step optical breakdown process. First, weak preionization of the fill gas must occur, followed by a rapid ionization growth process. The latter process is probably inverse bremsstrahlung heating. The details of the first process however remain unclear. In most cases the multiphoton ionisation is a relatively weak process. Di-

rect photoionization of some impurities in fill gas seems to be more likely [92]. Gamal and Evans in their theoretical study [97] suggest that for the most used ruby lasers the IB is not capable of producing the initial electrons in a neutral gas. For the range of laser intensities used the multiphoton ionisation is very unlikely (e.g. requires simultaneous absorption of 14 photons). In typical cases it is possible that a large number of impurity molecules are in the focal volume.

One would expect that focusing the laser on the anode should be the optimum discharge configuration. Then the rapid bridging of the gap due to the positive streamer is very efficient. One possible reason of easiness and quickness of gap breakdown might be the generation of soft x-ray radiation (0.5 - 3 keV) laser beam - target interaction reported in [116 - 118]. The preionisation produced by this radiation leads rapidly to the total breakdown of the gap. The dependence of breakdown properties on the gap filling gas has been found and in [104] it has also been found that for laser triggered switches the mixture of equal parts of nitrogen and argon is the best, and that Ar facilitates the breakdown in all investigated gas mixtures.

Another parameter of interest is the electrode material which will primarily affect the term N_0 , the number of initial electrons. Khan and Walsh [110], having assumed that electron and ion emission at the electrode are of thermoionic origin, have associated performance of various materials with the temperature rise after irradiation by a pulsed laser. The formula they derived considering the effect of electrode materials is:

$$T = \frac{2AI}{(\pi\rho ck)^{1/2}} [t^{1/2} - (t - \tau)^{1/2}], \quad (14)$$

where A is the fraction of incident light absorbed, I the power per unit area of beam, ρ the material density, c the material specific heat, k the thermal conductivity, t the time after laser heating starts and τ the duration of laser pulse. Khan and Walsh in their experiments got good fit with this formula for brass and tungsten electrodes. With tungsten electrodes the delay time was half of that for brass electrodes and observed peak currents were 160mA and 70 mA, respectively.

The plasma generation by *XeCl* excimer laser pulse during laser photoablation process was studied in [119, 120], where three stages in generation of plasma plume during the laser irradiation were distinguished:

- i) interaction of the laser beam with the target material resulting in heating of surface layers to the temperature of boiling T_k ,
- ii) the evaporation of the material of surface ,
- iii) interaction of the laser beam with the evaporated materials and breakdown
- iiii) interaction of the laser radiation with plasma of created plasma.

In [121] Vogel and Höft studied minimum conditions for the formation of surface craters by irradiation. The critical power for crater formation was found to be of 10^7 W cm^{-2} (according to this they concluded that crater formation by ion bombardment will require an ion current density of 10^6 A/cm^2). By their calculations the surface temperature of irradiated target reaches to a value of 3000°C within 1 ns (Intensity of laser radiation was $2.5 \times 10^9 \text{ Wcm}^{-2}$). This rapid increase of the temperature can provoke the explosive ejection of matter of target.

The validity of a number of models of corona discharges and of the formation of corona discharges can be proved experimentally with adequate spatially and temporally determined initiating

One purpose of the present work is to determine the formative time of corona pulses with the uncertainty of few nanoseconds. For this reason there is an ultimate need to work out the experimental methods enabling to initiate corona pulses with the same uncertainty and thus to determine the formative times.

2 Experimental

2.1 Experimental set-up and apparatuses

2.1.1 Experimental set-up

In this chapter mainly additional information to experimental results presented in papers [A1 -A5] added in the appendix of this thesis is

given. The Author's publications dealing with the problems of corona discharges and initiating of corona pulses are presented in the list of publications as [A1 - A11]

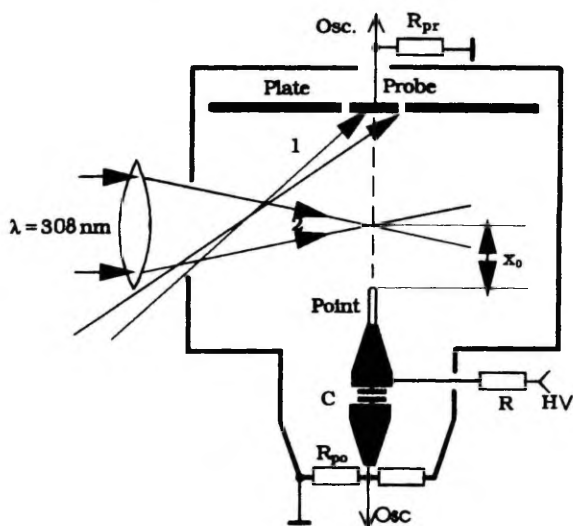


Figure 1 Experimental set -up.

1 - primary electrons are released at the probe electrode

2 - primary elections are created at the gap axis
by a focused laser beam

$R = 20 \text{ k}\Omega$, $C = 2000 \text{ pF}$, $R_{po} = 50, 470 \Omega$, $R_{pr} = 470 \Omega, 1.3 \text{ k}\Omega$

HV - high voltage supply

The experiments were carried out using two different experimental devices with nearly the same discharge gap geometry. The gap spacing was 40 mm and the point electrode was a hemispherically capped wire of diameter 1 mm. The opposite electrode was a disc with the diameter of $\geq 150 \text{ mm}$. Point electrodes made of different materials (*Al*, *Pt*, *Mo*, *Cu*) were used. The experimental device for corona studies in nitrogen was located in a stainless steel chamber, which was furnished with quartz windows, the plane had a probe electrode of diameter of 1.5 cm in its centre (Figure 1). In studies of discharge in ambient air the discharge gap was electrically shielded and the disk electrode had a hole of 4 mm in diameter in its centre for directing X-ray radiation

through it along the gap axis to the point electrode. In this device the probe electrode in the centre of the plate was absent (Figure 2).

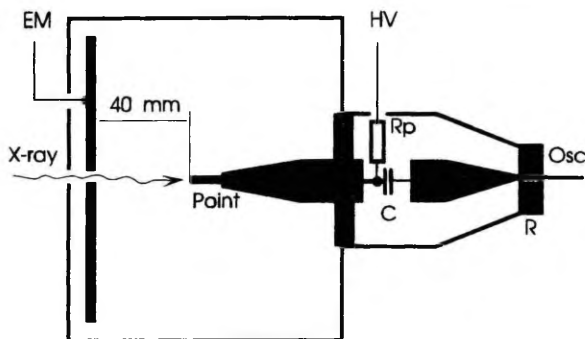


Figure 2. Experimental set-up in air:

X-ray - x-ray pulse generator

EM- electrometer; $R_p = 10 \text{ k}\Omega$; $C = 1 \text{ nF}$;

R - disc-like low inductance $50 \text{ }\Omega$ resistor

For the nanosecond resolution measurements of the current of streamer pulses a 350 MHz bandwidth oscilloscope of $50 \text{ }\Omega$ input resistance was used: a $50 \text{ }\Omega$ coaxial feedthrough of the gap was fitted with a $50 \text{ }\Omega$ transmission line. Light from corona was detected by an image intensifier and/or photomultiplier. It was possible to use different resistances in the plate and point circuits.

Mainly two different ways of corona initiation was used: With X-ray pulse directed along the gap axis, and with the ultraviolet light pulse from XeCl excimer laser (308 nm) directed perpendicularly to the gap axis and focused at the gap axis. In some experiments [A1] axial longitudinal triggering was used, where the laser beam was directed through the hole in the plate along the gap axis to the point electrode and focused on the distance of few millimetres from the point surface. The gap configuration was almost the same as described above, the experimental set-up is described in [A1] and presented in Figure 1 of that paper.

2.1.2 The X-ray source

The X-ray pulse generator with corona plasma cathode is based on the principles published in [122]. The X-ray generator is presented schematically in Figure 3A. The cathode of the device (Figure 3B) consists of a fine (diameter $d = 0.05$ mm) *W* wire which is helically wound around the quartz tube of 8 mm in diameter and 5 cm in length. The inner surface of this tube is covered with *Al* folio which is connected to the circuit ground.

The negative HV pulse from the output of pulse generator is delivered to the helical winding. The amplitude of applied HV pulse can be regulated from 6 to 30 kV, the halfwidth of the pulse is about 120 ns. The anode made of *Ta* is placed at the distance of 4 cm from the cathode. The X-ray tube has a lavsan window and can be evacuated with silica-gel trapped rotatory vacuum pump to a residual pressure of 10^{-3} Torr.

The HV pulse causes the liberation of electrons due to the field emission and the formation of a plasma sheath under the effect of displacement current [122]. Electrons from the plasma sheath are accelerated in the electric field between the cathode and anode, thus forming an e-beam which, reaching the anode causes the X-ray pulse. The generated X-rays, after passing the lavsan window, can be directed through the hole in the plate electrode into the discharge gap. The X-ray pulse is detected with the PM tube supplied with scintillator in front of its window. Detected X-ray pulses were about twice shorter in duration than the applied voltage pulse (60 - 70 ns). The quantum energy of the X-ray radiation is determined by absorption measurements. Two different detector systems were used in these measurements: the PM tube with scintillator coupled with oscilloscope and the ionisation chamber coupled with electrometer. In all measurements both the devices gave the mean quantum energy within the limits 5 - 6 keV. The intensity of X-ray radiation depends on applied voltage and vacuum in the chamber of X-ray tube. During the measurements the value of residual pressure was held constant $\approx 10^{-2}$ Torr, which corresponded to the maximum intensity of radiation. The intensity of X-rays can be attenuated stepwise by putting *Al* folios

between the window of the tube and discharge gap. The used repetition rate of X-ray pulses was 10 pps.

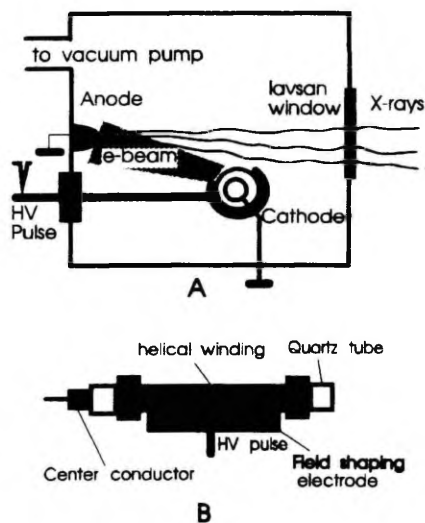


Figure 3 A - The scheme of the X-ray generator tube
B - The construction of the cathode

The number of electron-ion pairs created by a single X-ray pulse was measured by the help of ionising chamber. The measuring device consists of electrometer, which worked at the charge measuring regime, and of ionising chamber of 100 cm^3 volume. The front and back sides of the chamber are made of stainless steel grid, fine wires are placed in the central part of the chamber, which are insulated from the sides and can be stressed relatively to the sides by the galvanic voltage supply of 32V; the polarity can be changed. The measured number of electron-ion pairs was 10^7 for the maximum pulse intensity. To eliminate the number of electrons created by photoeffect from the walls of the chamber, the polarity of applied voltage was changed. Only negligible effect was registered.

2.1.3 The excimer lasers

The XeCl excimer lasers used have been constructed at the Laboratory of Gas Discharges of Tartu University [123] and have the following output parameters. The wavelength $\lambda = 308$ nm, the maximum energy per pulse $I_0 \approx 80 - 100$ mJ, the duration of pulse of a long pulse laser is ≤ 100 ns and that of short pulse laser is about 10 ns. The waveforms of the laser pulse intensities are presented in Figure 4. The cross section of the laser beam is approximately (1×2) cm², the divergence of the laser beam is estimated to be in the order of 1 mRad. The laser beam can be directed into the discharge gap using surface coated mirrors and quartz optics and it can be attenuated stepwise by the help of calibrated metal grids and gradually by a diaphragm of changeable size.

The number of charged particles generated by a single laser pulse was measured at first as in the case of X-rays, by the help of the ionisation chamber-electrometer. The laser beam was focused through the small hole in the wall of the chamber on the centre of it and the generated charge was measured. Another way to determine the charge created by laser was focusing the laser beam between two parallel plates (1×1 cm²) which were placed at the distance of 5 mm from each other. Voltage 100 - 600 V was applied between the plates. The generated current pulse was registered with the help of the oscilloscope and the number of charged particles was determined from it. The third method of determining of the number of charged particles was measuring current pulse parameters in point circuit of the discharge gaps. In this case the laser beam was focused on the midgap above the point electrode tip and the charge of current pulse in the gap circuit was determined as a function of gap voltage. The current was detected by the help of oscilloscope of higher sensitivity (0.1 mV/cm, 1 MHz bandwidth) as a drop of voltage over the resistor R (1.3 k Ω - 1M Ω). So the circuits were mismatched and the recorded signals were integrated. During these measurements the gap voltage was low $U \leq 3$ kV. From 1.5 to 3 kV the measured charge does not depend on voltage, thus the avalanche multiplication did not take place. From this value of charge the number of charge carriers was calculated. At higher gap voltages the increase in charge was registered, consequently the detectable avalanche multiplication took place. This last method enabled to

measure the number of charged particles originated by a laser pulse in nitrogen. The number of charge carriers which

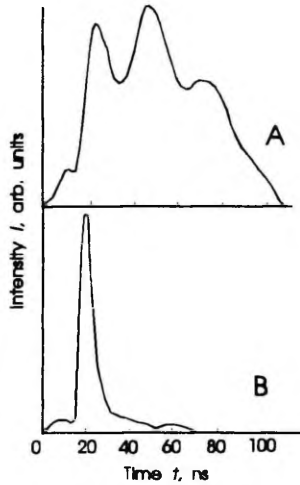


Figure 4. A - Waveform of the long pulse laser
B - Waveform of the short pulse laser

corresponds to the maximum laser intensity I_m both in air and nitrogen was nearly the same and had the order of magnitude of 10^8 . However, the number of carriers created by a 10 ns pulse is somewhat less than that produced by a 100 ns pulse. Registered generated charges are in accordance with results reported in [124] for analogous lasers and experimental conditions.

2.1.4 Gases.

Gas mediums chosen for experiments are air and nitrogen. The most available and usual discharge medium in laboratories is ambient air. Most of the studies have been up till now carried out in air. That gives us a good chance to compare experimental results with a number of earlier studies. Moreover, air has from a practical point of view a great importance. On the other hand, air is a mixture of gases which, from the viewpoint of discharge, have very different electrical properties. To simplify the matter under the study it seems to be reasonable to get rid

of attachment problems originating from the electronegativity of oxygen. Consequently, there is a necessity to carry out a series of experiments for comparison in the other main component of air, in nitrogen. Shortly, the choice of nitrogen is based on the following arguments:

- 1) Both air and nitrogen are molecular gases
- 2) Nitrogen appears to be one of the main components of air
- 3) As nitrogen is a free electron gas, it enables to suppress the influence of negative ions on the discharge. Consequently it gives a possibility to estimate the role of negative ions in the discharge processes
- 4) The efficiency of photoionisation as a possible secondary mechanism is much lower in nitrogen than in air.

Nitrogen of purity of 99,996 % was used for filling the discharge chamber, the pressure was set at atmospheric pressure.

The stabilised high voltage power supplies in use had an output range of voltages 400 V - 15 kV and allowed to vary the voltage with the smallest step of 10 V.

2.2 Experiment

2.2.1 Positive point.

The formation of spontaneous streamers and initiating streamers with X-rays is discussed in more detail in the paper [A2], the laser initiation of streamers is the subject of studies in papers [A3], discussed in [A4], some of the results are published in [A5] and [A6]. Mainly only additional experimental data to those presented in the articles in the appendix of the thesis are presented in this chapter.

X-ray initiating , air.

Both spontaneous (noninitiated) and initiated positive corona pulses were under observation. In air the sequence of different noninitiated DC corona types does not differ from that described earlier by several investigators [7 Ch.13, 15,16]. The first detectable discharge type is burst pulses which are registered ~ 200 V below the onset potential U_0 of preonset streamers. This form of discharge spreads along the point surface. Visually a very weak illumination on the point electrode tip

surface can be seen. The area covered by the luminous layer on the point electrode is nearly 0.2 mm^2 . Current pulses of very small amplitude and corresponding light pulses can be registered. Light and current pulses were recorded by a 250 MHz bandwidth oscilloscope. With voltage increase their amplitude and duration as well as their repetition rate rises. At voltages close to U_0 the amplitude of larger burst pulses achieves 0.2 mA and their duration is nearly $1 \mu\text{s}$, the corresponding light pulse is considerably shorter ($\approx 70 \text{ ns}$) (Figure 1A in [A2]). At voltages $U > U_0$ both burst pulses and streamers exist simultaneously. The onset potential U_0 depends on humidity and pressure of ambient air and varies for different days of experiment from 7.8 to 8.0 kV. The peak value of the largest current pulses of streamers is 9 mA and their halfwidth is $\approx 100 \text{ ns}$. The noninitiated streamers are recorded in the range of $\approx 200 \text{ V}$. They have a branched structure and some of the branches develop up to $\approx 10 \text{ mm}$ from the point. At higher voltages the discharge exists in the form of steady glow, its current increases from $0.5 \mu\text{A}$ at 8.5 kV up to $9 \mu\text{A}$ at 14 kV.

In the narrow range of voltage near the inception voltage the burst-to-streamer transition is observable: the steep current rise of a streamer pulse is preceded by a step (Fig 1B in [A2]). The recorded current waveform is very similar to the avalanche-to-streamer transition in homogeneous field, (Figure 5 - this is a reproduction of a figure 5.14 from 37). The magnitude of the step is close to that of burst pulses and its duration does not exceed 20 ns. With the voltage increase the duration of step diminishes quickly and already of 50 volts above U_0 it is difficult to separate the step from the main pulse. With the increase in voltage the amplitude of the step decreases. The corresponding light pulses are presented in Figure 6. Similar temporal development of luminosity near the point electrode has been registered by several authors [125]. In homogeneous field the observed delay is supposed to correspond to the radial development of discharge, what will be followed by originating of a streamer from this area [126]. At the onset a prepulse starts about 20 ns before the streamer rise. The light pulse of a streamer has a comparatively long rise time. With the increase in of voltage only 10 V the rise time of a streamer pulse shortens to about 10 ns, and further increase in voltage results in the further shortening of the rise time, at the same time the shortening of the time interval between the prepulse (burst pulse stadium) and the rapid growth of the

streamer can be observed. At about 50 V above U_0 the burst stage is not detectable already.

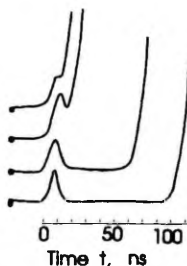


Figure 5. The transition to streamer in homogeneous field.
(Figure 5.14 from [37])

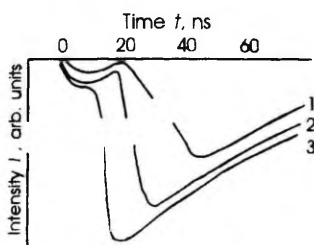


Figure 6. Light pulses of burst-streamer transition
1 - $U = 7.78\text{kV}$; 2 - $U = 7.79\text{kV}$; 3 - $U = 7.80\text{kV}$

When the X-ray pulse generator is switched on the initiation of bursts occurs at $\approx 400\text{ V}$ below U_0 . The current amplitude of these burst pulses about 100 V below U_0 is eight-fold compared with the current of spontaneous ones at the same voltage. Area covered by the light of initiated burst is nearly 1 mm^2 . In case of initiation the burst-streamer transition occurs at 90 V below U_0 . The transition from burst pulse to streamer has similar features as in the noninitiated case - it has a step or prepulse before the rapid current rise. It was convenient to study this phenomenon because of a low jitter in relation with the triggering X-ray pulse and good reproducibility. Near U_0 one X-ray pulse initiates more than one streamer. The average number of initiated

streamers per laser pulse determined with the pulse counter is presented in figures 2A and 3A in [A2], and it mainly depends only on the gap voltage, not so much on the X-ray intensity. The first of these streamers is quite well related to the X-ray pulse, the next one follows randomly with delay time of 1 ms and more. Time intervals between the X-ray pulse and corresponding corona pulse were registered by the digital timer with 10 ns resolution or on the oscilloscope screen with somewhat higher time resolution. The accuracy of measurements of delay time was determined by the relatively slow risetime of X-ray pulses. At voltages above U_0 initiated as well as spontaneous streamers exist. In Figure 2A in [A2] the first initiated streamer delay time t_d distribution for different voltages and mean delay time t_d dependence on voltage are presented; in Figure 3A in [A2] t_d and t_d dependencies on X-ray intensity are presented.

Laser initiating . Air.

The laser initiation of discharge has been under investigation in the papers [A1], [A3], [A6] and [A7], and discussed in [A4].

Primary electrons are created by the radiation of excimer laser beam directed perpendicularly to the gap axis and focused on the gap axis at some distance x_0 from the point electrode (See Figure 1). With transverse triggering one can neglect additional effects caused by the laser radiation at the electrodes as they occur in experiments described in [A1]. The maximum used intensity I_m near the beam focus does not exceed $5 \times 10^{10} \text{ Wcm}^{-2}$. This intensity I_m is considerably lower than needed for optical breakdown ($I \sim 10^{12} \text{ Wcm}^{-2}$ for $\lambda = 350 \text{ nm}$, [93]). In air the distance x_0 is established with the accuracy of some a tenth of millimetre. Due to the laser instabilities the position of the focal point varies from pulse to pulse within the same limits. In the case of experiments in nitrogen the accuracy is less than in the experiments carried out in air as in chamber the direct measurement of x_0 is impossible. Near the beam focus the dimensions of the trace created by the radiation at a photo plate are $\approx 0.01 \times 0.02 \text{ cm}^2$ and it remains nearly constant within limits of 0.6 cm along the beam axis. It is supposed that the ionisation by laser radiation mostly takes place within

this volume and thus the guessed value of the concentration of charged particles of a plasma ball in the beam focus is $\sim 10^{11} \text{cm}^{-3}$. In [124] the experimental conditions and gap parameters were very similar to ours, also the registered characteristics as the number of electron created by laser, were close to those we obtained.

It was possible to initiate streamers already at $U = 0.75 U_0$ (onset potential of spontaneous streamers $U_0 = 7.8 \text{ kV}$) as well as in the region of steady glow. The onset potentials of initiated streamers for different initiation intensities I and distances are presented in Figure 7.

Delay time t_d was measured from the rise of the laser pulse. At every applied voltage

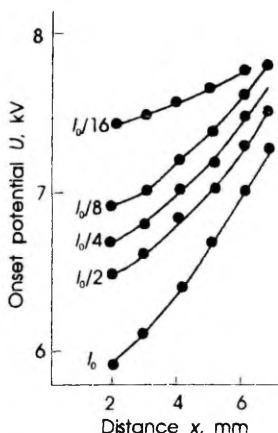


Figure 7. The onset potential U of initiated streamers as a function of initiating intensity I and distance x

U delay time t_d depended both on the distance x and intensity I and varied from 10 ns for $x = 1 \text{ mm}$ up to 350 ns for $x = 8 \text{ mm}$ (Figure 8, 9, 10) and Figure 5 in [A3]. In [127] was determined the critical gap length, where the rapid triggering transited to the long term triggering (10 - 11 mm). In our case the upper limit of triggering distance was 8 mm, what corresponds to the rapid triggering by the released electron. The initiation of a streamer by electrons detached from ions is not sufficiently effective. It is confirmed in experiment, where electrons were released from the cathode plate. After a quite long time lag (3.5

ms), what corresponds to the negative ions drift time across the gap, they were able to initiate only a burst pulse.

For all distances under observation the behaviour of curves $t_d = f(U)$ is similar. At every intensity $I = \text{constant}$ below

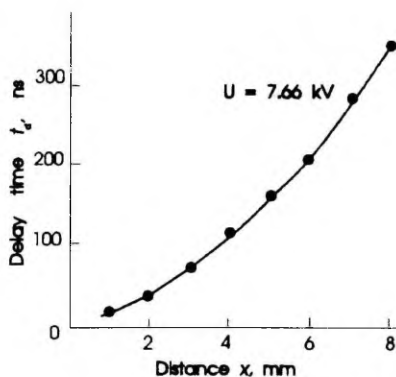


Figure 8. Delay time t_d as a function of the triggering distance x

the inception voltage of non-initiated streamers U_0 the delay time decreases with the voltage increase and achieves its minimum near the potential U_0 . Further increase in voltage leads to the increase in delay time, too. In the region of steady corona the delay time remains nearly constant. At every voltage the decrease in intensity causes the increase in delay time. The distance $x = 8$ mm was the maximum distance, where the initiating was observed in air. The dependencies of delay time on intensity of initiation are presented in Figure 8. Regardless of quite a long delay time t_d , the starting moment of the streamer had a very small jitter (< 2 ns) in relation with the triggering laser pulse. By appearance, as it was fixed by an image intensifier camera, there was no principal difference between streamers initiated at any voltages and spontaneous streamers, (Figure 11).

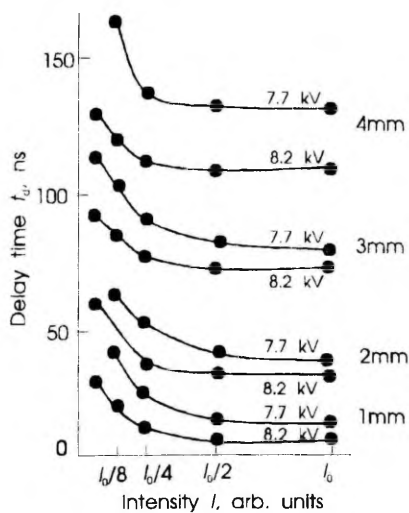


Figure 9. Delay time t_d as a function of the initiating intensity I for different distances x

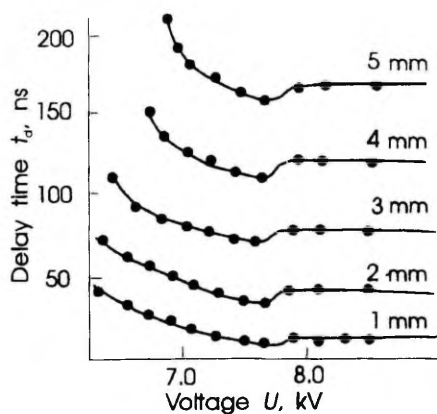


Figure 10. Delay time t_d as a function of gap voltage U for different triggering distances x

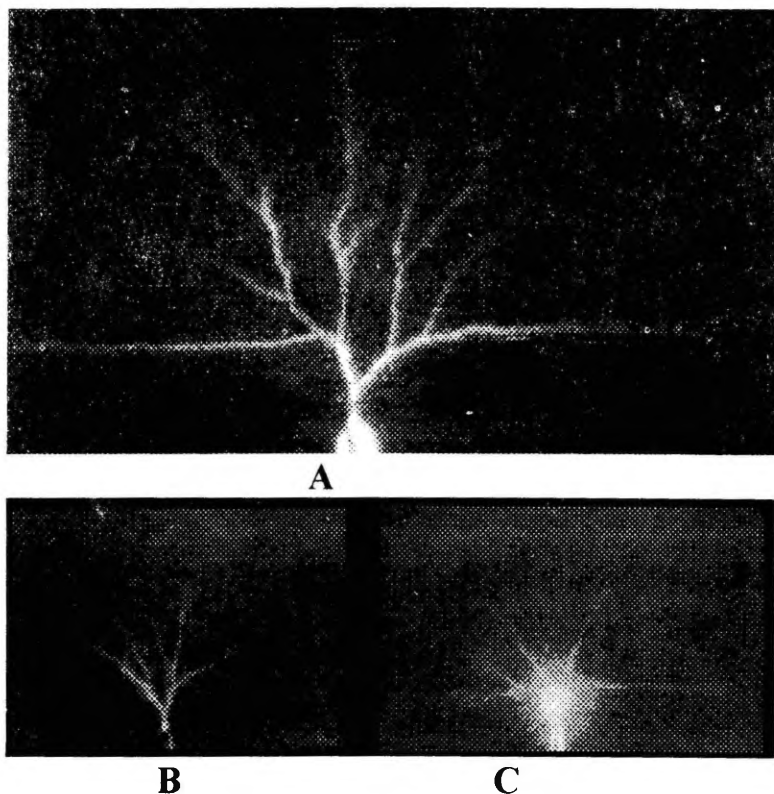


Figure 11 Photos of initiated streamers in air

A. A typical photo of a initiated streamer

Transversal triggering,

$x_0 = 2 \text{ mm}$, laser intensity I_0 , $U = 7.9 \text{ kV}$

B. - $x_0 = 6 \text{ mm}$, laser intensity $I = I_0/2$

, the gap voltage $U = 7.5 \text{ kV}$

C. $x_0 = 1 \text{ mm}$, laser intensity $I = I_0/2$,

the gap voltage $U = 10.6 \text{ kV}$

Laser initiating. Nitrogen

Noninitiated and laser initiated discharges in the case of positive point in nitrogen have been studied in papers [A1, A3, A4 and A7]. Experiments were carried out at atmospheric pressure. The problems concerning the purity and ageing of nitrogen gas are discussed in [A3].

The discharge chamber was evacuated by the help of an oil diffusion pump trapped by the liquid nitrogen and supported by a rotary pump. When the chamber was evacuated, it was warmed up to about 100⁰C during some hours. As the drift velocity of electrons depends on the humidity of nitrogen, the ageing of nitrogen gas was assumed to be also caused by the effect of humidity. To reduce that influence the gas was dried by the means of a bakeable silica-gel cell, which was placed into the discharge gap and during evacuating it was warmed up to some hundred degrees. The discharge gap was evacuated to the residual pressure of 10⁻⁵ Torr before filling with fresh gas, and the pumping period with silica-gel trap heating lasted about 3 hours. The measurements were performed after the discharge chamber and silica-gel trap were cooled down to ambient room temperature.

In nitrogen the onset potential of the discharge is considerably higher than in air: at 9.7 kV the first pulses of 0.25 μ A in amplitude are recorded, their duration $\approx 10^{-6}$ s is determined by the time constant of the recording system. The number of electrons $N \geq 10^6$ in a pulse is close to the calculated number of charge carriers in an avalanche at this voltage. According to the static picture from several pulses (observed by the image intensifier) a large area of the hemispherical part of the point electrode is covered by a very faint luminous layer.

At 9.9 kV a steady discharge establishes. Together with the voltage increase the DC current of steady discharge increases gradually from 1 μ A at the onset up to the 8 μ A at 14 kV . At the point surface near its tip a more intensive luminous spot with sharp borders is observable. The area of the spot is $(1.2 \div 1.5) 10^{-4}$ cm² and above it a faint luminous channel extends far into the gap. From time to time the spot jumps to another place. Only few jumps per minute occur. The jump is accompanied by a sudden change of DC current (Figure 12 - the bars indicate the extent of the current jumps) as well as by the streamer formation. It

is difficult to say whether there are streamers also during the constant current or not.

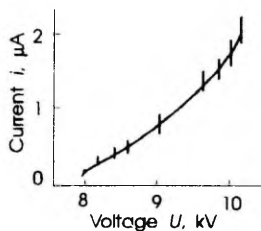


Figure 12. $I - U$ curve of steady discharge in nitrogen.

Bars indicate the range of fluctuations

The height of the current pulse of a streamer varies from 16 to 20 mA and the halfwidth of pulses is ≈ 800 ns. By appearance the streamers are less if any branched than in air. The length of a non-branched channel varies within the limits $0.8 \div 1.5$ cm and the channel is often deflected from the gap axis, the branching occurs mainly at the end of the streamer channel.

In dry nitrogen the extinction voltage differs from the inception one: the steady discharge exists down to 8.7 kV. The extinction current of discharge is $\approx 0.12 \mu A$. The same behaviour as at voltages above the inception voltage is observed: the sudden change of current is connected with streamer formation, and the length of streamer channel is diminishing with voltage decrease.

In non-dried nitrogen the extinction voltage equals to the inception voltage and the streamer is branched like in air.

Drift time and experimental ionisation integral

The noninitiated DC discharge as well the determination of drift time of electrons and finding of the experimental ionisation integral has been described in [A3]. The primary electrons are liberated from the probe by a 10 ns attenuated laser pulse. Analogous methods for releasing electrons in drift time measurements have been used in [128 - 130, 131]

The drift time t_{ca} is measured as a function of voltage (figure 3 in [A3]). The results for dry nitrogen are close to those calculated on the

basis of data from the literature [132 - 134]. The presence of water vapour reduces drastically the drift time (measurements without silica-gel trap after discharge had run some times).

The number of electrons leaving the cathode N_c and reaching the anode N_a is determined from the areas $\int i dt$ of current pulses of the probe and the point, respectively. During their drift the number of electrons changes due to the losses as well as due to the ionisation multiplication in a high field near the point.

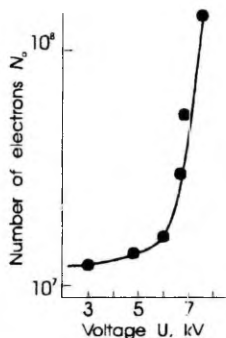


Figure 13 Number of electrons reaching the anode N_a as a function of the gap voltage U

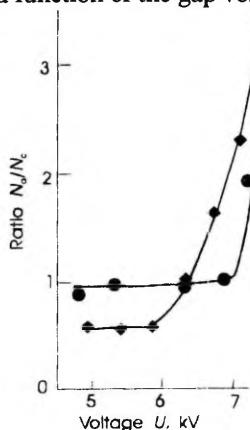


Figure 14. The ratio of N_a/N_c as a function of gap voltage
dots - dried nitrogen
diamonds - nondried nitrogen

In Figure 13 the number of electrons reaching the cathode as a function of gap voltage is given. Up to 4 kV in dry nitrogen within the limits of experimental errors there is no difference between N_c and N_a (in non-dried nitrogen $N_a/N_c < 1$) (Figure 14). As the value of the calculated ionisation integral $\int \alpha_0 dx$ is close to one in this range of voltage, it is possible to conclude that in this case the role of losses is negligible. At higher voltages ($U = 5 \div 8$ kV) N_a increases together with voltage but the waveform of current pulses does not change and the relation N_a/N_c does not depend on laser intensity. So the curve $\ln(N_a/N_c) = f(U)$ may be treated as a dependence for experimental ionisation integral.

At voltages $U > 8$ kV the waveform of current pulses of the point circuit changes. The simple waveform is replaced by a more complicated one (figure 2B in [A3]): there is a higher hump at the beginning of a current pulse. At higher voltages a steep current rise starts from this hump that is corresponding to streamer development as it is also confirmed by image intensifier observations. The onset voltage of an initiated streamer U_i depends on laser intensity, but independent of U_i there is a critical total number of charge carriers $N_{cr}^t = (2 \div 5)10^7$ (figure 2B in [A3]) near the point that must be achieved by the moment of transition.

Transversal triggering. Nitrogen

In the case of transfer triggering in nitrogen the dependencies $t_d = f(U)$ are recorded up to the distance $x_0 = 1.6$ cm (Figure 15). The long-pulse as well as the short-pulse laser are used, but the results do not depend remarkably on the pulse length. This maximum distance is limited by the dimensions of viewport of the discharge chamber and not by the jitter of t_d . Like in air the initiation of streamers is possible at voltages remarkably less than the inception voltage of non initiated discharge. Compared with air the dependence on laser intensity at $U = \text{constant}$ is considerably less. A typical curve of $t_d = f(U)$ is presented in Figures 4 and 6 in [A3]: delay time diminishes gradually with voltage increase.

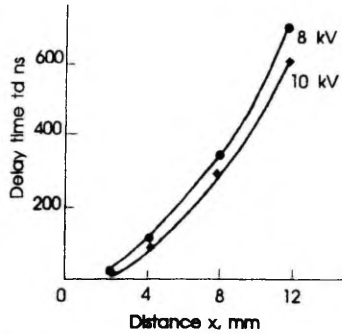


Figure 15. Delay time t_d as a function of triggering distance for different gap voltages

Spatial-temporal development of streamer was studied by the help of ICIC in framing mode. By appearance an initiated streamer had a branched structure, the length of branches increased with voltage increase. At higher laser intensities the branches developing towards the laser beam would prevail (Figure 16, 17) [A6, A7].

Streamer channel starts from the point. When it reaches some distance $x < x_0$, an intense branch parallel to the laser beam trace develops towards the laser. The position of this branch is well fixed from pulse to pulse and it has higher velocity of propagation v_B than others. The length of the branches increases with the increasing of intensity of the laser beam as well as with the increasing of the gap voltage U . Typical length of horizontal branches is 2.5 cm. At the initial stages the velocity of branches which develop towards the plane electrode v_A is less and they are randomly distributed in space. Increase in U causes the increase in length of these branches. If U exceeds U_0 they usually bridge the gap. The dependence of velocities v_B and v_A on the distances s from the point are presented in Figure 18 attenuating the laser pulse energy to $I_0/16$, the initiated streamer will not longer propagate along the preionised path, attenuation to $I_0/32$ stops the initiating.

In the case of longitudinal triggering of sufficient intensity a streamer with straight axial channel forms, but the laser beam of low intensity initiates streamers the appearance of which is very similar to the spontaneous ones. The propagation velocity of streamer during laser pulse is much

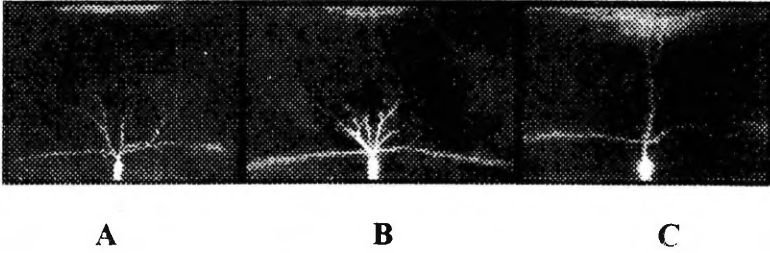


Figure 16 Initiated streamers in nitrogen

A - $x_o = 4$ mm, the gap voltage $U = 8.2$ kV,

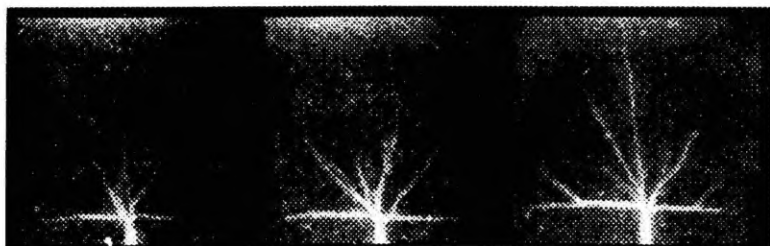
laser intensity $I = I_o$

B - $x_o = 2$ mm, the gap voltage $U = 10.1$ kV,

laser intensity $I = I_o/2$

C - $x_o = 10$ mm, the gap voltage $U = 14.4$ kV,

laser intensity $I = I_o$



A

B

C

Figure 18 Photos of initiated streamers in nitrogen,
laser intensity $I = I_0$, initiating distance $x_0 = 2\text{mm}$,

A - gap voltage $U = 8.3\text{ kV}$

B - gap voltage $U = 9.3\text{ kV}$

C - gap voltage $U = 10.3\text{ kV}$

higher than after the termination of it - $8 \cdot 10^7$ and $3 \cdot 10^6$ cm/s, respectively. More information about this experiments can be found in [A1].

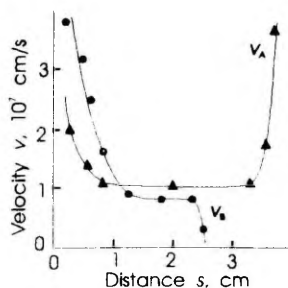


Figure 18. Velocities v_A and v_B as functions of the distance from the point

2.2.2 Negative point

Ambient air . X-ray initiation

Experiments were carried out in ambient air at atmospheric pressure. Different samples of *Al* and *Pt* points were used. An X-ray pulse generator was used for corona initiation. Previously the parameters of discharge were measured without X-ray initiation. A low current I - U curve was registered. I - U curve depends strongly on the material of the point and its prehistory. Typical $I = f(U)$ dependencies for *Al* and *Pt* points are presented in Fig. 1 in [A2]. The I - U curve for *Pt* in air is similar to that of in pure nitrogen, but in case of *Al* point remarkable increase in current is registered only near the onset potential of corona pulses U_o . In case of *Pt* point diffuse light is visible already of 1 kV below the onset potential, but it is absent for *Al* point. The onset potential of spontaneous corona pulses varies in big limits ($U_o = 7.5 - 7.9$ kV) and depends on point material as well as on prehistory of the point. Corona current pulse has a rise time < 2 ns, its peak value near the U_o is practically the same for all points. To study the initiation of corona pulses by X-ray radiation the time intervals between the beginning of X-ray

pulse and corona pulse (delay time t_d) are measured for different points and voltages. While at any voltages under observation there is also a chance of arising of spontaneous pulses, the mean number of spontaneous pulses per second (pps) \bar{n}_1 is determined at every voltage as well as the mean number of pps in the presence of X-ray radiation \bar{n}_2 . The repetition rate of generated X-ray pulses is 10 pps. The number of corona pulses per second is determined (Figure 5 in [A2]). Near the onset U_o where spontaneous corona pulses are almost absent ($\bar{n}_1 = 0.46$) not every X-ray pulse initiates a corona pulse ($\bar{n}_2 = 8.1$) and t_d is distributed over a large time interval. Already at $U = 7.60$ kV each X-ray pulse initiates a corona pulse ($\bar{n}_1 = 5.8$, $\bar{n}_2 = 16.1$) and 30% of pulses have t_d less than 30 ns. At more than 500 V above U_o spontaneous pulses prevail and it is difficult to determine the influence of X-ray radiation. In the case of *Al* point (Fig. 5B in [A2]) X-ray initiation is more efficient. It is possible to create a corona pulse already below the onset $U = 7.7$ kV and at $U = 7.85$ kV each X-ray pulse initiates a corona pulse ($\bar{n}_1 = 0$, $\bar{n}_2 = 10.4$). At a voltage 20 V higher than that, a single X-ray pulse creates even more than one corona pulse ($\bar{n}_2 = 13.5$). Delay time t_d distribution is presented only for the first corona pulse. Strong effects are observed when a *Pt* point is coated with a thin layer of transformer oil. Low current mode of discharge is practically absent (the current is at least two orders of magnitude less than in case of uncoated point). Onset potential of spontaneous pulses rises remarkably, in some experiments (it depends on the thickness of oil layer) it rises more than 3 kV, but initiated pulses start nearly at the same voltage as in case of noncovered point and initiation is effective ($\bar{n}_1 = 0$, $\bar{n}_2 = 9.45$; Fig. 5C in [A2]). At higher voltages ($U = 8.4$ kV) a single X-ray pulse initiates a series of corona pulses ($\bar{n}_2 = 124$). Beyond this, the following trends are observed: in case of *Pt* points the onset potential is systematically lower than that for *Al* point and a new oxidised *Al* point has higher onset potential than the used one.

I-U curves for dried and nondried nitrogen were measured in addition to the results published in [A2] (Figure 19). The extinction current

for dried nitrogen was $\approx 70 \mu A$, for nondried nitrogen it was somewhat larger $\approx 100 \mu A$. The part of $U-I$ curve with negative slope as in Korge's measurements was not observed, the low current region was not under observation any more.

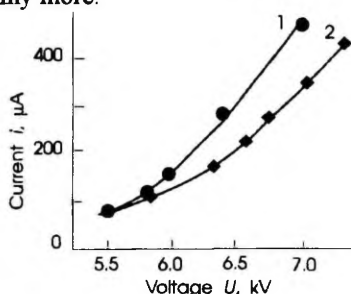


Figure 19. $I-U$ curve in the case of negative point in nitrogen
1 - dried nitrogen ; 2 - nondried nitrogen

Corona pulses triggered by directing the laser beam to the point electrode surface indicate that in this case the thermal effects caused by laser radiation are dominating [A1]. In this case it is possible to initiate corona pulses with very low intensity of laser radiation .

3. Discussion

3.1. Main results and open problems

3.1.1. Negative point

It is known that at high fields ($E > 10^7$ V/cm) in a homogeneous gap at higher (few atmospheres) gas pressures the breakdown characteristics differ considerably from those at low pressures, and the most relevant features of this difference are [135]:

- (i) The sparking potential is not well defined even under well controlled experimental conditions. It trends towards some upper limit. This trend is known as conditioning.
- (ii) A marked departure from Paschen's law has been found; the applied E/p across the gap field at higher pressures became so low that it would give very little gas amplification.
- (iii) The sparking potential has a very marked dependence on the cathode material and state. Some cathode dependent processes or

processes which are negligible at lower pressures are introduced at higher E/p values, and they dominate the breakdown mechanism.

Some evidence exist [136] that at these field strengths considerable field emission of electrons from the cathode occurs. The exact role played by this emission in the producing of breakdown is yet unclear, but it is made sure that in the development of the emission localised sites on the cathode and positive ions on cathode insulated layers participate in some cases.

Despite of the number of investigations there is no generally accepted theory or means of predicting the breakdown voltage. The basic difficulty is that the surface-gas interface is a very complex physical system, and experiments in which a strict control of all possible relevant parameters such as thickness of the oxide layer, the presence and nature of inclusions, the size of dust particles and surface topography, are needed to ascertain the parameters which are significant. The problem has much in common with that of the vacuum breakdown [137].

In discharge gaps under observation the Laplacian field at the point surface is $> 10^5$ V/cm. So, it is natural to suppose that processes leading to the formation of a corona are close to those taking place in the formation of a breakdown in homogeneous field at high pressures. The latter is supported by the common characteristics of these discharges:

- field strength at the point is close to the breakdown field in homogeneous field
- there is a stage of low-current discharge, its current-voltage follows the Fowler-Nordheim type of dependence [35]

Taking into consideration above listed arguments and experimental results of the present work, the following evolution of discharge for negative point-to-plane corona is assumed: a low-current discharge determined by a Fowler-Nordheim type of emission precedes the corona pulse in electronegative gas as well as the transition to a strong current discharge in pure nitrogen. Corona pulse and the transition are both triggered by an electron emission due to the breakdown of dielectric layer. In the later stages the discharge is sustained mainly by γ_i secondary mechanism.

Moreover, it is assumed that there is no principal difference between the triggering processes of corona at atmospheric pressure and mechanism of prebreakdown events in homogeneous field.

In pure nitrogen as well as in ambient air the low-current stage of discharge preceding the formation of strong-current discharge (in N_2) or corona pulse (in air) was observed. Current-voltage (I - U) curve of this discharge followed the Fowler-Nordheim type of dependence [A5]. In the case of measurements in air the curve had a strong dependence on surface properties of the point [138]

According to the results of measurements in the case of negative point electrode, a hypothesis that the negative corona formation takes place due to the **dielectric switching mechanism** like in vacuum breakdown [82] and arc formation in gases [139] has been established in the paper [A5]. Similarities between the breakdown events in vacuum and high pressure gas have been confirmed in several publications, detailed studies of the characteristics of electrode emissivity have been made for prebreakdown currents in vacuum [82]. The model of an emission site assumes a metal-insulator emission regime, i.e. the presence of foreign insulator inclusions on the electrode surface that are in intimate contact with the substrate of metallic cathode. Similar assumption was already given by Loeb [52] who stressed the decisive role of dust particles or other foreign inclusions on the point surface for the effective triggering of discharge.

In addition to the general sequence of discharge formation processes observed during the measurements at least two results, which support the proposed dielectric switching mechanism can be concluded.

Firstly, if the dielectric switching mechanism is valid then according to [82] the emissivity of a cathode must depend strongly on the surface temperature. Indeed, in experiments it was possible to initiate corona pulses by directing focused excimer laser beam to the point surface considerably below the onset potential [A1]. The initiation of a discharge with laser pulse in experiment shows the current peak i_{max} dependence on the temperature ($T \sim I$) of the point surface. The amplitude of initiated pulse i_{max} may be considered proportional to the quantity of emitted electrons at voltages below the onset of corona pulses. Linear dependence $\ln(i_{max}) = f(\sqrt{U})$ (Fig. 7

in [A1]) indicates [137] that the height of initiated corona pulse is correlated with the emissive site temperature, thus being caused by field assisted thermoionic emission.

Secondly, according to [139] the charging of insulating layer must precede the discharge formation. The charge of positive ions will accumulate on the insulator surface, until the created electric field of this charge is sufficient to cause the breakdown of this insulating layer. In case of using X-ray radiation [A1] the efficiency of corona initiation depends on point material and the presence of insulating layers. The presence of insulating layer leads to considerable increase in efficiency of initiation. In this case charging of an insulator on the point electrode surface is caused by photoeffect. Its efficiency is different for different points: charging of large oxide layers on *Al* point is more effective than that of microinclusions on *Pt* point. Oil layer on *Pt* point plays similar role to oxide layer on *Al*: it suppresses low-current region, X-ray radiation charges the layer to high densities of positive ions causing the lowering of corona pulse onset potential.

These discussed experimental facts cannot be explained solely in terms of ionisation processes in gas, but electrode surface properties as well as the interaction of electrode surface with ambient gas must be taken into consideration.

Although the methods of initiating negative corona used in the work support the established hypothesis, it does not give unambiguous answer to the Trichel pulse formation mechanism because of the following arguments:

- (i) In the case of laser initiating, a significant heating of the electrode surface takes place, thus this case might not to be in consistent with the formation of noninitiated corona pulses
- (ii) In the case of x-ray initiating the jitter of delay times is too large for adequate determination of formative times.

The validity of the proposed corona formation model can be proved by correct and exact measurements of formative times and the comparison of obtained results with those estimated by the model. For this purpose an adequate initiating of discharge with low jitter is needed. It can be realised by irradiation of cathode surface with weak

short-wave radiation, which is able to generate initial electrons by photoeffect.

Another possibility for proofing the model validity is the investigation of the sputtering of the electrode during discharge. The proposed mechanism of emission is substantiated by the electrode sputtering because of the forming of the conducting channel through the insulate layer [139]. The sputtering is observed in [140], but the moment of sputtering in correlation with corona pulse evolution has not specially investigated. If the time moment of sputtering will coincide with the corona pulse inception, it could be an evidence of validity of the proposed negative corona switching mechanism.

Although the first reports on the possibility of negative corona inception due to the dielectric film breakdown were published as earlier as in 1941 [52], the systematic investigations, which could unambiguously prove the validity of proposed dielectric switching mechanism are still absent.

It is reasonable to suppose that the discharge formation characteristics depend on the surface properties of the cathode. The validity of the model can also be proved by investigation of the discharge formation characteristics on the cathode surface properties. During the measurements the next complications must be taken into account.

- (i) The properties of emission sites at the electrode surface vary within large limits already in vacuum: there are point and extended sites, virgin and relaxed sites, $I-U$ - curve of a site has hysteresis, etc. [1, 82]
- (ii) The presence of gas adds new complications: it is difficult to separate the initiating process from the ionization mechanism in gas [2]. The emission ability of a site diminishes with the pressure increase due to gas absorption [1]
- (iii) previously existing dielectric layers may be destroyed by ion bombardment [138], due to surface-discharge interaction the surface may be covered by the layers of decomposition products [141].

According to the above-mentioned difficulties the preliminary surface processing and choice of gas mixtures as well as the study of

electrode surface before and after discharge runs play a decisive role. Furthermore, besides the traditional recording of current waveform a number of different characteristic dependencies must be recorded. The unsolved problems cannot be solved using only traditional methods of gas discharge investigation. The explanation of the effects of humidity and other impurities demands mass spectrometric investigations of the composition of gases. The influence of electrode surface effects forces us to use electron microscopy and Auger spectroscopy.

3.1.2 Positive point.

It has been experimentally proved that in the case of a large number of primary electrons a streamer forms at voltages considerably lower than the inception voltage as well as in the range of steady corona.

For streamer formation an ionisation instability must develop in a spatially localised region. The local increase in ionisation leads to the increase in the space charge field in this region. A streamer starts when the space charge field achieves a critical value. These conditions are common in different experimental conditions.

At the inception voltage of streamers in a homogeneous field the number of charge carriers in a single avalanche is high enough to reach the critical field but if the gap is undervolted a large amount of primary electrons and/or an accumulation period of space charge are needed for streamer formation.

In a highly divergent field in air even at the inception voltage a space charge accumulation precedes the streamer formation as the number of charge carriers of an avalanche is much less than the critical number and so the streamer formation has a multiavalanche nature. The increase in the inception voltage in nitrogen is caused by the low value of secondary emission coefficient.

Accomplished measurements and calculations enable us to determine the formative time of streamers with quite a good accuracy enabling to state the model of multiavalanche nature or streamer formation.

For the positive point-to-plane corona a detailed discussion is presented in [A3] in the appendix of the thesis. The main results and discussed problems are only shortly listed here:

- (i) It has been concluded on the basis of measurements that the steady discharge in nitrogen can be considered a typical glow. The problem of feedback mechanism of discharge in nitrogen has been discussed in the same chapter (Ch.4.1 in [A3]) and it has been found out that the photoionisation does not have a significant role.
- (ii) In the case of laser initiating the space charge field occurring near the point electrode before streamer start has been estimated (Ch.4.2 in [A3]). A disc-like approximation has been used in calculations. The results achieved for initiating conditions are in accordance with the general streamer formation criterion: the space charge field strength is close to that of the applied field.
- (iii) The initiation of streamers in the region of steady glow in air has been achieved. Two initiation methods, optical with the laser pulse, and electrical, with supplying additional comparatively small but short voltage pulses to DC voltage, have been reported. The initiation of streamer in the case of steady glow in air has been assumed to be possible due to the formation of spatially localised region of increased ionisation rate (Ch. 4.2 in [A3]).
- (iv) In the case of transverse triggering the measured delay times have been found to be $t_d = \Delta t + t_f$, where Δt is the electron drift time from the place of its release to the border of the ionisation zone, and t_f is the formative time, i.e. the time needed for the accumulation of critical space charge in the ionisation zone. The measured and calculated values of t_d have been presented (Ch.4.3., Figure 6 in [A3]).
- (v) A model of space charge accumulation and calculation of formative time has been presented (Ch.4.4 in [A3]). Corresponding results have been represented in Figures 8 and 9 in [A3].

Nevertheless, in the case of longitudinal axial triggering (published in [A1]) due to the thermal effects we can say nothing about the formation processes of spontaneous corona pulses, the described method enables to get a discharge channel well localised in space and

time. The obtained straight channel make it possible to investigate the processes in the discharge channel.

Open problems

There are several unsolved problems in this field. Some of the most essential are:

- (i) The actual spatial distribution of charge carriers near the point during the space charge accumulation.
- (ii) The mechanism of a streamer formation in the case of steady corona remains still obscure.
- (iii) The mechanism of a non initiated streamer formation and development during the sudden change of current of steady discharge in nitrogen.

Related problems. Ageing

In experiments in nitrogen two striking effects of gas ageing were registered: firstly, the changes in current-voltage curve in the course of time, and secondly, the increase in drift velocity (Ch. 4. in [A3]. Similar drift velocity changes can be found from transient current pulse waveforms registered in [128 - 130], where the attaching properties of water vapours in nitrogen were investigated. Already Loeb and Miller [55 - 56] have assumed that operating discharge liberates gases like O_2 and H_2O from the electrode. Van Brunt has suggested that the conditioning (ageing) effects in the gas may be due to the release of H_2O during the discharge and the nature of the presence of H_2O can significantly affect the nature of negative ions through cluster formation [142]. It has also been confirmed in [131] that the presence of small traces of water vapour in nitrogen leads to the increase in the drift velocity. By these circumstances listed above it was assumed that the ageing was caused in a great deal by the liberation of water vapours from the electrodes and walls of the discharge chamber.

Inserting bakeable silica-gel cell into the discharge gap reduces the observed ageing effects remarkably (Figure 3 in [A3]). This reduction might be affected, of course, by the absorption of other impurities

(pump oil vapour) in the chamber, but taking into account all above cited facts and opinions, the substantial role of water vapours is obvious.

Conclusions

The most important results of the present work are:

1. The methods of initiation of corona by x-ray and by excimer laser pulses were worked out;
2. The streamer initiation by laser radiation was found to be possible 2-3 kilovolts below the onset of spontaneous streamers as well as in the region of steady glow;
3. Using the initiation, the methods for measuring the times of formation of positive corona pulses were worked out;
4. The model of a streamer formation by multiavalanche mechanism was established;
5. The calculations of formative times according to this proposed model are in consistent with experiments;
6. In the case of negative point electrode, the "dielectric switching mechanism" was proposed to be responsible for inception of negative corona.

Acknowledgements

I greatly acknowledge to all my colleagues in Gas Discharge Group for good advises and permanent support me over the years.

My deepest gratitude goes to my long-time supervisor Matti Laan, who introduced me to the gas discharge investigations, and further collaboration with who leads at last to make the dissertation to come true.

I am also indebted to Hans Korge and Mart Aints for valuable discussion that help to interpret the results.

Thanks to Ants Tiirik and Tõnu Asu for their efforts in keeping our laser and all the apparatuses working.

I would like to thank Marika Liivamägi for proof-reading of the manuscript.

Publications

- A1. Laan M, Paris P, Perelygin V 1992 Laser action on corona pulses. *Acta Phys Slov* **42** 91-97
- A2. Laan M and Paris P 1992 Streamer initiation by x-ray pulse *Acta et Comment. Univ. Tartuenssis: Methods of study of electrical processes in gases and aerosols* **950** 14 - 22
- A3. Laan M, Paris P 1994 The multiavalanche nature of streamer formation in inhomogeneous field. *J Phys D: Appl Phys* **27** 1 - 9
- A4 Laan M and Paris P 1992 Formation of corona pulses *9th symp. on elementary processes and chemical reactions in low temperature plasma* (Small Carpathy, Slovakia) Inv. papers 201 -216
- A5 Korge H, Laan M, Paris P 1993 On the formation of the negative corona. *J Phys D: Appl Phys* **26** 231-236
- A6. Laan M, Paris P 1992 Multielectron initiation of a streamer by the laser radiation. *Contr Papers XXI Int Conf ESCAPIG, St Petersburg* 269-270
- A7. Paris P Aints M and Haljaste A 1993 Development of a laser-initiated streamer *21th Int. Conf. on Phenomena in Ionized Gases* (Bochum, Germany) Proceedings II 263 - 264
- A8. Laan M, Paris P, Perelygin V 1991 Propagation of HF discharge along the preionized channel. *XV Int Symp Phys Ion Gases, Dubrovnik*
- A9. Laan M, Paris P, Perelygin V 1990 Laser assisted streamer development. *Contr Papers Int Conf ESCAPIG 90, Orleans* 371-372
- A10. Лаан М, Парис П, Перельгин В 1990 Иницирование импульсов отрицательной короны. *Тезисы Всесоюз конф Газового Разр, Омск I* 190-101
- A11. Куду К, Лаан М, Парис П 1992 Импульс тока отрицательной короны в азоте. *Тезисы Всесоюз конф Газового Разр, Казань* 98-99

References

- 1. Latham R. V., Bayliss K.H. and Cox B.M. 1986 Spatially correlated breakdown events initiated by field electron emission in vacuum and high-pressure SF₆ - *J.Phys. D:Appl Phys.* vol.19, 219-231
- 2. Heylen A.E.D. 1991 Similarities between high electric field emission and consequent breakdown processes in compressed gases and vacuo. - *Gaseous Dielectrics VI, Ed. by L.G. Christophorou and J. Lucas, Plenum Press; New York, 151-158*
- 3. Crichton G C and Williams W T 1983 Influence of electrode radius of curvature on the temporal characteristics of the electron avalanche to corona transition - *XVI Int. Conf. on Phenomena in Ionized gases (Düsseldorf)* 176 - 177

4. Crichton G C, McAllister I W and Brengsbo E 1979 Positive corona onset in atmospheric air - a multiple avalanche process. *XIV Int. Conf. on Phenomena in Ionized gases (Grenoble)* C7 - 287 - C7-288
5. Belasri A, Boeuf J P and Pitchford 1993 Cathode sheath formation in a discharge sustained XeCl laser - *J Appl Phys* **74** (3) 1553 - 1567
6. McAllister I W , Crichton G C, Brengsbo E 1979 Experimental study on the onset of positive corona in atmospheric air. *J Appl Phys* **50** (11) 6797 - 6805
7. Loeb L B 1965 *Electrical Coronas* (Berkeley and Los Angeles: University of California Press)
8. Nasser E 1971 *Fundamentals of gaseous ionization and plasma electronics*. Wiley-Interscience, J Wiley and Sons, N.Y., London, Sydney, Toronto
9. Sigmond R S 1978 Corona discharge *Electrical breakdown of gases* ed J M Meek and J D Griggs (New York: Wiley)
10. Sigmond R S and Goldman M 1982 Corona discharge physics and applications *Electrical breakdown and discharges in gases Part B* ed E E Kunhardt and L H Luessen (New York and London: Plenum Press) 1-64
11. Goldman M and Sigmond R S 1982 Corona and insulation - *IEEE Transactions on Electr. Insulation* **EI-17** 2 90 - 105
12. Miyoshi Y, Hosokawa T 1973 The formation of a positive corona in air. *J Phys D: Appl Phys* **6** 730 - 733
13. Acker F E, Penney G W 1968 Influence of previous positive streamer on streamer propagation and breakdown in a positive point-to-plane gap. *J Appl Phys* **39** 5 2363 - 2368
14. Berger G, Johnson P C , Goldman M 1972 Influence of an electrical discharge on the development of a subsequent discharge in a positive point-to-plane gap *IEEE Int Conf on Gas Discharges* (London) 236 -238
15. Amin M R 1954 Fast time analysis of intermittent point-to-plane corona in air. I The positive burst pulse corona. *J Appl Phys* **25** 2 210-16
16. Amin M R 1954 Fast time analysis of intermittent point-to-plane corona in air. II The positive pre-onset streamer corona. *J Appl Phys* **25** 3 358-363
17. Giao T N, Jordan J B 1968 Modes of corona discharges in air. *IEEE* **5** 1207-12
18. Giao T N, Jordan J B 1968 The positive point plane corona in air and N_2 *IEEE Transaction on Power Apparatus and System* **X**
19. Gallinberti I 1972 A computer model for streamer propagation. *J Phys D: Appl Phys* **5** 2179 - 2189
20. Gallinberti I, Gleijeses B 1978 The field computation in filamentary gas discharges. *Atti Ist veneto sci lett* .. **136** 75- 99
21. Marode E 1975 The mechanism of spark breakdown in air at atmospheric pressure between a positive point and plane. I. Experimental: Nature of the streamer track. *J Appl Phys* **46** 5 2005- 2015
22. Marode E 1975 The mechanism of spark breakdown in air at atmospheric pressure between a positive point and plane. II. Theoretical : .Computer simulation of the streamer track. *J Appl Phys* **46** 5 2016- 2020
23. Pedersen A, McAllister I W, Crichton G C 1984 Formulation of the streamer breakdown criterion and its application to strongly electronegative gases and gas mixtures. *Archiv für Elektrotechnik* **67** 395 - 402
24. Pedersen A 1989 On the electrical breakdown of gaseous dielectris. *IEEE transaction and Electric. Insul.* **24** 5 721 -739
25. Ibrahim A A and Singer H 1982 Calculation of corona discharges in positive point-to-plane gaps *7th Inter Conf Gas discharges and applications* London 128-131
26. Ibrahim A A, Singer H 1984 Investigation of the positive point to plane corona in air *IV Int Symp Gaseous Dielectrics* Knoxville 106-114
27. Dhali S K , Williams P F 1985 2-D numerical simulation of streamers in atmospheric pressure N_2 . *5th IEEE Pulsed Power Conf. Alington Dig Techn Pap* New York 410- 413

28. Dhali S K , Williams P F 1983 Numerical simulation of space-charge -controlled transport. *4th IEEE Pulsed Power Conf Albuquerque Dig Techn Pap* New York 227- 230
29. Dhali S K , Williams P F 1985 Numerical simulation of streamer propagation in nitrogen at atmospheric pressure. *Phys Rev* **31** 2 1219 - 1221
30. Dhali S K , Williams P F 1987 Two-dimensional studies of streamers in gases. *J Appl Phys* **62** (12) 4696 - 4707.
31. Haydon S C 1972 The role of medium energy metastable particles in gas breakdown in nitrogen. *Tokyo Seminar on Gas Breakdown and its Fundamental processes* 33a-35b
32. Hartmann G, Gallimberti I 1975 The influence of metastable molecules on the streamer progression. *J Phys D: Appl Phys* **8** 670 - 680
33. G Hartmann 1982 Theoretical evaluation of the threshold field for a DC positive corona discharge in SF₆ *7th Inter Conf Gas discharges and applications* London 231-235
34. Weissler G L 1942 Positive and negative point-to-plane corona in pure and impure hydrogen, nitrogen, and argon. *Phys Rev* **63** 3-4 96-107
35. Korge H 1992 Investigation of negative point discharge in pure nitrogen at atmospheric pressure. Thesis Tartu 9
36. Korge H Kudu K and Laan M 1979 The discharge in pure nitrogen at atmospheric pressure in point-to-plane discharge gap *3rd Int. Symp. on High Voltage Engineering* (Milan) paper 31.04
37. Raether H. 1964 *Electron avalanches and breakdown in gases* (London: Butterworths)
38. Булашенко О М 1987 Ступенчатая ионизация, как механизм распространения плазменного стримера. *Физ. процессы в приборах электрон. и лазерн. техн.* М 64 - 67
39. McAllister I W, Pedersen A 1983 Paschen's law and the prediction of discharge onset in strongly electronegative gases and gas mixtures. *Proc XVI Int Conf Phenomena in Ionized Gases* Düsseldorf 130-131
40. Marode E, Bastien F, Bakker M 1979 A model of the streamer-induced spark formation based on neutral dynamics. *J Appl Phys* **50** 1 140 - 146
41. Tzeng Y, Kunhardt E E 1983 New insight into streamer development. *4th IEEE Pulsed Power Conf Albuquerque Dig Techn Pap* New York 451 - 452
42. Gilbert A, Bastien F. 1989 Fine structure of streamers. *J Phys D: Appl Phys* **22** 1078 - 1082
43. Даусон Дж Винн У 1968 Модель распространения стримера в кн Петер Г Электронные лавины и пробой в газах Мир
44. Badaloni S, Gallimberti I 1972 Basic data of air discharges
45. Femsler R F 1984 General model of streamer propagation. *Phys Fluids* **27** (4) 1005 - 1012
46. Wright J K 1964 A contribution to the theory of impulse corona and the long sparks. *Proc. Roy. Soc. A* **280** 23 - 26
47. Kondo K , Ikuta N 1980 Highly resolved observation of the primary wave emission in atmospheric positive-streamer corona. *J PhysD: Appl Phys Letter to the editor* **13** L33 - L 38
48. Stritzke P, Sander I , Raether H 1977 Spatial and temporal spectroscopy of a streamer discharge in nitrogen. *J Phys D: Appl Phys* **10** 2285 - 2300
49. Trichel G W 1938 The mechanism of the negative point-to-plane corona near onset. *Phys Rev* **54** 1078-1089
50. Torsethaugen K. and Sigmond R.S. 1972 The Trichel pulse phase of negative coronas in the Trichel pulse regime in air - *Proc. 11th Int. Conf. on Phenomena in Ionized Gases (Prague) Contr. Papers*, 195

51. Sigmond R S 1993 The influence of the external circuit on Trichel pulse coronas. *4th Int Symp High Pressure Low Temp Plasma Chem Bratislava Contrib Papers XV-XX*
52. Loeb L B, Kip A F, Hudson G G, Bennett W H 1941 Pulses in negative point-to-plane corona. *Phys Rev* **60** 714-22
53. Amin M R 1954 Fast time analysis of intermittent point-to-plane corona in air. III The negative point Trichel pulse corona. *J Appl Phys* **25** 5 627-33
54. Moore D B, English W N 1949 Point-to-plane impulse corona. *J Appl Phys* **20** 370-75
55. Miller C G, Loeb L B 1951 Positive coaxial cylindrical corona discharge in pure N_2 , O_2 , and mixtures thereof. *J Appl Phys* **22** 4 494-503
56. Miller C G, Loeb L B 1951 Negative coaxial cylindrical corona discharge in pure N_2 , O_2 , and mixtures thereof. *J Appl Phys* **22** 5 614-21
57. English W N 1948 Positive and negative point-to-plane corona in air. *Phys Rev* **74** 2 170-78
58. Weissler B L 1943 Positive and negative point-to-plane corona in pure and impure hydrogen, nitrogen and argon *Phys Rev* **63** 96 - 107
59. Giao T N, Jordan J B 1968 Modes of corona discharges in air. *IEEE Trans on PAS vol PAS-87* **5** 1207-12
60. Giao T N, Jordan J B 1970 Trichel streamers and their transition into the pulsless glow discharge. *J Appl Phys* **41** 10 3991-99
61. Kondo Y, Miyoshi 1978 Pulsless corona in negative point to plane gap. *Jap J Appl Phys* **17** 4 643-649
62. Torsethaugen K. and Sigmond R.S. 1972 The Trichel pulse phase of negative coronas in the Trichel pulse regime in air - *Proc. 11th Int. Conf. on Phenomena in Ionized Gases (Prague) Contr. Papers*, 195
63. Gardiner P S, Craggs J D 1977 Negative ions in Trichel corona in air. *J Phys D: Appl Phys* **10** 1003-9
64. Александров Г Н 1963 О природе импульсов тока отрицательной короны *ЖТФ* **33** 2 223 - 230
65. Zentner R 1970 Über die Ausstiegszeiten der negativen Koronaentladungsimpulse *Z angew (Math) Physik* **29** 294-301
66. Zentner R 1970 Stufenimpulse der negativen Koronaentladung *Elektrotechn. Z.* **91** 303-5
67. Scott D A, Haddad G N 1987 Negative corona in nitrogen-oxygen mixtures. *J Phys D Appl Phys* **20** 1039-44
68. Scott D A, Haddad G N 1986 Negative point-to-plane corona pulses in oxygen. *J Phys D Appl Phys* **19** 1507-1517
69. Cross J A, Morrow R, Haddad C N 1986 Negative point-plane corona in oxygen. *J Phys D: Appl Phys* **19** 1007 1017
70. Morrow R, Lowke J J 1981 Space charge effects on drift dominated electron and plasma motion. *J Phys D Appl Phys* **14** 2027-34
71. Morrow R 1965 Theory of stepped pulses in negative corona discharges. *Phys Rev A* **32** 6 3821-24
72. Morrow R 1985 Theory of negative corona in oxygen. *Phys Rev A* **32** 3 1799-1809
73. Cernak M, Hosokawa T and Odobina I 1992 Complex form of Trichel pulses in N_2 containing small admixtures of SF_6 . critical test of Morrow's theory. *Proc X Int Conf Gas Discharges and their Applications (Swansea)* 238-240
74. Cernak M, Kaneda T, Hosokawa T 1989 First negative corona pulses in 70% N_2 + 30% SF_6 mixture *Jap J Appl Phys* **28** 10 1989-1996
75. Cernak M, Hosokawa T, Odobina I 1993 Experimental confirmation of positive-streamer-like mechanism for negative corona current pulse rise. *J Phys D: Appl Phys* **26** 607-618

76. Cernak M, Hosokawa T 1988 Initial phase of negative point-to-plane breakdown in N_2 and $N_2 + 10\%CH_4$: verification of Morrow's theory. *Jap J Appl Phys* **27** 6 1005 - 1009
77. Ikuta N, Kondo K 1976 A spectroscopic study of positive and negative coronas in N_2O_2 mixtures *Pros IV Conf on Gas Discharges* 227 - 230
78. Kondo K, Ikuta N 1980 Highly resolved observation of the primary wave emission in atmospheric positive - streamer corona. *J Phys D.: Appl Phys* **13** L33 -38
79. Hosokawa T, Kondo Y, Miyoshi Y 1969 Prebreakdown phenomena of negative point-to-plane air gap. *Electric. Engineer. Jap.* **89** 9 1823 - 1832.
80. Gallimberti I 1987 Breakdown mechanism in electronegative gases *Pros V Int Symp Gaseous Dielectrics (Knoxwill)* 61 - 79
81. Cernak M, Hosokawa T 1987 Similarities between the initial phase of a transient nonuniform glow discharge in the negative corona Trichel pulse formation in an electronegative gas. *Appl Phys Lett* **52**(3) 185-187
82. Latham R V 1988 High-voltage insulation. New horizons. *IEEE Trans. Electr. Insul.* **23** 881-893
83. Latham R V 1981 High voltage vacuum insulation. London New York Toronto Sidney San Fransisco Academic Press
84. Guile A E, Latham R V , Heylen AEP 1988 Similarities between electron emission and consequent breakdown processes in high pressure gases and in vacuum *IEEE Proc.* **133A** 280-283
85. Grey Morgan C 1978 Irradiation and time lags *Electrical breakdown of gases* ed J M Meek and J D Graggs (New York: Wiley)
86. Miyoshi Y, Hosokawa T 1973 The formation of a positive corona in air. *J Phys D:Appl Phys* **6** 730 - 733
87. Verhaart H F A, van der Laan P C T 1982 Fast current measurements for avalanche studies *J Appl Phys* **53** 1430 - 1436
88. Meyerand R G and Haugh A F 1963. Gas breakdown at optical frequencies. *Phys. Rev. Lett* **11** 401
89. Minck R W 1964. Optical frequency electrical discharges in gases *J. Appl. Phys* **35** 252
90. Зельдович ,Райзер Ю П. 1964 О лавинной ионизации газа под действием светового импульса. *ЖЭТФ* **47** 3 (9)
91. Райзер Ю П .1980. Основы современной физики газового разряда. Москва, Наука,
92. Grey Morgan C 1978. Laser induced electrical breakdown in gases (in *Electrical breakdown of gases* , ed. Meek J M and Craggs J D) John Wiley & Sons , Chisester New York-Brisbane-Toronto
93. Rosen D I , Weyl G 1987 Laser-induced breakdown in nitrogen and rare gases at 0.53 and 0.35 μm . *J Phys D: Appl Phys* **20** 1264-1276
94. Dhali S K, Williams P F 1987 Twodimensional studies of streamers in gases. *J Appl Phys* **62** 4696-707
95. Gray Morgan C 1986 Laser produced plasmas. *Proc Nato Adv Study Inst B* **149** 363- 379
96. Gamal Y E E-D, Azzoz I M 1992 On the effect of laser pulse length on the threshold of breakdown of argon. *Proc X Int Conf Gas Discharges and their Applications* (Swansea) 628-631
97. Evans C J, Gamal Yosr E E-D 1980 Laser induced breakdown of helium. *J Phys D: Appl Phys* **13** 1447-58
98. Gamal Y E E-D, Abdel-Moneim N M 1987 Theoretical study of electrical breakdown in nitrogen induced by laser radiation at 1.06 μm . *J Phys D: Appl Phys* **20** 757-61
99. Gamal Y E E-D, Abdel-Moneim H M 1989 Investigation of electrical breakdown of electronegative gases by laser irradiation. *J Phys D: Appl Phys* **23** 851-855

100. Клинов В К, Назаркин А В, Норинский Л В, Рогов В С 1989 О роли квантовых эффектов при пробое газов лазерным излучением. *Квантовая электроника* **16** 10 2127 - 2135
101. Nakamura K, Suzuki T, Yamabe C, Horii K 1992 Fundamental research for laser triggered lightning - laser-triggered spark gap without the irradiation of the surface of electrodes using UV lasers *Proc X Int Conf Gas Discharges and their Applications* Swansea 588-591
102. Frost C A, Woodworth J R, Olsen J N, Green T A 1982 Plasma channel formation with ultraviolet lasers. *Appl Phys Lett* **41**(9)
103. Williams P F 1991 Laser triggering of gas filled spark gaps. *Gaseous dielectrics VI* ed Christophorou L C Plenum Press New York - London 331-338
104. Guenther A H 1983 Recent advances in laser-triggered Switching. *Proc Int Conf Biying- Shanghai* 187-200
105. Guenther A H, Bettis J R 1978 The laser triggering of high-voltage switches. *J Phys D: Appl Phys* **11** 1577-1612
106. Kawada Y, Hosokawa T. 1987 Breakdown mechanism of a laser triggered spark gap in a uniform field gap. *J Appl Phys* **62** (6) 2237-2242
107. Гайдаренко Д В, Леонов А Г, Новопранцев И В 1989 О порогах плазмообразования на поверхности металлов под действием ультрафиолетового лазерного излучения. *Письма в ЖТФ* **15** 3 75 - 79
108. Dougal R A, Williams P F 1986 Fundamental processes in the laser-triggered electrical breakdown of gases: Unconventional geometries. *J Appl Phys* **60** (12) 4240-4247
109. Dougal R A, Williams P F 1984 Fundamental processes in the laser-triggered electrical breakdown of gases. *J Phys D: Appl Phys* **17** 903-918
110. Khan S H, Walsh 1971 Effect of cathode material in a laser triggered spark gap. *J Phys D: Appl Phys* **4** 344 - 347
111. Bradley L P 1972 Preionization control of streamer propagation. *J Appl Phys* **43** 3 886 - 890
112. Александров Г Н, Иванов В Л, Кадзюв Г Д, Парфенов В А, Пахомов Л Н, Петрунькин В Ю, Подлевский В А, Селезнев Ю Г 1977 Исследование влияния высокоионизированного канала, создаваемого мощным ОКГ, на развитие разряда в длинном воздушном промежутке *Журнал технической физики* **47** 10. 2122 - 2124
113. Акманов А Г, Ривлин Л А, Шильдяев В С 1968 Оптически инициируемый направленный электрический пробой в газе. *Письма в ЖЭТФ* **8** 8
114. Норинский Л В 1971 Иницирование направленного электрического пробоя в газе излучением третьей гармоники неодимового лазера. *Квантовая электроника* **5**
115. Greig J R, Femsler R F, Murphy D P, Pechacek R E, Perin J and Raleigh M 1982 Laser guided electric discharges in the atmosphere *Proc VII Int Conf Gas Discharges* London 464-468
116. Kawada Y, Hosokawa T 1987 Breakdown mechanism of a laser triggered spark gap in a uniform field gap *J Appl Phys* **62** (6) 2237 - 2242
117. Sato S, Kobayashi Y, Yasojima Y, Murai Y 1988 Soft X-ray radiation from laser plasma (abstract). *Rev. Sci. Instrum.* **59** 8 1850
118. Friedorowicz H, Bamik A, Parys P, Patron Z and Pisarczyk T 1993 High intensity laser interaction with gas puff targets *Inter Conf Phenomena in Ionized Gases Bochum III Invited and additional papers* 132-140 XXI
119. Brcka J, Kreuty E V, Voss A 1992 Ionic properties in plasma generated by XeCl laser ablation process. *Electrotechn Cas* **43** 4 118-121
120. Арутюнян Р В, Баранов В Ю, Большов Л А, ..1987 Динамика плазмы образованной при воздействии излучений XeCl лазера на

металлическую поверхность . М ЦНИИ атоминформ Препринт ИАЭ - 4443/7 12

121. Vogel N, Höft H 1989 Cathode spot Energy Transfer simulated by a focused laser beam. *IEEE Transaction on plasma science* 17 5
122. Levatter J I, Sandstrom R L, Morris J H 1983 The corona-plasma cathode: a new long-life e-beam cathode. *IEEE Pulsed Power Conf Albuquerque*, Dig Techn Pap. N.Y 755-757
123. Асу Т, Лаан М, Ейрикс А 1988 Характеристики эксимерного лазера с длительности импульса 100 нс. *Учен. зап. Тарт. ун-та* 824 43-51
124. Soulem N, Pignolet P, Peyrous R, Held B, Loiseau J F 1992 Laser investigation of positive point-to-plane corona discharge in ambient air. *Proc X Int Conf Gas Discharges and their Applications* Swansea 286-289
125. Crichton G C, Williams W T 1983 Influence of electrode curvature on the temporal characteristics of the electron avalanche to corona transition. *Proc Int Conf Phenomena in Ionized Gases (Düsseldorf)* 176-177
126. Омаров О А, Рухадзе А А 1980 О проявлении плазменной стадии развития лавины при искровом пробое газов. *Журн. техн. физ.* 50 3 536 - 539
127. Gosho Y, Saeki M 1987 Triggering of DC positive corona by pulsed UV radiation. *J Phys D: Appl Phys* 20 526 - 529
128. Wang W C, Lee L C 1987 Photodetachment cross section of negative halogen ions in discharge media. *J Phys D: Appl Phys* 21 675-682
129. Wang W C, Lee L C 1985 Electron attachment to H₂O in Ar N₂, and CH₄ in electric field. *J Appl Phys* 57 (9) 4360 - 4367
130. Wang W C, Lee L C 1985 Shortening of electron conduction pulses by electron attachers. *5th IEEE Pulsed Power Conf Alington* Dig Techn Pap N.Y. 37-39
131. Gosho Y, Harada A 1983 A new technique for measuring negative ions mobilities at atmospheric pressure. *J Phys D: Appl Phys* 16 1159 - 1166
132. Brown S 1959 Basic data on plasma physics
133. Wetzer J M, Wen L 1991 Different avalanche types in electronegative gases. *J. Phys. D: Appl. Phys.* 24 1964 - 1973
134. Loeb L B 1965 *Electrical Coronas* (Berkeley and Los Angeles: University of California Press)
135. Dutton J 1978 Spark breakdown in uniform fields *Electrical breakdown of gases* ed J M Meek and J D Graggs (New York: Wiley)
136. Blair D T A 1978 Breakdown voltage characteristics *Electrical breakdown of gases* ed J M Meek and J D Graggs (New York: Wiley)
137. Chatterton P A 1978 Vacuum breakdown *Electrical breakdown of gases* ed J M Meek and J D Graggs (New York: Wiley)
138. Laan M. and Perelygin V. 1991 The dependence of negative corona on electrode surface properties - *Proc. 20th Int. Conf. on Phenomena in Ionized Gases (Pisa)* Vol. 4, 929-930
139. Guile A.E. and Hitchcock A.H. 1975 Oxide films on arc cathode and their emission and erosion - *J. Phys. D: Appl. Phys.* Vol. 8, 663-669
140. Kennedy J T, Wetzter J M, van der Laan P C T 1992 Experimental study of space charge effects in avalanches in atmospheric nitrogen. *10th Int. Conf on Gas Discharges and their Applications* (Swansea) 1 516-519
141. Hadidi K. and Goldman A. 1991 Current stability of negative corona discharges in SF₆ and delayed spark breakdown - *Gaseous Dielectrics VI* Plenum Press, New York and London, 399-405
142. Van Brunt R J 1982 Effects of H₂O on the behavior of SF₆ corona *Proc VII Int Conf Gas Discharges and their Applications II (London)* 255 - 258
143. Kondo K 1990 Characterisation of x-rays emitted from 351 nm laser produced plasmas for x-ray shadowgraphy. *J Appl Phys* 67 6 2693 - 2699

Koroonalahenduse initseerimine

Peeter Paris

Kokkuvõte

Käesolevas töös uuriti gaaslahenduse initseerimise võimalusi ja lahenduse formeerumise protsesse atmosfäärirõhu lähedastel rõhkudel mittehomogeenses väljas teravik-plaat lahendusvahemikus.

Töö eesmärgiks oli nii negatiivselt kui ka positiivselt pingestatud teraviku korral sobivate initseerimismeetodite leidmine ja lahenduse formeerumisaegsde mõõtmine ning mõõtmistulemuste põhjal koroonla formeerumismehhanismide täpsustamine.

Formeerumisaegade mõõtmine on kõrgrõhulise gaaslahenduse korral praktiliselt ainus otsene informatsiooni saamise meetod nendest protsessidest, mis toimuvad gaasis algelektroni(de) tekkehetkest kuni detekteeritava voolu või valguse tekkimiseni.

Formeerimisaegade mõõtmine nõuab mittehomogeenses välja korral adekvaatset initseerimist, s.t., et algelektronid tuleb tekitada ajas ja ruumis hästi kontrollitult ja lokaliseeritult (vastavalt nanosekundilise ja kümnendikmillimeetrilise täpsusega).

Töö tulemusena:

1. Töötati välja koroonla initseerimise viisid ja meetodid röntgenkiirguse ja eksimerlaseri välke abil. Laseriga initseerimisel oli initseeritavate koroonaimpulsside väärin (jitter) initseeriva laservälke suhtes väiksem kui 2 nanosekundit.
2. Positiivselt pingestatud teraviku korral leiti eksperimentaalselt, et striimereid on võimalik initseerida nii pingetel allpool spontaanste striimerite läve (kasutatud laservälke energiatega kuni paar kilovolti allpool läve), kui ka pideva koroonla esinemise piirkonnas. Nimetatud eksperimentaalse tulemuse põhjal oletati, et neis pingetes piirkondades on striimereid võimalik esile kutsuda suure arvu algelektronide tekitamisega lahendusvahemikus. Töös põhjendati

seda striimeri formeerumise paljulaviinse iseloomuga mittehomogeensete väljade korral. Erinevate laviinide kattumisel toimub teraviku lähedal positiivse ruumlaengu akumulatsioon, mis peale seda kui ruumlaengu tihedus ruumiliselt lokaliseeritud piirkonnas on ületanud kriitilise väärtuse, kutsub esile striimeri tekke.

3. Kasutades leitud initseerimisviise töötati välja meetod lahenduse formeerumisaegade mõõtmiseks. See on esimene teadaolev formeerumisaegade mõõtmine antud tingimustes.
4. Töös leiti positiivse koroona korral kvantitatiivne mudel, mille põhjal arvutatud formeerumisajad on kooskõlas eksperimendiga.
5. Püstitati hüpotees, et negatiivselt pingestatud teraviku korral on lahendust käivitavaks mehhanismiks teravikelektroodi pinnal oleva dielektrikukile (oksiidikile) läbilöök ("dielectric switching mechanism), mille tulemusena lahendusvahemikku emiteeritav elektronide purse käivitab lahenduse. Edasisel lahenduse arengul on alalhoidvaks sekundaarmehhanismiks teraviku pinna ioonpommitamine.

Oletati, et negatiivse koroona formeerumine toimub analoogselt läbilöögi formeerumisele vaakumis ning et puudub põhimõtteline erinevus atmosfäärirõhul koroonalahendust käivitavate protsesside ja homogeense välja läbilöögieelsete protsesside vahel.

6. Täiendava eksperimentaalse tulemusena saadi teljesuunalisel laseriga initseerimisel nii ruumis kui ka ajas hästi lokaliseeritud mööda sirget leviv striimer. See avab võimalused uurida striimeri kanalis toimuvaid protsesse piisava ajalise ja ruumilise lahutusega.

LASER ACTION ON CORONA PULSES¹⁾

LAAN, M.,²⁾ PARIS, P.,²⁾ PERELYGIN, V.,²⁾ Tartu

The influence of UV laser radiation on the formation and development of corona pulses were investigated. In the case of a positive point a nonbranched streamer was obtained which had good reproducibility in time and space. In the case of a negative point the formation of discharge pulses below the onset potential is explained by thermoionic emission, at higher voltages electron explosive emission is supposed to be active in pulse formation.

I. INTRODUCTION

Corona pulses have several interesting applications in plasma chemistry. However, many details of their nature have not been elucidated so far. The aim of our study was to investigate the corona pulse formation and development under the influence of UV laser radiation.

II. EXPERIMENTAL SET-UP

Corona pulses were investigated in a point-to-plane discharge gap (Fig. 1). The distance between the electrodes was 40 mm. The point electrode was a hemispherically capped platinum wire 1.2 mm in diameter. A plane electrode 150 mm in diameter was made from stainless steel grid. The discharge chamber was evacuated to residual pressure of 5×10^{-6} Torr and then filled with pure nitrogen up to the atmospheric pressure. Radiation from the UV pulse excimer laser ($h\nu = 4\text{eV}$, pulse energy $\leq 30\text{ mJ}$, pulse duration $\approx 60\text{ ns}$, repetition rate 5 p.p.s., the laser pulse shape is presented in Fig. 3) was directed along the discharge gap axis and focused by help of the lense ($F=180\text{ mm}$) at the distance of $\approx 5\text{ mm}$ from the point. Maximum mean intensity (Fig. 3) of laser radiation was $I_0 \approx 5 \times 10^7\text{ W/cm}^2$. Radiation intensity was changed by calibrated grids. The plane electrode was grounded over the resistor $R = 50\Omega$. Light emitted by the discharge was detected using a movable slit 1 mm height, a monochromator M and a fast photomultiplier PM.

1) Contribution presented at the 8th Symposium on Elementary Processes and Chemical Reactions in Low Temperature Plasma, STARÁ LESNÁ, May 28-June 1, 1990

2) Tartu University, TARTU, Estonia

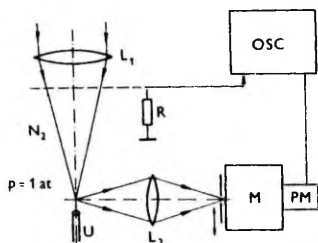


Fig. 1. Experimental set-up. osc - Oscilloscope, M - monochromator, PM - photomultiplier.



Fig. 2. Streamers fixed by image intensifier. a - spontaneous streamer, b - laser assisted streamer.

III. POSITIVE POINT

Experimental results

If there was no laser radiation, streamers were detected when the voltage exceeded $U_0 = 11.4\text{kV}$ (Fig. 2a) and at $U = 11.8\text{kV}$ a steady-state corona was established. All discharge characteristics were very similar to those found in [1]. As it was recorded at low voltage ($U = 0.3\text{kV}$) $\sim 10^7$ electrons were created along the gap axis by laser radiation. If $I = I_0$, then starting from $U = 9\text{kV}$ a nonbranched

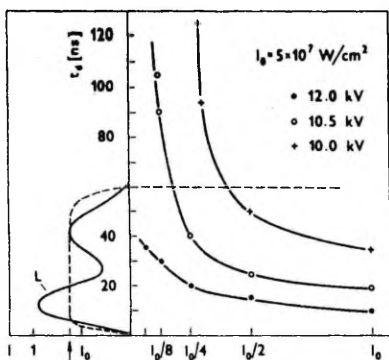


Fig. 3. Delay time t_d dependence on laser intensity for different voltages; L - laser pulse.

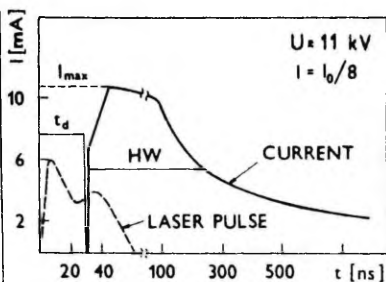


Fig. 4. A typical current pulse.

streamer (Fig. 2b) developed along the laser beam path and at $U = 10.5$ kV a streamer channel bridged the gap. Laser assisted streamer parameters were very stable in time and space. Delay time t_d depended both on voltage and intensity of laser radiation (Fig. 3) and had a jitter < 2 ns for $t_d < 60$ ns. The half-width (HW) of a single streamer trace on the photo was ≈ 0.1 mm and the HW of 600 overlapped streamer traces was 0.3 mm. Near the onset potential U_0 nonaxial branches started near the point and with the decrease of radiation intensity the axial branch became fainter and its length diminished. If $I = I_0/16$, the structure of the streamer resembled that of a spontaneous streamer. Current pulse amplitude i_{max} (Fig. 4) increased from 4 mA ($U = 9$ kV) to 20 mA ($U = 12$ kV). The current pulse duration exceeded 4 μ s and HW of a current pulse at the same voltage did not depend on the intensity of laser radiation I . The duration of the light pulse ($\lambda = 337$ nm) emitted from the channel part 1 mm in length was < 15 ns. The propagation velocity of the channel was determined. It depended strongly on the presence of laser radiation. At higher I , the velocity had the value of up to 8×10^6 cm/s. After the termination of the laser pulse the velocity diminished quickly to the value of 3×10^6 cm/s for all voltages used in the experiment.

Discussion

According to experimental results the following qualitative explanation of the laser-assisted streamer formation and development may be proposed. Near the laser beam focus primary electrons are generated. They move towards the point electrode in the DC field which is superimposed by a weak laser field. The electrons absorb energy from the laser field by induced free-free transition. This process

influences mainly the tail of the electron distribution function, which causes the increase of the ionization rate [2]. It makes the streamer formation possible at voltages below the onset potential. After that the streamer develops along the weakly preionized (and/or excited) path created by the laser beam. The streamer velocity increase in the laser field can be explained by the radiation influence on the distribution function as well. Such a laser-assisted streamer is a convenient object for further theoretical investigation.

IV. NEGATIVE POINT

Experimental results

It is known [3] that under pure conditions in nitrogen there are two different steady state modes of a point-to-plane discharge. Transition from one state to another occurs with the appearance of the current and light pulses similar to those in the case of a Trichel pulse in air. Our conditions were not pure enough and for that reason the discharge near the onset potential existed in a pulsed form. The onset potential of spontaneous Trichel pulses was 9.2 kV. The current pulse achieved its maximum value of 5 mA after 5 ns, it was followed by a slow decay and after 1.5 μ s a quasistationary value of 0.2 mA was established ("tail" of the pulse). After the filling of the discharge chamber with pure gas the tail lasted longer than after some days of work (Fig. 5). When the discharge chamber was refilled, the previous pulse duration was achieved. If the laser radiation was directed into the discharge gap, current pulses were recorded already at $U = 2$ kV. Charge $q = \int i dt$ created per pulse as a function of voltage is presented in Fig. 6 ($I_0 = 3 \times 10^7 \text{ W/cm}^2$). If $U < 7$ kV, q strongly depended on the laser pulse intensity, the duration and the shape of the current pulse corresponded to the shape of the laser pulse.

Typical schematic current pulses for $U > 7$ kV are presented in Fig. 7. The amplitude value i_{max} of the sharp peak at the beginning of the current pulse as well as its shape were correlated with the laser pulse intensity and its "fine" structure. For $t > 60$ ns the current pulse time dependence did not differ from the shape of the spontaneous pulse. If $I \sim 10^7 \text{ W/cm}^2$, the current pulse had a delay time of $t_d \approx 5$ ns from the beginning of the laser pulse. If $I \sim 10^6 \text{ W/cm}^2$ and $U = 8.3$ kV, $t_d = 90$ ns. The laser radiation energy concentration was high enough to cause thermoionic emission from the point. Thus if we suppose that i_{max} was determined by the surface temperature T ($T \sim I$) and the field strength E ($U \sim E$), $\ln(i_{max})$ must be a linear function of \sqrt{U} [4]. As we can see in Fig. 8 the assumption of a thermoionic nature of the electron emission explains the results recorded in the experiment quite well. The main conclusions are :

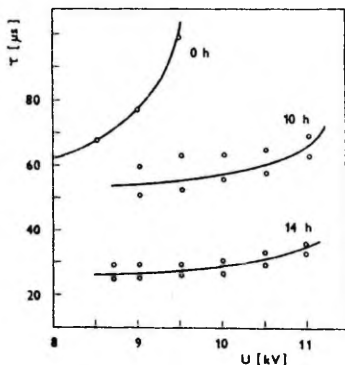


Fig. 5. Trichel pulse duration as a function of voltage for different conditions.

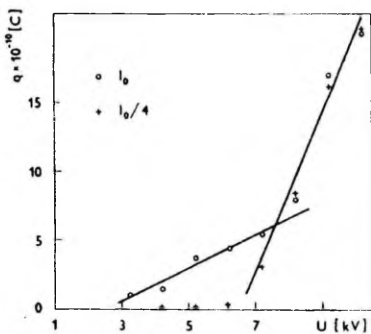


Fig. 6. Charge per pulse ($q = \int idt$) as a function of voltage for different intensities I .

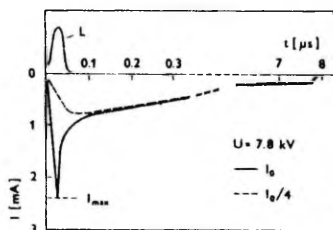


Fig. 7. Schematic representation of current pulses.

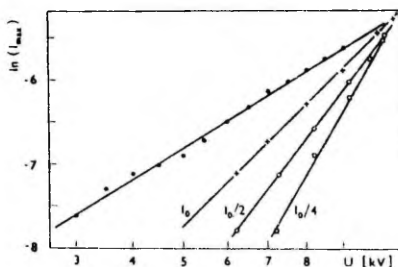


Fig. 8. Logarithm of the i_{max} as a function of \sqrt{U} for different intensities I .

1. The magnitude of the first peak of the current pulse is the function of E and T .
2. It is possible to create typical Trichel pulses on voltages remarkably lower than the onset of a spontaneous one. Consequently the formation of a Trichel pulse is not determined only by ionization processes in the gas.
3. The role of the laser radiation diminishes with the voltage increase, near the spontaneous pulse onset the dependence of i_{max} on the radiation intensity (surface temperature) is weak.

4. The current pulse tail duration has a strong dependence on impurities.

V. DISCUSSION

Usually the formation of the Trichel pulse is explained by the gas ionization by electrons accelerated in the electric field. This model was used in Morrow's theory [5]. The existence of a step in the leading part of the current pulse was explained by a different influence of the γ_p and the γ_i mechanism [6]: at the beginning of the pulse γ_p is active, in the later stages it is replaced by a more effective γ_i mechanism. As a result of our measurements another explanation of the pulse formation is available. In [7] it is mentioned that field emission can play a role in pulse formation. Field emission is effective from the micropoints (or dielectric films) on the electrode surface [4]. As a result Joule heating of these irregularities and their explosion take place. Such a process is an effective source of electrons. We suppose that the step in the leading part of the current pulse as well as the "precursor" before the pulse [8] are due to explosive emission. Below the onset potential an additional source for electrode heating is needed (in our case - laser radiation).

The fact that for $t > 60$ ns the shapes of the Trichel pulses below and above the onset potential are the same indicates that ionization mechanisms in these stages do not differ. Recently the results of spectroscopical measurements of the Trichel pulses have been presented [9,10]: the ionization mechanism by the electron impact with the N_2 ground state is active only in the first ten nanoseconds, when the field strength near the point electrode is high enough, later ionization by means of the metastable A -state takes place. Consequently, the duration of the current tail is connected with the concentration of the A -state metastables. If the discharge occurs, a small amount of admixtures is released from the electrode surface. A possible maximum concentration of impurities is too low to stop the Trichel pulse by quenching the metastables. More realistic is an assumption that these admixtures (as it is shown in [11]), which have a lower ionization potential than N_2 , modify the electron distribution function and as a result the rate coefficient of the A -state excitation diminishes: with an increasing admixture concentration the tail duration of the current pulse diminishes.

REFERENCES

- [1] Korge, H., Kudu, K., Laan, M.: *3rd ISHVE*, paper 31.04, 1979.
- [2] Popov, A. M., et al, *Thermophys. High Temperatures USSR*, vol. 27 (1989), 173.
- [3] Korge, H., Laan, M., Susi, J., *Acts Comment. Univ. Tartuensis*, no. 824 (1988), 25. (in Russian).

- [4] Korolev, Yu. D., Mesysts, G. A., in *Field emission and explosive processes in gas discharge*. Novosibirsk 1982 (in Russian).
- [5] Morrow, R., *Phys. Rev. A32* (1985), 1799.
- [6] Morrow R., *Phys. Rev. A32* (1985), 3821.
- [7] Černák, M., *Proc. 17 th ICPIG*, Contr.papers (1985), 573.
- [8] Černák, M., Kaneda, T., and Hosakava, T., *Jap. Appl. Phys.* 28 (1989), 1989.
- [9] Korge, H., Laan, M., Susi, J., *9 th ESCAPIG*, Cont. papers (1988), 115.
- [10] Korge, H., Kuusk, U., Laan, M., Susi, J., *Plasma Phys. USSR*, 17 (1991), 473.
- [11] Apollonov, V., et al. *Lett. Techn. Phys. USSR*, 13 (1987), 1363.

Received October 18th, 1990

Accepted for Publication January 4th, 1991

ВЛИЯНИЕ ЛАЗЕРНОГО ИЗЛУЧЕНИЯ НА КОРОННЫЕ ИМПУЛЬСЫ

Исследовано влияние УФ лазерного излучения на коронные импульсы. В случае положительного острья получен одноканальный стример, который имел хорошую повторяемость как в пространстве так и во времени. В случае отрицательного острья формирование импульса при подпороговых напряжениях объяснимо термомиссией, при более высоких напряжениях – взрывной эмиссией.

STREAMER INITIATION BY X-RAY PULSE

M. Laan, P. Paris

For the experimental investigation of a streamer formation the experimental equipment must be well synchronized with the moment of creation of triggering electrons. A good synchronization (which has a nanosecond jitter) in homogeneous field is achieved by liberating the first electrons from the cathode with a short UV pulse. It is impossible to use this method in a positive point-to-plane discharge gap, as the first electrons must be created in a small volume near the positive point. In [1] a streamer was initiated by $XeCl$ laser ($\lambda = 308$ nm) pulse. Although a good synchronization was achieved, additional difficulties arose in further interpretation since the laser radiation caused a remarkable vaporization of point electrode material.

The aim of this paper is to investigate the streamer formation using the X-ray radiation as a source of first electrons.

Experimental set-up. All the experiments were carried out in laboratory air at atmospheric pressure. Positive D.C. corona in a point-to plane discharge gap was investigated. Distance between the electrodes was 4 cm. The point electrode was a hemispherically capped Pt wire 1 mm in diameter. Plane electrode was a Al disc, 15 cm in diameter, with 4 mm hole in its center, that makes it possible to direct X-ray radiation along the discharge gap axis.

The X-ray source had a plasma cathode described in [2]. The anode was placed at 4 cm from the cathode. The working pressure was 0.1 Pa. The X-ray tube had a lavsan window. 30 kV negative pulse, half-width of which was 110 ns, was supplied to the cathode. X-ray pulse had a half-width of 70 ns (Fig. 2). The position of X-ray pulse related to the voltage pulse was determined with accuracy of some nanoseconds. 10 pps repetition rate of X-ray pulses was used. In absorption measurements for X-ray quantum energy determination two different detector systems were used: scintillator + photomultiplier and ionization chamber + electrometer. The mean quantum energy was within limits of 5-8 keV. An X-ray pulse originated nearly 10^7 charged particles per cm^3 as

determined by ionization chamber.

Light and current pulses were recorded by a 450 MHz bandwidth oscilloscope. For registration of current pulses a 50 Ω coaxial design of the point electrode connection was used [3]. Light from corona was detected by image intensifier and photomultiplier. Time intervals between the X-ray pulse and corresponding corona pulse were registered by the digital timer with a resolution of 10 ns.

Results. Both spontaneous (noninitiated) and initiated positive corona pulses were under observation. In case of positive corona the first observable discharge pulse is a burst pulse which spreads along the electrode surface. With increase in voltage a so-called preonset streamer develops into the discharge gap up to the distance of 10 mm from the point. The voltage region where these streamers exist is about 200 V. The steady state corona will be established at higher voltages [4]. In our case when the X-ray radiation is missing, burst pulses are registered \approx 200 V below the onset potential U_0 of preonset streamers. With increase in voltage their amplitude and duration, as well as their repetition rate also rise. Some tens volts below U_0 the burst pulse current has the duration up to 1 μ s and its amplitude achieves 0.1 mA. Corresponding light pulse is considerably shorter (\approx 70 ns) - Fig. 1A. Area covered by the luminous layer on the point electrode is nearly 0.2 mm². At the potential U_0 , some larger bursts transit to streamer - Fig. 1B. As no attention was paid to the air humidity and the air pressure stabilization, there are variations of ± 20 V of U_0 in different days. The burst-to-streamer transition is observable only in the narrow region of voltages: at the onset U_0 the duration of the burst pulse stage of $\tau = 15 - 20$ ns and 50 V above U_0 , the burst stage is already not observable.

When the X-ray pulse generator is switched on, the initiation of bursts occurs \approx 400 V below U_0 . The current amplitude of these burst pulses about of 100 V below U_0 is eight-fold, compared with the current of spontaneous ones at the same voltage. Area covered by the light of initiated burst is nearly 1 mm². In case of initiation the burst-to-streamer transition occurs at 80 V below U_0 , corresponding $\tau = 30$ ns, at 10 V higher potential $\tau = 20$ ns and 20 V higher - $\tau = 10$ ns. Near U_0 one X-ray pulse initiates more than one

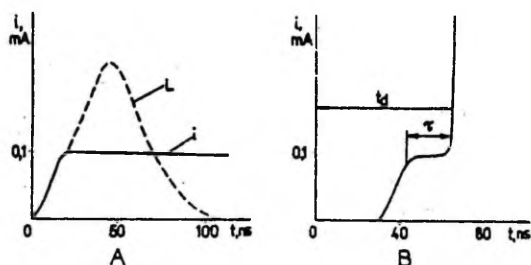


Fig.1. Sketches of burst pulse (A) and burst-to-steamer transition (B). Solid line presents the time dependence of burst pulse current, dashed line - the same dependence of light B - t_d - time interval between the beginning of the X-ray pulse and the streamer formation, τ - duration of the burst stage. Transition occurs at $U_0 = 7.82$ kV.

streamer. The first one is quite well related to the X-ray pulse, the next one follows randomly with the delay time of 1 ms and more. At voltages above U_0 exist both initiated and spontaneous streamers. In Fig. 2 delay time distribution of the first initiated streamer for different voltages and mean E_d dependence on voltage are presented; in Fig. 3 - t_d and E_d dependencies on X-ray intensity are presented.

Discussion. It is accepted that in a homogeneous field the formation of a streamer is possible when a number of charged carriers achieve the value of 10^8 in an avalanche [5]. The existence of such a mystic number demands further explanation especially in the case of inhomogeneous point-to-plane geometry where near the onset potential U_0 the magnitude of a single avalanche is several orders less than 10^8 [4].

For that reason another formulation seems to be more preferable: streamer formation occurs at the moment when the ionized gas achieves a plasma density i.e. the Debye length r_D becomes less than the characteristic dimension of ionized gas region d [6,7]. In our case it means that burst-to-streamer transition is possible when the ionized gas density in a thin layer near the point surface achieves the

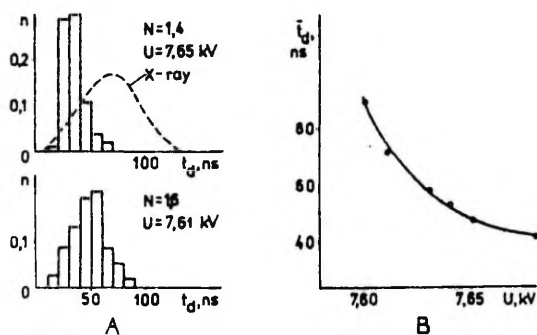


Fig. 2. Delay time t_d dependence on voltage.
 A : n - relative number of first streamers which have delay time t_d ; N - mean number of streamers created by a single X-ray pulse. Onset potential $U_0 = 7.82$ kV. Dashed line - shape of the X-ray pulse.
 B : Mean delay time \bar{t}_d dependence on voltage.

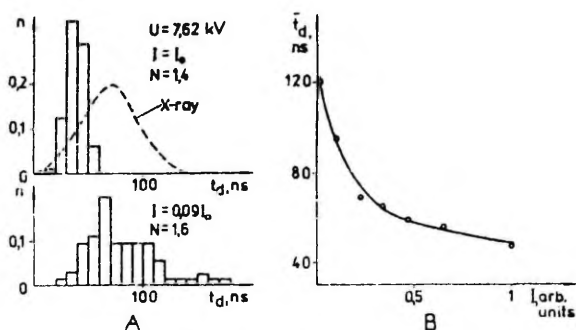


Fig. 3. A : Distribution of delay time t_d for different X-ray intensities. B : Mean delay time \bar{t}_d dependence on X-ray intensity; intensity I_0 corresponds to the charged particles concentration 10^7 cm $^{-3}$ per X-ray pulse. In all cases the jitter of τ is much smaller than that of $(t_d - \tau)$.

plasma density.

To prove the validity of this assumption the electron density in burst pulse must be estimated. Using experimental data for burst current $i = 0.1$ mA and for area covered by burst $S \approx 0.2$ mm², and supposing that drift velocity of electrons $v \approx 2 \cdot 10^7$ cm/s ^{*)}, from relation $i/S = nev$ the electron concentration $n = 10^{10}$ cm⁻³ is determined. The same order of magnitude was valued for n in avalanche head when streamer formation takes place in homogeneous field [6]. Corresponding value of Debye length r_D for electron temperature $T_e < 5$ eV is less than 10^{-2} cm. The plasma layer thickness can be estimated from the results of [8] where the light distribution for steady state corona was determined. The main part of light was emitted from the layer which thickness < 0.2 mm. The thickness of the region where the main part of charged particles is situated must be close to this value. So the assumption that burst pulse creates a plasma layer near the electrode surface is quite realistic, and all effects characteristic to plasma must occur: electrons are locked to the ions (due to ambipolar diffusion), the field strength in plasma body is low and enhancement of field strength near the cathode side border of plasma takes place (due to separation of positive and negative space charge to the distance of Debye length). A nice presentation of all these effects is given in [9].

The sketches of the burst pulse formation for $U \approx U_0$ are presented in Fig. 4. To trigger the ionization the first electron must appear near the border of ionizing zone (where $\alpha - \eta = 0$; α , η - first Townsend coefficient and attachment coefficient, respectively). An avalanche starting from this electron radiates photons able to ionize gas. If such a photon is absorbed near the border of ionizing zone, it creates a new equivalent avalanche (Fig. 4A), i.e. the role of feedback in this sequence of avalanches is played by photoionization. The site in space where a photon is absorbed is accidental, so the sequence of avalanches will

*) This value of v corresponds to reduced field strength $E/p = 60$ V/cm·Torr. In plasma such a high field can exist only for a short time.

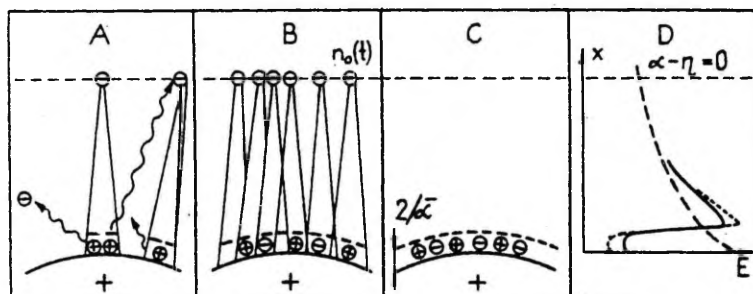


Fig. 4. Different stages of burst pulse development.

A - development of first avalanches; B - stage of overlapping avalanches, $n_0(t)$ - density of electrons created by an X-ray pulse; C - plasma layer; D - sketch of distribution. $\bar{\alpha}$ - mean value of α ; dashed line initial field; solid line - burst pulse stage; dotted line - steady state corona.

spread over the electrode surface. The main part of charges are created in a layer of $2/\bar{\alpha}$ thickness. ($\bar{\alpha}$ - mean value of α in ionizing zone). As a drift velocity of ions is low, the accumulation of positive space charge occurs in this layer. At atmospheric pressure and for the used point radius, an extended layer of space charge causes the diminishing of the field [10]. Whereas the concentration of triggering electrons n_0 near the border of ionizing zone increases then, starting from a moment governed by chance avalanches will overlap (Fig. 4B). It causes further diminishing of the field. By that reason the loss of electrons in the layer due to drift to the anode decreases. This stage of discharge is already observable in experiments and it is named as a burst pulse.

In the case of X-ray preionization triggering, electrons are created homogeneously near the point, and several parallel avalanches will develop towards anode and their concentration n_0 rises linearly in time. If the X-ray intensity is high, the stage a is absent and t_d varies within narrow limits (Fig. 3). 10-fold decrease of intensity leads to the increase of jitter t_d , the density of n_0 is too low for overlapping of avalanches and the conditions of ionization are similar to a single electron initiation. The last stage

(burst pulse stage) in plasma formation is presented in Fig. 4C. When a plasma density of ionized gas is achieved, the field distribution completely differs from the Laplacian field (Fig. 4D). The light emitted by burst pulse belongs to the 2^* system of nitrogen. The excitation of 2^* system by electron impact is possible only in the high field. Since the plasma concentration is $\approx 10^{10} \text{ cm}^{-3}$, the high field can exist only few tens of nanoseconds, later the excitation is not effective. This estimation corresponds well to the experiment (Fig. 1A). Plasma layer can exist near the anode for a long time. There are two loss mechanisms of electrons in plasma body: attachment and leakage to the anode. So the formation of negative ions is a result (not reason!) of existence of the low field strength near the point electrode. Burst pulse exists up to the moment when these losses are compensated by ionization in high field region on the cathode side of plasma layer. This explanation differs from Loeb's one [4]: he supposed that long duration of burst pulse current is connected with the ion component of current, and the duration of light pulse corresponds to the duration of time when electrons exist near the point. But as the mobility of ions is two orders less than that of electrons, there must be a peak at the beginning of current pulse which reflects electron movement. It was never observed in experiments.

At higher voltages ($U \geq (U_0 + 200)\text{V}$) there is an equilibrium between the loss and generation of electrons and steady state corona establishes.

Only the existence of plasma is not sufficient for streamer formation. A streamer can start from a site of plasma layer where the local ionization instability develops. There are the next experimental confirmation to this assumption:

- (I) If $U > U_0$, both burst-pulses and streamer exist.
- (II) Streamers can be suppressed by α -particles. An α -particle creates a big number of triggering electrons so the plasma layer is more homogeneous than it is in the case of single electron initiation, and the probability that instability may develop is lower.
- (III) The initiation of streamer is possible at the voltage region of steady state corona if ionization instability is created artificially. It was done this way in our old unpublished paper [11] where to D.C. voltage $U = 8 - 15 \text{ kV}$ a short (100 ns) pulse voltage ($U > 500 \text{ V}$) was added and a

streamer development was fixed.

(IV) In this paper burst-to-streamer transition occurs only for $\tau < 30$ ns (Fig. 2B), i.e. only when the field strength in plasma is high and so the probability that ionization instability may develop is high too.

R e f e r e n c e s

1. Laan, M., Paris, P. Perelygin, V. Laser-assisted streamer development // Abstracts of invited talks and contr. papers-ESCAHPIG 90 - Orleans - 1990. - P. 371-372.

2. Levatter, J.S., Sandstrom, R.L., Morris, J.K. The corona-plasma cathode: a new long-life e-beams cathode for X-ray preionization // 4 IEEE Pulsed power Conf.(Albuquerque, N.M., 1983).- Dig. techn. Pap.- N.Y. - 1983. - P. 755-757.

3. Korge, H., Laan, M., Paris, P. On formation of negative corona pulse // J. Phys. D: Appl. Phys. - in print.

4. Loeb, L.B. Electrical coronas.- Berkeley; Los Angeles: Univ. of Calif. Press - 1965. - 694 p.

5. Raether, H. Electron avalanches and breakdown in gases - London. - 1964.

6. Omarov, O.A., Ruchadze, A.A., Schneerson, G.A. On plasma mechanism of high pressure gas breakdown in high electric field // Sov. J. Techn. Phys. - 1979. - V. 49.- P. 1997-2000 (in Russian).

7. Omarov, O.A., Ruchadze, A.A. Evidence of plasma stage of avalanche development in case of spark breakdown // Sov. J. Techn. Phys.- 1980. - V. 50. - P. 538-539 (in Russian).

8. Charrier, J., Boulloud, A. Positive Glow Corona Distribution of Light Emission in Point-to-Plane Gap // 8th. Int. Conf. Gas Discharges - Oxford, 1985.- P. 185-188.

9. Morrow, R., Lowke, J.J. Space-charge effects and drift dominated electron and plasma motion // J. Phys. D: Appl. Phys.- 1981.- V. 14.- P. 2027-2034.

10. Sigmond, R.S., Goldman, M. Corona discharge physics and application // Electrical breakdown and discharge in gases.- N.Y. and London: NATO, 1983. - P. 1-64.

11. Paris, P. Investigation of streamer characteristics on combined voltages (D.C. + pulse voltage) // Tartu Diploma Thesis.- 1978.- (in Estonian).

ИНИЦИИРОВАНИЕ СТРИМЕРА ИМПУЛЬСОМ РЕНТГЕНОВСКОГО ИЗЛУЧЕНИЯ

М. Лаан, П. Парис

Резюме

Целью работы являлось исследование формирования стримера в сильнонеоднородном разрядном промежутке острие - плоскость. Разряд инициировали при помощи импульсов рентгеновского излучения (средняя энергия кванта - 5 кэВ, длительность импульса - 140 нс). Рентгеновский импульс создавал в воздухе 10^7 см^{-3} заряженных частиц. Измерено время формирования разряда в зависимости от интенсивности излучения при разных напряжениях. Найдено, что для формирования стримера необходимо существование плазменного слоя вблизи острия.

THE MULTI-AVALANCHE NATURE OF STREAMER FORMATION IN INHOMOGENEOUS FIELDS.

Matti Laan and Peeter Paris

Institute of Experimental Physics and Technology

University of Tartu, EE2400 Tartu, Estonia

The streamer formation in a positive point-plane gap both in air and nitrogen has been studied. The primary electrons were created by the laser radiation. This gave the opportunity to initiate streamers in a wide range of voltages including the range of steady corona in air as well as to determine the formative time lags. A streamer starts when the space charge density reaches a critical value in a spatially localised region. In a divergent field the streamer formation is preceded by the accumulation of space charge i. e. it has a multiavalanche nature. A model for calculation of formative time lags is presented. For a virgin gap the model describes fairly the accumulation process. For the voltage range of steady corona in air only the qualitative description of the mechanism is given.

1. Introduction

In a homogeneous field a streamer starts at voltages where the number of charge carriers of an avalanche $\exp(\int \alpha_0 dx)$ (α_0 - the first Townsend coefficient for Laplacian field) reaches a critical value $N_{cr} \sim 10^8$. In this case the field intensity of the space charge of ions becomes comparable to the intensity of the applied field. However it is possible to reach the same critical space charge field when a large number of avalanches develop within the diffusion radius of an avalanche. Thus the critical total number of carriers can be reached at lower fields as was demonstrated in experiments with α - particles [1, Ch 5].

In inhomogeneous fields the streamer formation is possible at voltages where the mean number \bar{N} of charge carriers of a single avalanche is less than 10^8 . In that case the avalanche-to-streamer transition is explained by the stochastic nature of the avalanche growth [2], the larger avalanches ($N > \bar{N}$) grow into streamers. In a point-plane gap (hemispherical 0.1 cm in diameter point, the gap spacing - 4 cm) in air the calculated number \bar{N} for Laplacian field at the onset potential $U_0 \approx 8$ kV of a cathode-directed streamer is $\sim 10^4$, the

development of an avalanche of $N \sim 10^8$ carriers has a very low probability [1, Ch 3]. Such a large difference of $N_{cr}/\bar{N} \sim 10^4$ rather indicates that in a highly divergent field the streamer formation has the multiavalanche nature : the critical conditions are achieved by the accumulation of the cloud of positive ions from several avalanches.

This paper describes the formation of a streamer without external triggering (a non initiated streamer) as well as the formation of initiated streamers. Initiated streamers start due to a high number of primary electrons which are created by laser radiation. With this method of streamer initiation

(i) the time moment and the place of liberation of primary electrons can be fixed, and

(ii) the number of primary electrons can be varied easily.

These factors allow the formative time lags to be determined as a function of voltage and the number of primary electrons.

2. Experimental set-up, methods .

2.1. Discharge gap

A positive DC corona is studied in a point-plane gap (figure 1). The gap spacing is 4 cm, the point electrode is a hemispherically capped wire of diameter 0.1 cm. The points made of different materials (Pt, Al, Cu, Mo) are used. The plane electrode is an aluminium disc of diameter 20 cm with a probe electrode of diameter 1.5 cm in its centre. The point electrode is stressed. The stabilised power supply allows the voltage to be varied with the smallest step of 10 V.

2.2. Gases.

Experiments are carried out in ambient air and in nitrogen. The discharge in nitrogen is studied in a stainless steel chamber. It is evacuated to 10^{-5} Torr by the help of an oil diffusion pump trapped by liquid nitrogen. The chamber is raised to 100^0 C in a few hours and is then filled with nitrogen (99.996% of N_2 , the content of H_2O is less than 0.005 gm^{-3}) and the pressure is set at atmospheric pressure. In such a medium the "ageing" of the gas takes place. There are two most striking effects of ageing:

- (i) current-voltage curve of negative corona changes with as previously described [3,4].
- (ii) recorded drift times of electrons from the cathode to anode decrease drastically with time.

It is known [5] that small traces of water vapour in nitrogen lead to the increase in the drift velocity. For this reason it is assumed ageing is

primarily caused by liberation of water vapour from the electrodes and the walls of the chamber. To reduce the influence of water vapour a bakeable trap with silica-gel is set into the chamber. As a result the changes of the current-voltage curve of the negative corona slow down considerably and the drift velocity is maintained constant for a long time. Of course, the stabilization of discharge parameters may be caused by other impurities (like the vapour of the diffusion pump oil), which are also absorbed by silica gel.

2.3. Primary electrons.

Primary electrons are created by the radiation of excimer lasers (wavelength $\lambda = 308$ nm) which have different pulse lengths (10 ns and 100 ns) but nearly the same maximum pulse energy ≈ 100 mJ. The stepwise attenuation of laser radiation is carried out by the means of calibrated grids. Two different ways for production of primary electrons are used:

1) Electrons are released from the cathode by photoeffect: a divergent laser beam is directed to the probe electrode (figure 1, 1). To avoid side effects (like heating of the electrode surface) the illuminated area at the probe is ≈ 1 cm in diameter and the energy of a laser pulse does not exceed some millijoules. Changing the attenuation of laser radiation the number of released electrons varies from 10^6 to 10^7 . The estimated order of magnitude of the coefficient of secondary emission γ is $\sim 10^{-8}$.

2) Electrons are created by laser beam directed perpendicularly to the gap axis and focused on the gap axis at some distance x_0 from the point electrode (figure 1, 2). With transverse triggering one can neglect additional effects caused by the laser radiation at the electrodes. The maximum intensity I_m used near the beam focus does not exceed 5×10^{10} Wcm $^{-2}$. The intensity I_m is considerably lower than needed for optical breakdown ($I \sim 10^{12}$ Wcm $^{-2}$ for $\lambda = 350$ nm, [6]). The total number of charge carriers released by a laser pulse is determined in a parallel plate gap of 1 cm spacing. The laser beam is focused to the mid-gap and the charge of current pulse in the gap circuit as a function of gap voltage is determined. From 1.5 to 3 kV the charge does not depend on voltage. From this value of charge the number of charge carriers is calculated. The number of charge carriers which corresponds to I_m both in air and nitrogen is nearly the same and has an order of magnitude of 10^8 . The number of carriers created by a 10 ns pulse is somewhat less than that produced by a 100 ns pulse.

In air the distance x_0 is established with the accuracy of some tenth of mm. Due to the laser instabilities the position of the focal point varies from pulse to pulse within the same limits. In the case of experiments in nitrogen the accuracy is less as experiments are carried out in the chamber and the direct measurement of x_0 is impossible. Besides this the role of laser instabilities in nitrogen is somewhat larger as the chamber is situated at a greater distance from the laser than the gap in air.

Near the beam focus the dimensions of the trace created by the radiation at a photo plate is $\approx 0.01 \times 0.02 \text{ cm}^2$ and it remains nearly constant in limits of 0.6 cm along the beam axis. It is supposed that the ionisation by laser radiation mostly takes place within this volume and thus the guessed value of the concentration of charged particles of a plasma ball in the beam focus is $\sim 10^{11} \text{ cm}^{-3}$. This concentration is high enough to lock electrons to ions as it is proved by the computer calculations [7], a plasma ball exists for a long time and only a small leak of electrons towards the anode occur. This viewpoint is also supported by our measurements (figure 9): the plasma ball is created by a 10 ns laser pulse but the duration of the flux of electrons to the anode exceeds 80 ns.

2.4. Measurements of current and time intervals

The DC current is measured by an ammeter in the circuit of the plate and the probe connected in parallel. For the nanosecond resolution measurements of the current of streamer pulses a 350 MHz bandwidth oscilloscope of 50Ω input resistance is used: a 50Ω coaxial feedthrough [4] (figure 1, $R_{po} = 50 \Omega$) is fitted with a 50Ω transmission line. In the case of detecting low-current pulses (less than 10^{-4} A in height, see sections 3.1 and 3.2) in the probe and the point circuits the larger values of resistors are used ($R_{po}, R_{pr} = 470 \Omega, 1.3 \text{ k} \Omega$), and signals are recorded by the help of an oscilloscope of $1 \text{ M}\Omega$ input resistance. Therefore the circuits are mismatched and the recorded signals are integrated.

The waveform of a laser pulse is recorded by a fast photodiode situated close to the discharge gap.

The time intervals are determined from the screen of oscilloscope. The time interval between the low-current pulses in the probe and the point circuits (drift time t_{ca} ; see section 3.2, figure 2A) is measured with the accuracy of $0.05 \mu\text{s}$. The time interval between the leading edges of laser pulse and streamer pulse (delay time t_d , see section 3.3)

is measured with a higher precision. To achieve it a variable delay cable is switched in series with the photodiode. The accuracy of delay time measurements is 4 ns and it is determined mainly by the reproducibility of the adjustment of variable delay.

The light emitted by discharge is detected by a fast photomultiplier and a static image intensifier.

2.5. Formulas for calculations.

For computer calculations carried out by the Mathcad program various data are used. Numerical values of the constants in the expressions are given for our gap geometry; voltage U is in volts, pressure p is in Torr, distance x from the point tip is in cm.

The reduced field intensity E/p ($\text{Vcm}^{-1} \text{ Torr}$) along the gap axis is calculated according to the expression

$$E(x)/p = 3.6 \cdot 10^{-5} U (x + 0.05)^{-2} \exp(2(x + 0.05)).$$

Up to the distance $x = 1$ cm it is a good fit [8] to the electric field distribution, obtained by the method of charge simulation [9]. At larger distances x the field is calculated according to the formula derived in [10] in hyperbolic approximation

$$E(x)/p \approx \frac{1}{p} \cdot \frac{1.4 \cdot U}{x(2 \cdot a - x) + (a - x) \cdot r}, \quad a = 4 \text{ cm and } r = 0.05 \text{ cm}.$$

The ionisation coefficient α is in cm^{-1} . The approximations from [11] are used:

$$\alpha/p = 8.6 \exp(-254/E/p) \quad \text{for air and}$$

$$\alpha/p = 8.8 \exp(-275/E/p) \quad \text{for nitrogen.}$$

The drift velocity v_e of electrons is in cm/s. For air the expression from [13] is used

$$v = 10^6 (E/p)^{0.715}.$$

For nitrogen two different quadratic fits are derived: the first

$$v = 10^6 (0.27 + 0.471 E/p - (E/p)^2) \quad E/p < 20$$

is based on experimental data from [14, Ch 1], the other one

$$v = 10^6 (0.7 + 0.35 E/p - 5.643 \cdot 10^{-4} (E/p)^2)$$

is for higher fields and the data are from [15].

3. Results.

3.1. Types of non initiated positive corona.

In air the sequence of different corona types does not differ from that described earlier by several investigators [15, ch 3]. The first detectable

discharge type is a burst pulse which spreads along the point surface. It is possible to observe burst pulses about 200 V below the inception voltage U_0 of onset streamers. At voltages close to U_0 the amplitude of larger burst pulses achieves 0.1 mA and their duration is nearly $1\mu\text{s}$, the corresponding light pulse is shorter ($\approx 70\text{ ns}$). At voltages $U > U_0$ both burst pulses and streamers exist. U_0 depends on humidity and pressure of ambient air and varies from 7.8 to 8.0 kV. No dependence on electrode material is mentioned. In the narrow range of voltage near the inception voltage the burst-to-streamer transition is observable: the steep current rise of a streamer pulse is preceded by a step. The recorded current waveform is very similar to the avalanche-to-streamer transition in homogeneous field [1, Ch 5]. The magnitude of the step is close to that of burst pulse and its duration does not exceed 20 ns. With the voltage increase the duration of step diminishes quickly and already 50 volts above U_0 it is difficult to separate the step from the main pulse. The burst-to-streamer transition is described in more detail elsewhere [16]. The peak value of largest current pulses of streamers is 9 mA and their half width is $\approx 100\text{ ns}$. The streamers are recorded in the range of $\approx 200\text{ V}$. They have a branched structure and some of branches develop up to 10 mm from the point. At higher voltages the discharge exists in the form of steady glow, its current increases from $0.5\mu\text{A}$ at 8.5 kV up to $9\mu\text{A}$ at 14 kV.

In nitrogen the onset potential of the discharge is considerably higher: at 9.7 kV the first pulses of $0.25\mu\text{A}$ in amplitude are recorded, their duration $\approx 10^{-6}\text{ s}$ is determined by the time constant of the recording system. The number of electrons $N \geq 10^6$ in a pulse is close to the calculated number of charge carriers in an avalanche at this voltage. According to the static picture from several pulses (observed by the image intensifier) a large area of the hemispherical part of the point electrode is covered by a very faint luminous layer.

At 9.9 kV a steady discharge is established. With the voltage increase the DC current of steady discharge increases gradually from $1\mu\text{A}$ at the onset up to the $8\mu\text{A}$ at 14 kV. At the point surface near its tip a more intensive luminous spot with sharp borders is observable. The area of the spot is $(1.2 \div 1.5)10^{-4}\text{ cm}^2$ and above it a faint luminous channel extends far into the gap. From time to time the spot jumps to another place. Only few jumps per minute occur. The jump is accompanied by a sudden change of DC current (e.g. at $U = 10.1\text{ kV}$ the current changes within the limits $1.8 \div 2.2\mu\text{A}$) as well as by the

streamer formation. It is difficult to say whether there are streamers also during the constant current or not. The height of the current pulse of a streamer vary from 16 to 20 mA and the halfwidth of pulses is ≈ 800 ns. By appearance the streamers are less if any branched than in air. The length of a non branched channel varies within the limits $0.8 \div 1.5$ cm and the channel is often deflected from the gap axis, the branching occurs mainly at the end of the streamer channel.

In dry nitrogen the extinction voltage differs from the inception one: the steady discharge exists up to 8.7 kV. The extinction current of discharge is $\approx 0.12 \mu\text{A}$. The same behaviour as at voltages above the inception voltage is observed: the sudden change of current is connected with a streamer formation, the length of streamer channel is diminishing with voltage decrease.

In non dried nitrogen the extinction voltage equals to the inception one and the streamer is branched like in air.

3.2. Determination of drift times and ionisation integral

Most of the experiments are carried out in nitrogen. The primary electrons are liberated from the probe by a 10 ns laser pulse.

The drift time t_{ca} is measured (figure 2A) as a function of voltage (figure 3). The results for dry nitrogen are close to that calculated on the bases of data from the literature (section 2.5). The presence of water vapour reduces drastically the drift time.

The numbers of electrons leaving the cathode N_c and reaching the anode N_a are determined from the areas $\int i dt$ of current pulses of the probe and the point, respectively. During their drift the number of electrons changes due to the losses as well as due to the ionisation multiplication in a high field near the point. Up to 4 kV in dry nitrogen within the limits of experimental errors there is no difference between N_c and N_a (in non dried nitrogen $N_a/N_c < 1$). As the value of calculated ionisation integral $\int \alpha_0 dx$ is close to one in this range of voltage it is possible to conclude that in this case the role of losses is negligible. At higher voltages ($U = 5 \div 8$ kV) N_a increases with voltage but the waveform of current pulses does not change and the relation $N_a/N_c = f(U)$ does not depend on laser intensity. So the curve $\ln(N_a/N_c) = f(U)$ may be treated as a dependence for experimental ionisation integral. In figure 4 the experimental points, a quadratic fit of $\ln(N_a/N_c) = \int \alpha_0 dx = 5.2 \cdot 10^{-5} U^2 - 0.61$ as well as the calculated curves $\int \alpha_0 dx = f(U)$ for Laplacian field are presented.

At voltages $U > 8$ kV the waveform of current pulses of the point circuit changes. The simple waveform is replaced by a more complicated one (figure 2B): there is a higher hump at the beginning of a current pulse. At higher voltages from this hump a steep current rise starts (figure 2B) that is corresponding to streamer development as it is also confirmed by image intensifier observations. The onset voltage of an initiated streamer U_i depends on laser intensity: in the case of four-fold increase in intensity U_i diminishes from 8.7 kV to 8.2 kV. But independent of U_i there is a critical total number of charge carriers

$N_{cr}^t = (2 \div 5)10^7$ (figure 2B) near the point which must be achieved by the moment of transition.

In the case of similar experiments in air the time interval between anode and cathode current pulses is nearly 3.5 ms and it corresponds to the drift time of negative ions. Using a hemispherical 1 mm point only large burst pulses are initiated in the region of onset streamers.

3.3. Measurements of delay times

Experiments are carried out in both ambient air and nitrogen. The primary electrons are created by a focused laser beam at the distance x_0 from the point. The long-pulse as well as the short-pulse laser are used, but the results do not depend remarkably on the pulse length. Delay time t_d needed for the start of an initiated streamer depends on voltage U , laser intensity I and distance x_0 . Delay time is determined only for these values of x_0 , I and U for which the jitter of t_d does not exceed some nanoseconds.

By appearance an initiated streamer has a branched structure, the length of branches increases with voltage increase. At higher laser intensities the branches developing towards the laser beam will prevail [17, 18].

In air the maximum distance is $x_0 = 0.8$ cm. At larger distances independent of laser intensities used the initiated streamers are not observed. For all distances under observation the behaviour of curves $t_d = f(U)$ is similar. The results for $x_0 = 0.5$ cm and for the long laser pulse are presented in figure 5. At every intensity $I = \text{constant}$ below the inception voltage of non initiated streamers U_0 , the delay time decreases with the voltage increase and achieves its minimum near the potential U_0 . Further increase in voltage also leads to the increase in delay time. In the region of steady corona the delay time remains nearly constant. At every voltage the decrease in intensity causes the increase in delay time.

In nitrogen the dependencies $t_d = f(U)$ are recorded up to the distance $x_0 = 1.6$ cm. This maximum distance is limited by the dimensions of viewport and not by the jitter of t_d . As in air the initiation of streamers is possible at voltages remarkably less than the inception voltage of non initiated discharge. Compared with air the dependence on laser intensity at $U = \text{constant}$ is considerably less. A typical curve of $t_d = f(U)$ is presented in figure 6: delay time diminishes gradually with voltage increase.

4. Discussion

A non homogeneous discharge gap may be divided into two typical zones [19]: the drift zone and the ionization zone. In our gap at voltages under observation the border of the ionization zone x_i is at the distance < 0.06 cm from the point tip.

4.1 Feedback mechanism in nitrogen.

Near the onset in air ($U \approx 8$ kV) the calculated (figure. 4) size of an avalanche $\exp\left(\int \alpha_0 dx\right)$ is two orders of magnitude less than that at the onset potential ($U \approx 10$ kV) in nitrogen. At the same time for a self-sustained discharge the replenishment factor $\gamma \exp\left(\int \alpha_0 dx\right)$ must be 1 (γ - the coefficient of secondary emission). This means that compared with air the efficiency of secondary process(es) in nitrogen is much less. It is widely accepted that in air the different discharge forms (burst pulses, streamers, steady corona) are supported by the photoionisation as a γ -mechanism, processes at the cathode play a minor role [15]. Only the results of experiments carried out in synthetic air [20] seem to prove that the development of the repetitive streamers is also supported by the cathode processes.

In nitrogen the photoionisation is not so effective and the role of the cathode becomes dominant. This viewpoint is supported by different experimental observations (see section 3.1):

(i) Instead of a luminous layer concentrated close to the point surface in the case of steady corona in air, the channel of the steady state discharge in nitrogen extends far to the gap and, as it was observed in purer conditions [21] the channel of a very weak luminosity bridges the gap. As the rule the channel of a steady discharge is deflected from the gap axis, most probably it starts from the edge of the probe where the field intensity is higher. Observed jumps of the DC current with corresponding replacement of the bright anode spot may be caused by a change in emissive site at the cathode.

(ii) The streamers in nitrogen are less branched and a non branched channel is deflected from the gap axis like the channel of steady discharge. So it is probable that a streamer develops preferably along the channel of a steady discharge, i.e. along the preionised path.

(iii) The difference between the inception and extinction voltages is not explainable supposing that the gas photoionisation as a feedback mechanism of steady corona is dominant.

(iv) The detected current pulses at the onset of discharge correspond to single avalanches, i.e. burst-pulse like mechanism is not active.

So it is quite reasonable to assume that the steady discharge in nitrogen is a glow with its typical cathode region at the plane electrode, and the preionisation ahead of a non initiated streamer in nitrogen is caused by the background steady discharge than by the photoionization

4.2 Conditions for streamer formation

Multi-electron streamer initiation both in air and nitrogen is possible in a wide range of voltages including the case of low fields ($U \approx 7$ kV) where the calculated number of the charge carriers of an avalanche is $\sim 10^2$ as well as in the region of steady corona. It is obvious that in all cases similar critical conditions must be established at the moment of a streamer initiation. Furthermore, these conditions must not differ from those for single electron initiation.

As has previously been demonstrated by experiments with α - particles in homogeneous field [1], the streamer formation is determined rather by the critical density of charged particles than by the size of a single avalanche. In our experiments only the critical number of charge carriers $N'_{cr} \sim 10^7$ near the point (see section 3.2) is directly determined. Due to the gap geometry most of charge carriers are created in a thin layer at the point surface. The area of this layer should not differ considerably from that for non-initiated streamer. A non-initiated streamer in nitrogen (section 3.1) starts from an anode spot of $\sim 10^{-4}$ cm² in area. So an estimated critical value of the charge surface density is $\sigma_{cr} \sim 10^{-8}$ (C/cm²). Calculated maximum field intensity ($E \sim 10^5$ V/cm) of the anode spot treated as a charged disc differs less than 40% from the value of Laplacian field intensity at the point surface at the inception voltage ($U_0 \approx 8$ kV) of streamers in air. This result coincides with the general formulation of the criterion for streamer formation: a streamer starts when the intensity of the space charge field is close to that of applied field.

In the case of steady corona in air the situation is more complicated. There are no problems with the achievement of a critical number of charge carriers as the point surface is covered by a laterally extended layer of ionised gas. According to the general analysis of corona

stability [19] this type of discharge is stable as an accidental current increase will also enhance the positive space charge layer and thus weaken the field at the point, ionisation is reduced and the original current is restored. The stability of steady discharge also follows from the analysis of its positive-slope I - U curve. For streamer formation the field at the cathode side of the layer must be high enough to ensure that ionization increases there. It becomes possible when in a spatially localized region of the layer the increase of ionization rate dn/dt for some reason occurs. It may lead to the spike-like extension of the region of ionised gas towards the cathode, i.e. a streamer forms. The cited model is supported by experimental results:

(i) In air a burst-pulse starts near the point tip and then due to the photoionisation spreads over the point. During its development a space charge layer forms at the point surface. At $U \geq U_0$ a burst may grow into a streamer (section 3.1). The probability of transition is determined by the competition between the cathode-directed extension of ionisation due to the accumulation of space charge in a limited area and the development of discharge to the lateral parts of the point. The last process diminishes the field at the cathode side of the layer and thus it lowers the probability of streamer formation. For this reason the transition occurs always at the initial part ($t < 20$ ns) of the burst as later the field is too weak to ensure the development of cathode-directed ionisation instability.

(ii) It is possible to create streamers in the region of steady corona in air (figure 5, $U > 8.5$ kV) where the point is covered by an extended ionized layer. In this case the local increase of dn/dt is caused by entering a large number of electrons created by a laser shot into the ionization zone in the limits of a small area.

(iii) Experiments with voltage pulses (1 kV in height and of 100 ns duration) superimposed to DC voltage demonstrate another possibility to create streamers in the steady corona region in air [17]. As a rule, a streamer starts from the lateral part of the layer where the layer is less homogeneous and so it is easier to achieve the local ionization instability.

Thus for the streamer formation independent of the magnitude of Laplacian field and the initial distribution of the field, a critical space charge density must be achieved in a spatially localised region.

4.3. Interpretation of delay times

In [22] the transverse triggering was also used and the experiments were carried out in similar conditions (point-plane gap, ambient air). In this paper the delay time t_d was interpreted as a time interval needed for streamer development from the anode to the cathode (the current pulses were recorded in the circuits of the probe and the outer part of the cathode), i.e. the drift time of the electrons to the ionisation zone nor the final time interval required for the space charge accumulation were taken into account.

We shall present the measured delay time (section 3.3) as $t_d = \Delta t + t_f$

After $\Delta t = \int_{x_0}^{x_i} \frac{dx}{v(E(x)/p)}$ the first electrons from a plasma ball

at the distance x_0 reach the border of ionisation zone at x_i and t_f (formative time) is the time interval needed for the accumulation of critical space charge in the ionisation zone. The measured values of t_d and the calculated values of Δt as a function of voltage both for air and nitrogen are presented in figure 6. As one can see:

(i) even in the case of large number of primary electrons and at the onset of streamers in air ($U \approx 8$ kV) an accumulation period precedes the streamer formation;

(ii) formative time $t_f = t_d - \Delta t$ in the region of steady corona in air increases with the voltage increase;

(iii) in nitrogen t_f diminishes with voltage increase and it is close to zero at the onset of non initiated discharge.

4.4 Model of space charge accumulation

The model describes the space charge accumulation in a virgin gap only and so the streamer formation in the region of steady corona is not treated here.

We assume that during the formative time t_f the flux of electrons $n_{ei}v_{ei}$ into the ionisation zone is constant (n_{ei} , v_{ei} are, respectively the concentration and the velocity of electrons at x_i). Most of the electrons enter the ionisation zone within the limits of a small area δS . In the ionisation zone the number of charge carriers N increases and during

the time interval δt $N(\delta t) = n_{ei}v_{ei}\delta t \delta S \exp(\int \alpha dx)$ positive ions

accumulate inside a thin disc-like volume situated close to the point surface. It is supposed that the ions are immovable during the accumulation.

During the accumulation the ionisation coefficient changes due to the space charge effects. The space charge causes the redistribution of the total field and α decreases [1, ch 3]. According to recent studies [23] in a homogeneous field at $E/p = 37 \text{ Vcm}^{-1}\text{Torr}$ the avalanche growth retards when the surface density of primary electrons is higher than 10^8 cm^{-2} . In our experiments the estimated density of primary electrons at x_1 exceeds this value and that is why the experimental ionisation

integral $\int \alpha dx$ is lower than that for Laplacian field (figure 4). The

actual smooth dependence of $\int \alpha(x,t) dx$ on time is unknown and it is replaced by a step-wise one: at the initial stage of accumulation the ionization occurs in Laplacian field, at the later stage the ionisation is

governed by $\int \alpha dx$ (figure 4). Furthermore, we suppose that there is no

remarkable difference of $\int \alpha dx$ for air and nitrogen. The estimated duration of initial stage is very short compared with that of t_f , e.g. at $U \approx 8 \text{ kV}$ and $n_{ei} \sim 10^{10} \text{ cm}^{-3}$ (this value of n_{ei} corresponds to our experimental conditions (figure 8)) the time interval for accumulation of 10^6 charge carriers is less than 1 ns.

After a formative time t_f the surface density $eN/\delta S$ (e - elementary charge) of space charge layer reaches its critical value σ_{cr} (section 4.2) and a streamer forms. Thus according to this rough model the formative times are calculated as

$$t_f(U, n_{ei}) = \frac{\sigma_{cr}}{en_{ei}v_{ei} \exp\left(\int \alpha dx\right)}$$

In this expression the concentration n_{ei} is a free parameter and its value has been chosen to achieve the best coincidence of the model with the experimental results.

The curves $t_f = f(U)$ ($x_0 = 3 \text{ mm}$) for air and for various laser intensities are presented in figure 7. Within the limits of its validity (i.e.

at voltages below the onset of steady corona) the model describes fairly well the accumulation process. It is likely that the increase in t_f in the voltage range of steady corona is caused by the decrease in the field at the cathode side of the ionized layer; thus for achievement of the critical field there, longer formative times are needed.

For all distances $x_0 > 2$ mm the coincidence with experimental results is similar. If the electrons are released closer to the point the experimental values of t_f are systematically longer than predicted by the model. This may be caused by the field reduction near the plasma ball created by the laser radiation: according to [18] the streamer branches never pass through the position of plasma ball.

The concentration of electrons n_{ei} reaching the ionisation zone varies in limits $(0.5 \div 3)10^{10} \text{ cm}^{-3}$, i.e. approximately 10^5 electrons per nanosecond pass the area $\delta S = 10^{-4} \text{ cm}^2$ at the border of the ionization zone. In figure 8 the dependencies $n_{ei} = F(I)$ for different x_0 in air are presented. The concentration n_{ei} logarithmically depends on laser intensity $n_{ei} = A \ln(I/I_0)$, the constant I_0 has a simple physical explanation: it is the minimum laser intensity which is able to ionize the gas and its estimated order of magnitude is $\sim 10^8 \text{ W/cm}^2$ (the corresponding energy of laser pulse is $\approx 2 \text{ mJ}$). The slope A is different for different x_0 : it describes the decrease of the number of electrons due to attachment during their drift towards the point.

The dependencies $t_f = f(U)$ ($x_0 = 4 \text{ mm}$) for nitrogen are presented in figure 9. The calculated curves are close to the points determined from the experiment for the whole range of voltage under observation.

There are several unsolved problems in this field. Some of these (the most exciting for us) are:

(i) The actual spatial distribution of charge carriers near the point during the space charge accumulation.

(ii) The mechanism of streamer formation in the case of steady corona.

(iii) The mechanism of non initiated streamer formation and development during the sudden change of current of steady discharge in nitrogen.

5. Conclusions.

It has been proved experimentally that in the case of a large number of primary electrons a streamer forms at voltages considerably lower than the inception voltage as well as in the range of steady corona.

For streamer formation an ionization instability must develop in a spatially localized region. The local increase in ionization leads to an increase of the space charge field in this region. A streamer starts when the space charge field achieves a critical value. These conditions are common in different experimental conditions.

At the inception voltage of streamers in a homogeneous field the number of charge carriers of a single avalanche is high enough to reach the critical field but if the gap is undervolted a large amount of primary electrons and/or an accumulation period of space charge are needed for streamer formation.

In a highly divergent field in air even at the inception voltage a space charge accumulation precedes the streamer formation as the number of charge carriers of an avalanche is much less than the critical number and so the streamer formation has a multi-avalanche nature. The increase of the inception voltage in nitrogen is caused by the low value of secondary emission coefficient.

Acknowledgements

One of the authors (M. L), would like to thank Professor R. S. Sigmond for discussions on the problems of corona discharges during his stay at the Norwegian Institute of Technology. The authors would like to thank Svein Sigmond for very useful discussions as well as the Norwegian Scientific Foundation (NAVF) for their scholarship. The study was supported by the Estonian Scientific Foundation.

REFERENCES

1. Raether H. 1964 *Electron avalanches and breakdown in gases* (London: Butterworths)
2. Pedersen A. 1989 On the electrical breakdown of gaseous dielectrics *IEEE Trans. on Electrical Insulation* **24** 721-739
3. Laan M, Paris P and Pereleyin V 1991 Laser action on corona pulses *Acta Phys. Slov.* **42** 91-97
4. Korge H, Laan M and Paris P 1993 On the formation of negative coronas *J. Phys. D: Appl. Phys.* **26** 231-236
5. McDaniel E W 1964 *Collision phenomena in ionized gases Ch 11* (New York - London - Sydney: John Wiley & Sons)
6. Rosen D I and Weil G 1987 Laser induced breakdown in nitrogen and rare gases at 0.53 and 0.35 μm *J. Phys. D: Appl. Phys.* **20** 1264-1276
7. Morrow R and Lowke J J 1981 Space-charge effects on drift dominated electron and plasma motion *J. Phys. D: Appl. Phys.* **14** 2027 - 2034
8. Abou - Seada M S 1980 Calculating of the high - frequency breakdown voltages of point-plane air gaps *IEEE IAS 15th Annual Meeting* 1118 - 1122
9. Abou - Seada M S and Nasser E 1969 Digital computer calculation of the potential and its gradient of a twin cylindrical conductor *IEEE Trans PAS* **PAS-88** 1802-1814

10. Coelho R, Debeau J 1971 Properties of the tip-plane configuration *J. Phys. D: Appl. Phys.* **4** 1266 - 1280
11. Granovski V L 1971 Electrical current in gas Ch. 2 (Moscow: Nauka) (in Russian)
12. Sigmond R S 1983 Basic corona phenomena: the role of space charge saturation and secondary streamers in breakdown *16th Int. Conf. on Phenomena in Ionized Gases (Düsseldorf) Inv. Papers* 174 -186
13. Brown S 1959 Basic data on plasma physics
14. Wetzer J M, Wen L 1991 Different avalanche types in electronegative gases *J. Phys. D: Appl. Phys.* **24** 1964 - 1973
15. Loeb L B 1965 Electrical Coronas (Berkeley and Los Angeles: University of California Press)
16. Laan M and Paris P 1992 Streamer initiation by x-ray pulse *Acta et Comment. Univ. Tartuensis: Methods of study of electrical processes in gases and aerosols* **950** 14-22
17. Laan M and Paris P 1992 Formation of corona pulses *9th symp. on elementary processes and chemical reactions in low temperature plasma* (Small Carpathy, Slovakia) *Inv. papers* 201 -216
18. Paris P Aints M and Haljaste A 1993 Development of a laser-initiated streamer *21th Int. Conf. on Phenomena in Ionized Gases* (Bochum, Germany) *Proceedings II* 263 - 264
19. Sigmond R S and Goldman M 1982 Corona discharge physics and applications *Electrical breakdown and discharges in gases Part B* ed E E Kunhardt and L H Luessen (New York and London: Plenum Press) 1-64
20. Kondo K and Ikuta N 1981 Highly resolved observation of the primary wave emission in atmospheric positive-streamer corona *J. Phys. D: Appl. Phys.* **13** Letter to the editor 1.33-1.38
21. Korge H Kudu K and Laan M 1979 The discharge in pure nitrogen at atmospheric pressure in point-to-plane discharge gap *3rd Int. Symp. on High Voltage Engineering* (Milan) paper 31.04
22. Soulem N, Pignolet P, Peyrous R, Held B, Loiseau J F 1992 Laser investigation of positive point-to-plane discharge ambient air . *10th Int. Conf on Gas Discharges and their Applications* (Swansea, U. K.) Vol. 1 286-289
23. Kennedy J T, Wetzer J M, van der Laan P C T 1992 Experimental study of space charge effects in avalanches in atmospheric nitrogen. *10th Int. Conf on Gas Discharges and their Applications* (Swansea, U. K.) Vol. 1 516-519

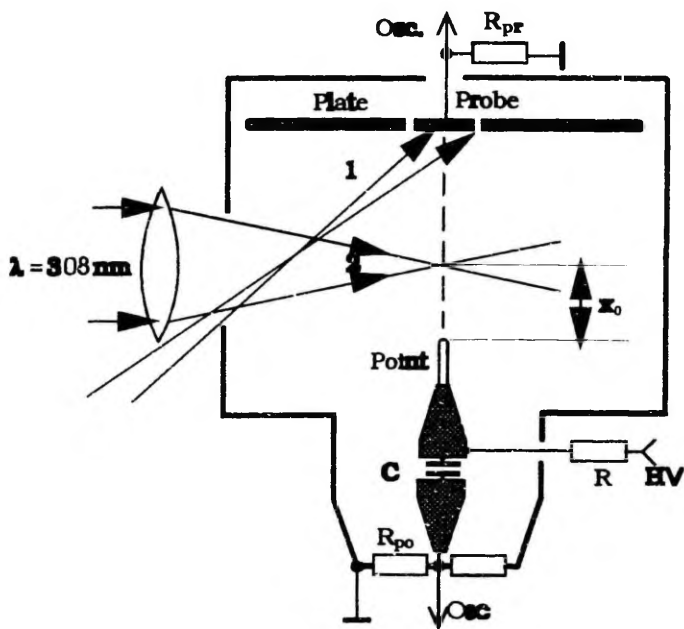


Figure 1 Experimental set -up.

- 1 - primary electrons are released at the probe electrode
- 2 - primary electrons are created at the gap axis by a focused laser beam

$$R = 20 \text{ k}\Omega, C = 2000 \text{ pF}, R_{po} = 50, 470 \text{ }\Omega, R_{pr} = 470 \text{ }\Omega, 1.3 \text{ k}\Omega$$

HV - high voltage supply

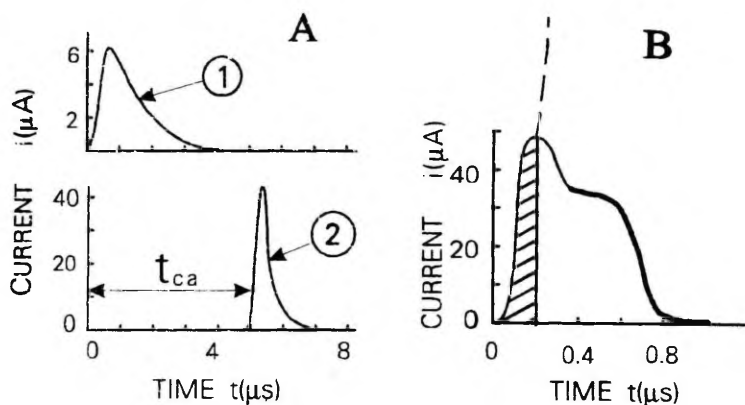


Figure 2 Sketches of current pulses.

A. Measurement of drift time t_{ca} :

1 - current pulse in the probe circuit

($R_{pr} = 1.3 \text{ k}\Omega$, time constant $\tau = 1.5 \cdot 10^{-7} \text{ s}$);

2 - current pulse in the point circuit

($R_{po} = 470 \text{ }\Omega$, $\tau = 5 \cdot 10^{-8} \text{ s}$)

B. Full line: current pulse in the point circuit

at $U > 8 \text{ kV}$ ($R = 50 \text{ }\Omega$)

Broken line: current pulse of a streamer.

The hatched area corresponds to the critical charge eN_{cr} .

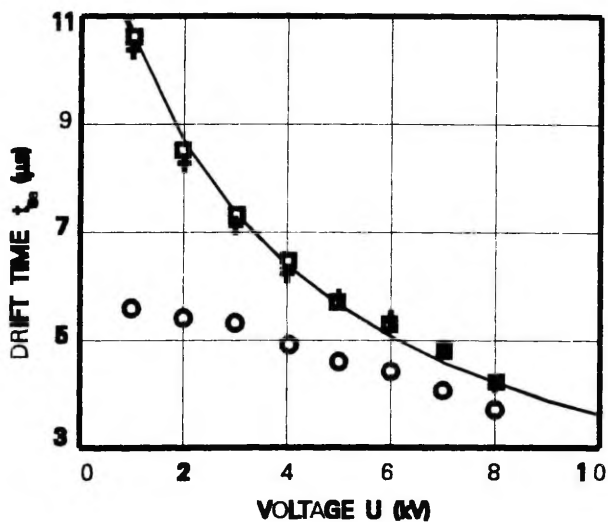


Figure 3 Drift time t_{ca} of electrons as a function of voltage.

O: non-dried nitrogen, 20 hours after filling with fresh gas.

+ and □: dry nitrogen, respectively 100 hours

and a month after filling.

Full curve: the calculated dependence.

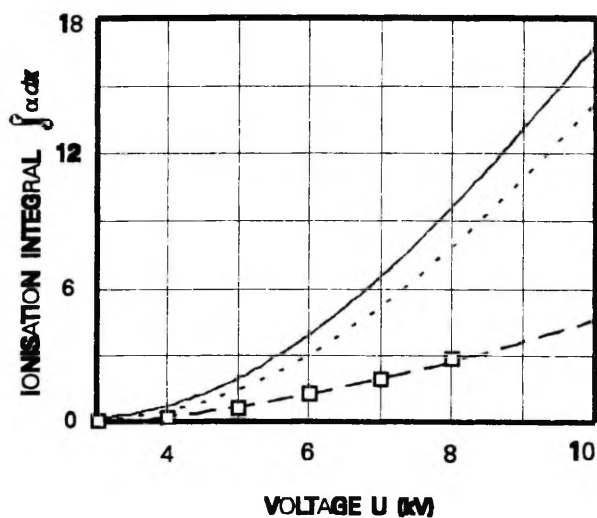


Figure 4 Ionisation integral as a function of voltage.

Full curve: air, Laplacian field.

Dotted curve: nitrogen, Laplacian field.

Curves for Laplacian field are calculated from the border of ionisation zone.

□: experimental results. Broken curve: a quadratic fit to experimental results.

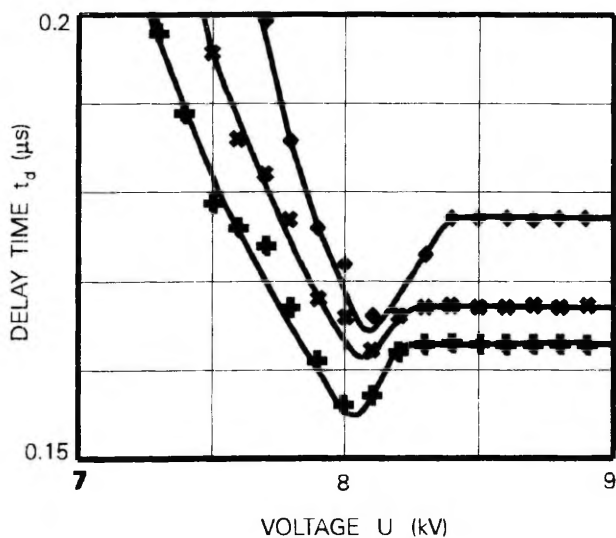


Figure 5 Delay time t_d in air as a function of voltage .

Electrons are created at $x_0 = 0.5$ cm from the point.

Voltage $U \approx 8$ kV corresponds to the onset of non initiated

streamers.

+: laser intensity $I = I_m$.

x: $I = I_m/2$.

◆: $I = I_m/4$.

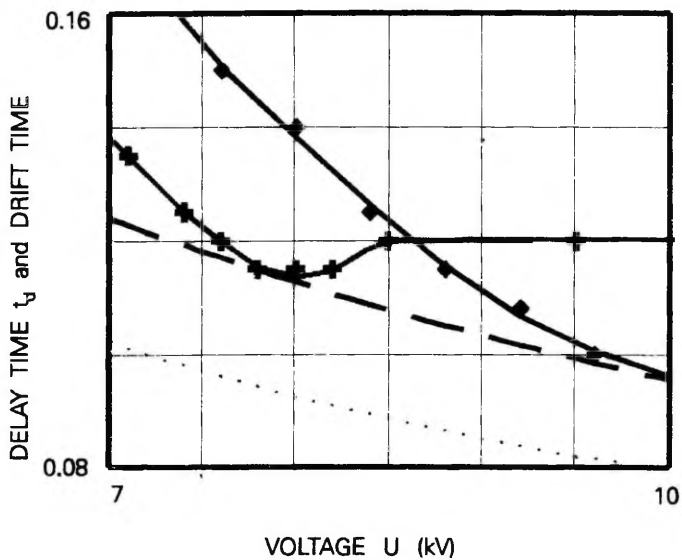


Figure 6 Delay time t_d and drift time Δt as a function of voltage.

Electrons are created at $x_0 = 0.4$ cm.

+: t_d in air.

◆: t_d in nitrogen.

Dotted curve: calculated Δt for air.

Broken curve: calculated Δt for nitrogen.

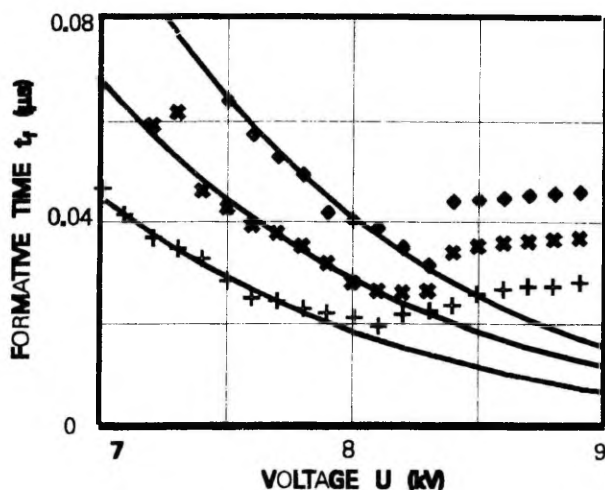


Figure 7 Formative time t_f in air as a function of voltage .

Electrons are created at $x_0 = 0.3$ cm

Full curves are calculated according to the model

+: $I = I_m$,

full curve corresponds to $n_{ei} = 2.8 \cdot 10^{10} \text{ cm}^{-3}$.

x: $I = I_m/4$, $n_{ei} = 1.85 \cdot 10^{10} \text{ cm}^{-3}$

♦: $I = I_m/8$, $n_{ei} = 1.26 \cdot 10^{10} \text{ cm}^{-3}$

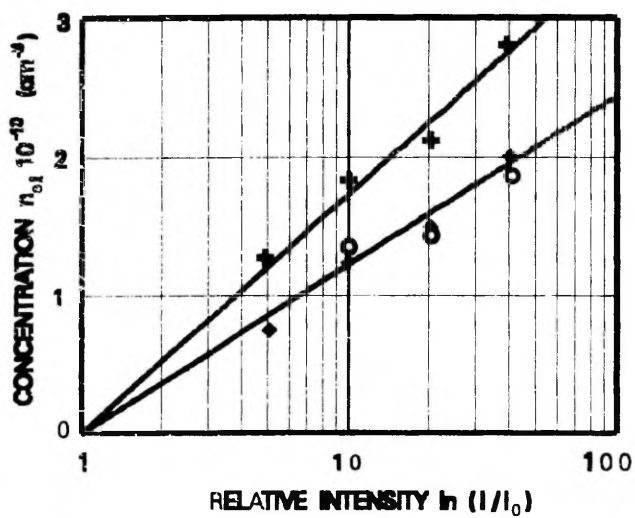


Figure 8 Concentration n_{ei} at the border of ionisation zone

as a function of relative laser intensity.

+: electrons are created at $x_0 = 0.3 \text{ cm}$.

◆: $x_0 = 0.4 \text{ cm}$. Circles: $x_0 = 0.5 \text{ cm}$.

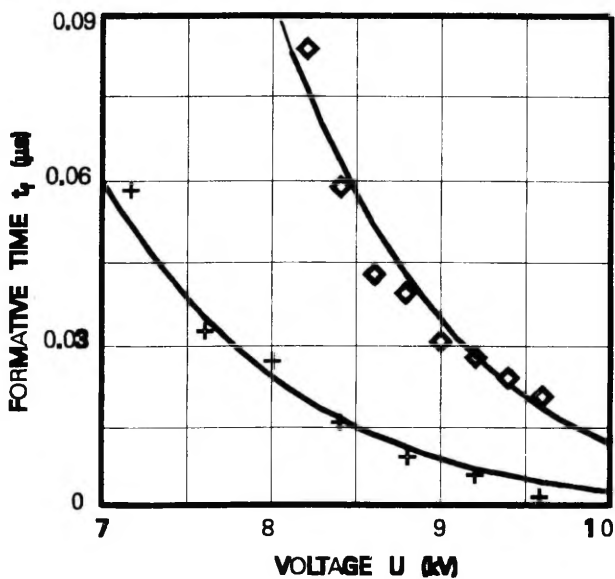


Figure 9 Formative time t_f in nitrogen as a function of voltage.

Full curves are calculated according to the model.

Electrons are created at $x_0 = 0.4$ cm.

+: 100 ns laser pulse,

full curve corresponds to $n_{ei} = 2.2 \cdot 10^{10} \text{ cm}^{-3}$.

◆: 10 ns laser pulse, $n_{ei} = 0.6 \cdot 10^{10} \text{ cm}^{-3}$.

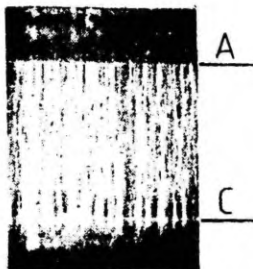
FORMATION OF CORONA PULSES

M.Laan and P.Paris
Tartu University
EE2400 Tartu, Estonia

In the 8 th symposium at Stára Lesná [1] Dr. Mirko Černák presented an extended survey on processes which take place in the case of D.C. corona formation. In our paper the main attention will be payed only to some new aspects connected with this topic.

During the recent years our interest in corona studies has been caused by a striking similiraty between corona formation and development of instabilities in high pressure bulk discharges in homogeneous field. As it is well established (2, ch. 7), the distortion of homogeneity of a bulk discharge is mainly determined by the processes occuring near both the oathode and anode. A typical picture of a bulk discharge is presented in Fig. 1. This discharge radiates mainly in ultraviolet part of spectra. The photo was taken using a spectral filter which cuts off the UV part and so it was possible to increase the contrast of channels. A bulk discharge consists of a big number of "minidischarges", each of which is linked to its own cathode spot, at the anode surface there are the anode spots.

Fig. 1. Discharge in homogeneous field; He/Xe/HCl mixture;
A - anode; C - cathode.



Formation of these spots and evolution of a minidischarge in its initial stage are close to those of in a point-plane gap. Furthermore, these processes are weakly

influenced by gas composition. In a point-plane gap and in molecular gases the discharge is localized near the point electrode and the influence of processes as well on the opposite electrode as in the gap are considerably suppressed. It gives a good opportunity to study separately the processes near the cathode and anode; finally it leads to the better understanding of instabilities that rise in a bulk discharge.

In this paper recent results of both positive and negative corona formation studies in molecular gases are presented.

EXPERIMENTAL SET-UP.

Nearly the same discharge gap geometry was used in all the experiments. The gap spacing was 40 mm and the point electrode was a hemispherically capped wire of 1 mm diameter. Point electrodes made of different materials were used. The opposite electrode was flat and its diameter was ≥ 150 mm. Pressure was varied from 60 to 760 Torr. Experiments were carried out in three different media:

(i) Ambient air: loss of electrons is determined by attachment.

(ii) Pure nitrogen: impurities have no remarkable influence on ionization and loss of electrons. The main loss mechanism of electrons is recombination.

(iii) Nitrogen: loss of electrons and/or quenching of metastables are determined by impurities.

Both spontaneous and initiated corona pulses were studied. Three different ways of corona initiation were used - Fig. 2. A X-ray pulse (mean quantum energy - 5 keV, pulse duration - 140 ns) originates in air 10^7 charged particles per cm^3 . A focused laser beam (quantum energy - 4 eV, energy per pulse - 100 mJ, pulse duration - 100 ns) creates in air 10^9 charged particles. If the beam is focused on the spot 5 mm from the point, (initiation I2) it causes the rise of point surface temperature to more than 1000 K. Maximum repetition rate of the initiating pulses was 20 pps.

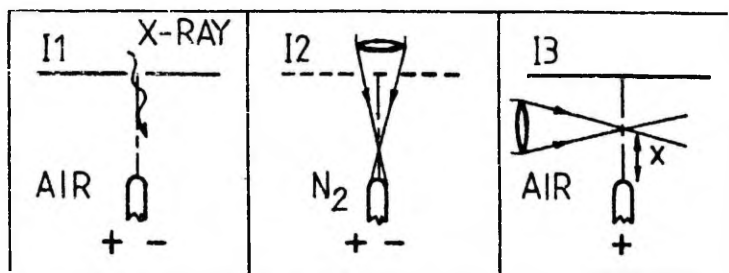


Fig. 2. I1 - corona is initiated by a X-ray pulse [3, 4]; I2 - corona is initiated by a laser beam directed along gap axis [5, 6, 7]; I3 - corona is initiated by a laser beam directed perpendicularly to gap axis [8].

NEGATIVE POINT.

It is possible to separate three different stages of negative corona, Fig. 3. The similar stages are observable also in case of bulk discharges.

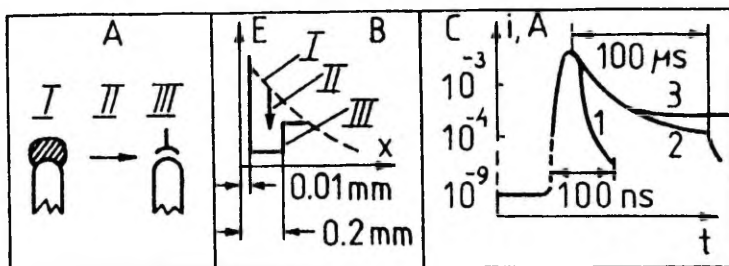


Fig. 3. Stages of negative corona. A - visual appearance of corona; B - sketch of the field distribution; C - current pulses; I, II, III - different stages of discharge; 1, 2, 3 - respectively air, nitrogen and pure nitrogen.

The first, low-current ($i < 10^{-9}$ A) steady discharge stage was in the first time studied in air by Loeb et al

[9], later it was observed by Weissler [10] in pure nitrogen. A detailed study was made by Korge et al [11] in pure nitrogen. By appearance the low-current discharge is a faint diffuse glow that covers the tip of the point. The low-current discharge is time dependent: at lower voltages, after a step-wise rising of the voltage its current and brightness decay in the course of time, Fig. 4A.

At higher voltages the current decay is replaced by a shorter or longer (up to 85 minutes) stagnation which later, in its turn, is replaced by current growth ending with a sudden transition into the strong-current discharge.

The similar I - U dependence for low-current discharge was registered in air [4], but the strong dependence on

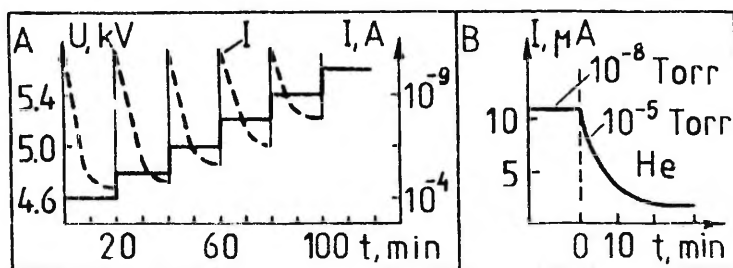


Fig. 4. A - current dependence on time in pure nitrogen [12]; B - gas influence to emissivity in vacuum [13].

point electrode material and properties of the point surface was observed. Further analysis of I - U curve indicates [4, 12] that the low-current discharge is determined by the field emission (FE) in the broad sense of the word. First of all FE is caused by foreign (dielectric) inclusion on point surface as in case of vacuum discharge [13]. The main difference, when compared with the vacuum discharge lies in the influence of gas composition and its pressure on electrode emissivity (Fig. 5, [14]).

In case of the final, the third stage of discharge it

is possible to separate a cathode spot, plasma and drift regions (Fig. 3). In Fig. 3B a sketch of corresponding field distribution is presented. Characteristics of the third stage depend on gas composition:

(i) In pure N_2 a steady strong current ($i \geq 10^{-4}$ A) discharge establishes. Its current is controlled by circuitry resistance [11].

(ii) In N_2 the form of the final stage depends on the running time of discharge [4, 5]. If the discharge chamber is filled with gas, there is a steady strong current discharge. At every fixed voltage its current decay in the course of time, Fig. 5. When after a pause the voltage supply was switched on, the current was higher than before the switch-off, later a current decay was

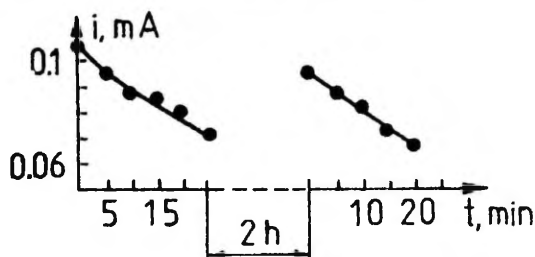


Fig. 5. Steady discharge in N_2 . $p = 400$ Torr, $U = 5.5$ kV.

observed again. After some running time of discharge the steady discharge was replaced by a pulsed one. The shape of a current pulse is similar to that in electronegative gases at lower pressures [15, 16]: a pulse has a long tail with duration of hundreds of μs .

(iii) Near the onset potential of corona in air there are always current pulses of comparatively short duration. With the increase in voltage repetition rate of pulses rises and at sufficiently high overvoltages a steady discharge forms.

We suppose that the final form of discharge is determined by the balance between the electron creation and

losses in plasma region i. e. plasma region is a "narrow site" which determines the discharge stability. Field strength in this region is low and even small deviation from ionization balance chokes up the discharge.

In air and other electronegative gases in plasma region prevails loss of electrons due to attachment. So the discharge near the onset potential of corona exists in pulse form. Only at higher voltages the electron loss is compensated by ionization and steady corona (negative glow) establishes. In pure N_2 and N_2 the situation is more complicated. In [17, 18] on the ground of spectroscopic measurements the evolution of electric field E/N and electron concentration n_e were determined. Already 20 ns after the beginning of transition to strong current discharge E/N is too low for the direct ionization by the electron impact with ground state molecules and the ionization is caused mainly by stepwise and/or associative ionization. The measurements in $N_2 + O_2$ and $Ar + O_2$ mixtures [19] also demonstrate the importance of nitrogen metastables in ionization. There is an equilibrium between associative ionization and recombination in plasma region in pure N_2 and the discharge is a steady state one. In N_2 occurs the accumulation of particles quenching metastables and by that reason current decays gradually. These particles may be liberated from electrodes and/or they are produced by reactions in discharge. Some of these are metastable: when there is no discharge, concentration of particles diminishes and after switching on discharge anew the current is higher (Fig. 5).

Presented interpretation connects the final form of discharge only with the processes in gas. But there is also a possibility that the described effects are linked with emissivity of the point electrode. Observed current decay of strong-current discharge in N_2 (Fig. 5) may be explained by the decrease of secondary emission coefficient γ similarly as it takes place in case of low-current discharge in pure N_2 (Fig. 4). A nice dependence of the final form of discharge on the point electrode emissivity are demonstrated

by the measurements of Černák and Hosokawa [20].

So the final understanding of described processes is open for further studies.

During the second stage of discharge the transition from low-current discharge (field distribution is the Laplacian one) to strong-current one (field distribution differs completely from that when the influence of space charges is negligible) takes place. While in pure nitrogen the transition occurs at $U = \text{const}$ [11] the increase in current is explainable by the increase in γ . In [5, 6] we supposed that the transition is caused by the explosive emission (EE) i. e. by sudden injection of charged particles into the discharge gap. Later studies [21] confirm this viewpoint. More detailed analysis [4] indicates that one must not imagine EE in its simplistic manner like heating of micropoints on the electrode surface by FE currents and following explosion of a point. Comparison of the transition stage with studies of both breakdown formation in vacuum [13] and glow-to-arc transition in gas discharges [22] leads to the conclusion that corona pulse formation is a special case of a wider phenomenon. Similarities between electron emission and consequent breakdown processes in high pressure gases and in vacuum are confirmed in [14, 23]. According to the detailed studies in vacuum [13] a typical electrode surface has a very high surface density of latent emission sites. The present-day model assumes the presence of foreign insulator inclusions on electrode surface. For electron emission first of all the breakdown of insulator is necessary, as a result of this a conducting channel is formed. The latter is the source of "hot" electrons which are emitted quasi-thermoionically. Emissivity of a site strongly increases with the rise of temperature. Sketches in Fig. 6 demonstrate that formation of corona follows the same patterns. These phenomena were pointed out in our experiments, too [3]. In sketch A (spontaneous pulses), positive ions created by a low-current discharge were set to dielectric layer, their space charge field causes the breakdown of the layer and formation of a conducting

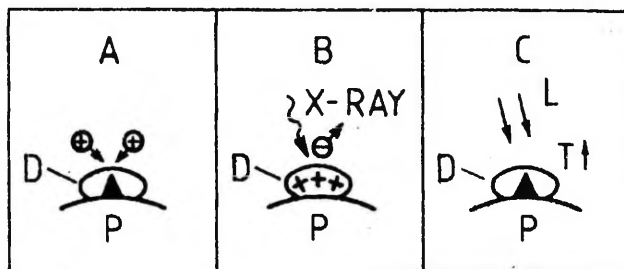


Fig. 6. A - electroforming of conducting channel; B - X-ray radiation charges a dielectric layer [3]; C - laser radiation heats the point [4, 5]; D - dielectric layer; P - point electrode.

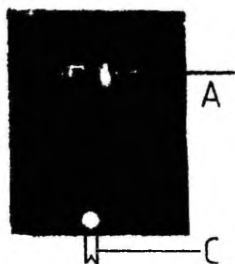
channel. In sketch B (initiation I1, Fig. 2) the point is covered by a thick insulator layer, so there is no low-current discharge. X-ray radiation charges the layer and a corona pulse is initiated. In sketch C (initiation I2, Fig. 2) laser radiation increases the point temperature and so emissivity of the emission sites rises considerably. Due to heating it is possible to initiate a typical corona pulse some kilovolts below the onset of spontaneous pulse. Further analysis and comparison with different experiments are presented in [3].

POSITIVE POINT.

From the viewpoint of distortion of discharge homogeneity processes at anode play more important role than those at cathode. This circumstance for rare gases is demonstrated in Fig. 7: in spite of a big difference in Laplacian field strengths near the point and the plane, the channels which develop far into the discharge gap, start from the anode.

As the mechanism of channel development in its initial stage weakly depends on gas composition it is more convenient to study the formation of discharge in the positive point-plane gap.

Fig. 7. Steady discharge in He;
negative point-plane gap;
 $p = 1$ atm, exposure 4 s.



A typical initial part of I - U dependence in air for a positive point-plane gap is presented in Fig. 8. There are three different regions: burst-pulses, onset streamers and positive glow.

Burst-pulses develop along the point surface. A burst is an avalanche generation, its secondary mechanism is gas photoionization. Largest bursts have a duration $\sim 1 \mu s$ and their current is ~ 0.1 mA. Increase in voltage leads to the development of onset streamers, which develop far into the discharge gap and have a branched structure. Rise time of the corresponding current pulses is ~ 2 ns, duration of the pulses is some hundreds of nanoseconds and the peak value of the pulse is ~ 10 mA. There is a steady discharge - steady

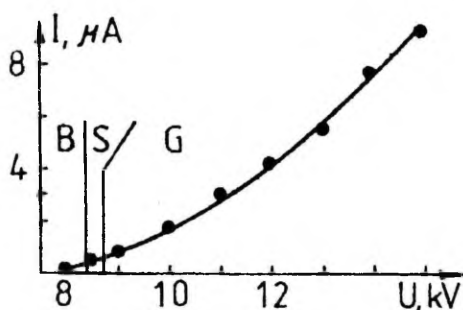


Fig. 8. I - U dependence in air; B - burst-pulses; S - onset streamers; G - steady glow.

glow at higher voltages. A luminous layer at point surface

corresponds to it visually.

There is well-known criterion of streamer formation in the homogeneous field: a streamer starts when the number of charged particles in avalanche head achieves 10^8 . In case of the inhomogeneous field the situation is more complicated as near the onset potential of the streamers the number of charged particles in an avalanche is 10^3 and so the streamer formation must be connected with the accumulation of charged particles from several avalanches. That is why another formulation of streamer formation [24] is more preferable: a streamer starts when the concentration of ionized gas achieves plasma density i. e. Debye length must be much smaller than the characteristic length of ionized gas region. In [3] the formation of a spontaneous streamer near its onset potential has been studied. To trigger the ionization the first electron must appear near the border of ionizing zone (Fig. 9A). An avalanche starting from this electron radiates photons able to ionize gas. If such a photon is absorbed near the border of ionizing zone, it creates a new equivalent avalanche. As photons are radiated in random directions, avalanche generation will spread over

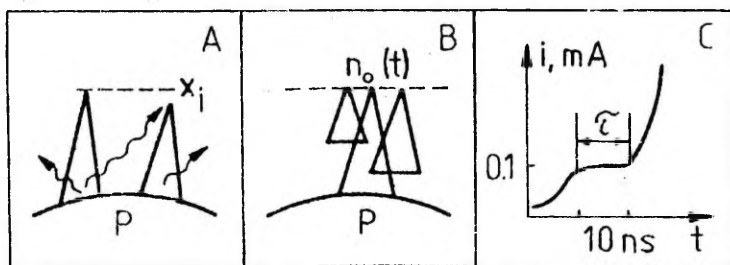


Fig. 9. A - initial stage of a burst; B - overlapping of avalanches; C - sketch of burst-to-streamer transition; P - point electrode; x_i - border of the ionizing zone; $n_o(t)$ - concentration of triggering electrons.

the electrode surface. At one random moment the concentration of electrons n_o near the border x_i is high

enough and avalanches will overlap (Fig. 9B). This stage can already be registered during the experiment. As it was estimated, the concentration in a burst achieves 10^{10} $1/\text{cm}^3$ and so we have a plasma layer near the point. Plasma layer can exist near the anode for a long time. There are two loss mechanisms of electrons in plasma body: attachment and leakage to the anode. Burst pulse exists till the moment these losses are compensated by ionization. Some larger bursts transform to the streamers. This transition is governed by chance.

It was supposed for a burst-to-streamer transition that there must be a local deviation δn_e from the equilibrium value of electron concentration n_e . It is more probable in high electric field, but high field cannot exist in plasma for a long time. Indeed, despite of a long duration of a burst pulse, transition occurs always at the beginning of a burst-pulse ($\tau < 15$ ns, Fig. 9C).

Our further studies confirm this assumption.

The first stage of burst development is very random as it is determined by the statistical nature of photon radiation and absorption. This makes the experimental study of streamer formation more complicate. Using discharge initiation by a X-ray pulses (Fig. 2, I'), it was possible to suppress this first stage. X-ray radiation creates the concentration of electrons $n_e(t)$ near the border of ionizing zone. The higher the intensity of X-ray radiation the less will be the role of photons emitted by avalanches and the moment of streamer formation will be better fixed. Delay time t_d (t_d - time interval from the beginning of a X-ray pulse to the streamer formation) distribution for two different X-ray intensities is presented in Fig. 10.

At lower intensities $I = 0.09 I_0$, t_d is distributed in a long time interval as the moment of overlapping of avalanches is comparatively random. If $I = I_0$, t_d is concentrated in short time interval. These two distributions demonstrate two different possibilities of initiation. At lower intensities initiation has a single electron nature, at higher intensities there is a multielectron initiation

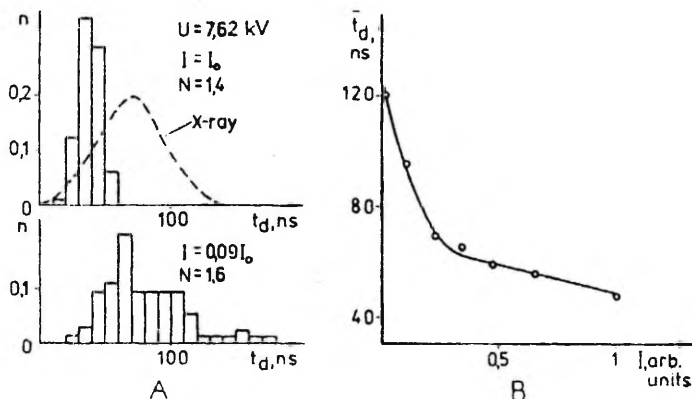


Fig. 10. X-ray initiation. A - probability of a streamer formation n as a function of t_d ; I_0 corresponds to 10^7 $1/\text{cm}^3$ charged particles in air; dashed line - the shape of a X-ray pulse. B - mean delay time \bar{t}_d dependence on X-ray intensity.

i. e. the time interval between the start of two successive avalanches which develop in limits of diffusion radius of an avalanche, is much smaller than the time needed for development of an avalanche to the anode. On the ground of dependence $\bar{t}_d = f(I)$ (Fig. 10B) it is also possible to separate the multi-electron initiation ($I > 0.3 I_0$) from the single-electron one ($I < 0.3 I_0$): for $I < 0.3 I_0$ the steep rise of \bar{t}_d is observable.

Now we can suppose that further increase in n_0 must lead to shorter \bar{t}_d and more narrow distribution of t_d . It was done by the initiation I3 (Fig. 2). These experiments were carried out also in air [7]. Laser beam originates N^L electrons at some distance x from the point. Their number diminishes due to attachment when drifting to the anode and $N_0 < N^L$ electrons enter ionizing zone at distance x_i . In ionizing zone the number of electrons rises as $N_0 \exp(\int \alpha dx)$ (α - Townsend ionization coefficient). Time t_d from the

beginning of a laser pulse to streamer formation varies from 350 ns ($x = 8$ mm) to 10 ns ($x = 1$ mm). Delay time $t_d = \Delta t + t_f$ (Δt , t_f - drift time from x to x_i and formation time, respectively) depends on both voltage and laser intensity; its jitter is not more than 3 ns. Using this method of initiation it was possible to originate a streamer already at voltage $U = 0,8 U_0$. It must be mentioned that at lowest potential U where the initiation was still possible, the calculated value of $\exp(\int \alpha dx)$ is as small as 50. Dependence $t_f = f(N_0)$ calculated accordingly to the model of multielectron initiation [2, ch. 4] well corresponds to the measured one [8].

Streamer current peak i_{max} dependence on voltage as well as photos of single initiated streamers registered by the help of an image intensifier are presented in Fig. 11. We can conclude that a streamer may be originated in a wide region of voltage and first of all there must be plasma for streamer formation. So in principle it is also possible to

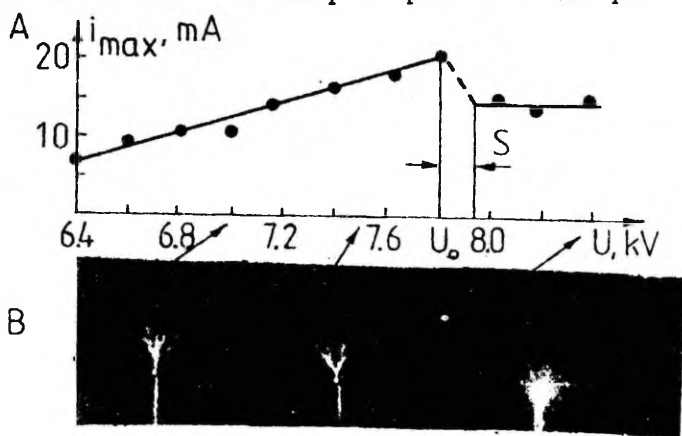


Fig. 11. A - current peak of initiated streamers i_{max} as a function of voltage; S - region of spontaneous streamers; B - static photos of single initiated streamers.

originate a streamer in the steady glow region if we create

a deviation of sufficient size δn_e from the equilibrium value of n_e in this region. It was done by supplying additionally a 100 ns duration pulses to D. C. voltage. Fig. 12.

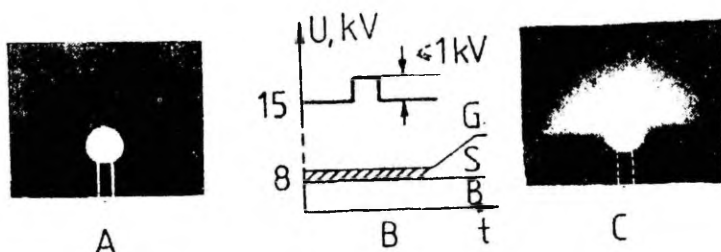


Fig. 12. A - D. C. voltage $U = 15$ kV, steady glow; B - D. C. + pulse voltage; C - discharge in case B; many overlapped streamers are fixed.

If there is only D. C. voltage the point is covered by the bright layer of steady glow. Additional voltage pulse causes a deviation from ionization equilibrium and a streamer starts. The same result is achieved at $U = \text{const}$ in steady glow region using laser initiation [3, Fig. 11: local increase of ionization is caused by electrons created by a laser pulse. From these studies follows that two conditions must be fulfilled to rise a streamer:

(1) Ionized gas must have plasma density.

(11) A streamer forms when the local deviation δn_e from the equilibrium value of electron density n_e takes place.

We want to express our special thanks to Dr. Mart Aints for many useful discussions we held together.

REFERENCES

- [1]. Čermák M., Acceleration of the glow-to arc transition induced by unconditioned cathodes: streamer-like instabilities of the cathode sheath, 8 th Symp. on elementary processes and ch. reactions in low

- temperature plasma, 1990, Stara Lesna, invited papers, part 1, p. 137 - 157.
- [2] Korolyev Yu. D. and Mesyats G.A., In: Physics of pulse breakdown in gases, Moscow: Nauka, 1991.
 - [3]. Laan M. and Paris P., Streamer initiation by X-ray pulse, Acta et Comment. Univ. Tartuensis, 1992, in press.
 - [4]. Korge H., Laan M., Paris P., On the formation of negative corona, J. Phys. D: Appl. Phys., in press.
 - [5]. Laan M., Paris P., Perelygin V., Laser action on corona pulses, Slovakian J. Phys., 1991, N° 5 - 6.
 - [6]. Laan M., Paris P., Perelygin V., Negative corona pulse initiation, Proc. 5 th SU Conf. Gas Discharges, 1990, Omsk, part 1, p. 191 - 192.
 - [7]. Laan M., Paris P., Perelygin V., Laser assisted streamer development, 10 th ESCAPIG, 1990, Orleans, Contr. papers, p. 371 - 372.
 - [8]. Laan M. and Paris P., Multielectron streamer initiation by laser radiation, 11 th ESCAPIG, 1992, S.Peterbourg, to be published.
 - [9]. Loeb L.B., Kip A.F., Hudson G.C., Bennet W.H., Pulses in negative point-to-plane corona, Phys. Rev., 1941, 60, p. 714 - 722.
 - [10]. Weissler G.L., Positive and negative point-to-plane corona in pure and impure hydrogen, nitrogen and argon, Phys. Rev., 1943, 63, p. 96 - 107.
 - [11]. Korge H., Kudu K. and Laan M., The discharge in pure nitrogen at atmospheric pressure in point-to-plane discharge gap, 3 rd Int. Symp. High Voltage Engineering, 1979, Milan, paper 31.04.
 - [12]. Korge H., Investigation of negative point discharge in pure nitrogen at atmospheric pressure, PhD thesis, 1992, Tartu.
 - [13]. Latham R.V., High voltage insulation. New Horizons, IEEE Trans. El. Insulation, 1988, 23, p. 881 - 893.
 - [14]. Latham R.V., Bayliss K.H., Cox B.H., Spatially correlated breakdown events initiated by field electron emission in vacuum and high pressure SF₆, J.

- Phys. D: Appl. Phys., 1986, 19, p. 219 - 231.
- [15]. Torsethaugen, Sigmond R.S., The Trichel pulse phase of negative coronas in the Trichel pulse regime in air, 11 th ICPIG, 1973, Prague, Contr. papers, p. 195.
 - [16]. Černák M. and Hosokawa T., Complex form of current pulses in negative corona discharges, Phys. Rev. A, 1991, 43, p. 1107 - 1109.
 - [17]. Korge H., Kuusk U., Laan M., Susi J., Evolution of excitation and ionization in transient stage discharge in nitrogen, Sov. Plasma Phys., 1991, 17, p. 473 - 480.
 - [18]. Korge H., Kuusk U., Laan M., Susi J., Excitation and ionization in the transient state discharge in pure nitrogen. In: Gaseous Dielectrics VI, edited by L.C. Christophorou and I. Sauers, 1991, N.-Y. Plenum Press, p. 95 - 100.
 - [19]. Scott D.A. and Haddad G.N., Negative corona in nitrogen-oxygen mixtures, J. Phys. D: Appl. Phys., 1987, 20, p. 1039 - 1044.
 - [20]. Černák M., Hosokawa T. and Inoshima M., Positive streamer-like instabilities on the cathode sheath of filamentary glow discharges, 20 th ICPIG, 1991, Barga.
 - [21]. Laan M. and Perelygin V., The dependence of negative corona on electrode surface properties, 20 th ICPIG, 1991, Barga, Poster Session P, N° 35.
 - [22]. Guile A.E. and Hitchcock A.H., Oxide films on arc cathode and their emission and erosion, J. Phys. D: Appl. Phys., 1975, 8, p. 663 - 669.
 - [23]. Guile A.E., Latham R.V., Heylen A.E.P., Similarities between electron emission and consequent breakdown processes in highpressure gases and in vacuum, IEEE Proc., 1988, 133A, p. 280 - 283.
 - [24]. Omarov O.A., Ruchadze A.A., Schneerson G.A., On plasma mechanism of high pressure gas breakdown in high electric field, Sov. J. Techn. Phys., 1980, 50, p. 536 - 538.

On the formation of negative coronas

Hans Korge, Matti Laan and Peeter Pärss

Department of Physics, Tartu University, EE2400 Tartu, Estonia

Received 24 March 1992, in final form 26 October 1992

Abstract. Negative coronas in nitrogen and in air have been studied. The transition from low-current discharge to strong-current discharge or to the spontaneous and initiated corona pulse regimes has been investigated. Corona pulses were initiated by an excimer laser pulse or by an x-ray pulse. The influence of point electrode surface conditions on the corona pulse formation has also been under observation. In the interpretation of the results the similarity of this transition to the electron emission and consequent breakdown processes in vacuum and other gases is emphasized. This approach permits an explanation of the existence of low-current discharge by Fowler-Nordheim type field emission and the transition to strong-current discharge or corona pulse by a large burst of electrons due to the breakdown of the insulator layer on the electrode surface.

1. Introduction

The DC corona of negative polarity in a point-to-plane discharge gap is observed.

Near the onset potential in electronegative gases the negative corona exists in pulse form which is preceded by a low-current ($i < 10^{-9}$ A) quasi-steady discharge as described by Loeb *et al* [1]; later it was observed by Weissler [2] in pure nitrogen. The systematic study of the leading edge of a negative corona current pulse was made by Zentner [3, 4]. He found that it had a complex structure: there was a step before the current reached its peak value.

It is impossible to explain the complex rise of the current pulse other than by a secondary (γ) mechanism. In his model, Morrow [5] explains the existence of the step by two different γ mechanisms: in the initial phase of the current pulse (the step) the secondary emission of electrons is caused by photons (γ_{ph}). This is then replaced by a more effective ion bombardment (γ_i). On the basis of their experiments Černák and Hosokawa [6, 7] concluded that Morrow's model is valid at lower pressures, but at higher pressures the observed waveforms are caused by a cathode-directed ionizing wave: the main current peak reflects the arrival of the ionizing wave at the point electrode.

Similarities between breakdown processes in vacuum and high-pressure gases have been stressed in the works of Latham, Guile and Heylen [8-11]. Prebreakdown phenomena are explained by field emission and breakdown by the dielectric switching mechanism.

Černák and Hosokawa stressed that the form of the leading edge of the corona pulse does not depend significantly on gas composition [12, 13]. Our investigations show that the existence of the low-current discharge is determined by surface conditions of the point electrode rather than other physical factors.

Thus there are good reasons for the application of the concept of field emission and the subsequent 'dielectric switching mechanism' to explain the existence of the low-current discharge and its transition to the strong-current one or to the corona pulse. Because the formation of a strong-current discharge in pure nitrogen and the evolution of a corona pulse in air are quite similar during the first tens of nanoseconds [14, 15], we are able to interpret from the above-mentioned viewpoint the experiments carried out in different gas media: pure nitrogen, impure nitrogen, and air.

2. Experimental details

In this section the selected results of our experiments in nitrogen in comparison with those in air are presented. Results of investigations in nitrogen were previously published mainly in the theses of different conferences; results in the case of air have not been published as yet.

Experiments were carried out using three different experimental devices, but the discharge gap geometry was nearly the same. The gap spacing was 40 mm and the point electrode was a hemispherically capped wire of diameter 1 mm. The opposite electrode was a disc and its diameter was ≥ 150 mm.

2.1. Experiment A: pure nitrogen

The results of our experiments in pure nitrogen were first described in [16]. The discharge chamber was evacuated to 5×10^{-6} Torr by the help of an oil diffusion pump trapped by liquid nitrogen. The chamber was warmed up to 100°C and the duration of a pumping cycle was at least 10 h. The chamber was filled with pure nitrogen (the content of nitrogen was not less than

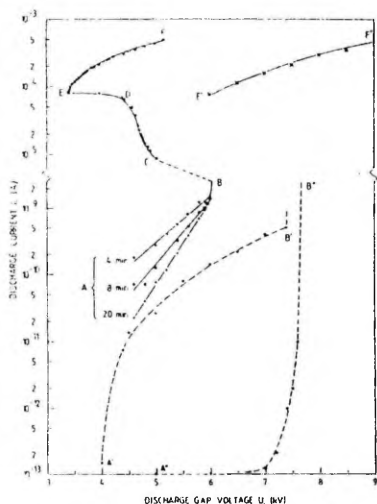


Figure 1. Current-voltage dependences: ABCDEF, pure nitrogen; AB and CDEF, low-current and strong-current discharge respectively; different curves AB correspond to the time being counted from the moment of stepwise raising of voltage; E'F', strong-current discharge in nitrogen; A'B', low-current discharge in air; Pt point, A''B'', low-current discharge in air, Al point.

99.996%, while that of oxygen, hydrogen and carbohydrates were each less than 0.001%). The pressure in the chamber was set at 770 Torr. In the discharge emission spectra of such a medium faint traces of CN appeared beyond the 2^+ system of N_2 ; no traces of OH were observed.

The platinum point electrode was mechanically polished and under 100-fold magnification its surface seemed smooth. Before use, the point electrode was cleaned in an ultrasonic bath. The points were used for a long time and the surfaces of used points were covered with craters, so the results for every point must be interpreted as for one 'conditioned' by discharge.

The current-voltage ($I-U$) discharge curve is represented in figure 1. Parts AB and CDEF correspond to the steady-state discharge. The part CDE with negative slope can only be registered using a large external series resistor ($\geq 10\text{ M}\Omega$).

The low-current steady-state discharge (part AB) appears as a faint diffuse light near the tip of the point and at every fixed voltage below about 5.9 kV its current diminishes in time (figure 2). At higher voltages, usually from 5.90 kV to 6.10 kV or more, this decay of current may be replaced by shorter or longer stagnation which may at any moment transform to an increase in current,

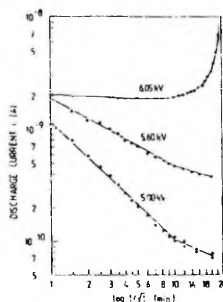


Figure 2. Current dependence on time $t = t(t^{-1/2})$ for low-current discharge in pure nitrogen.

ending with a sudden transition to the strong-current discharge. The time interval between the moment of applying sufficient voltage and the moment of transition varies within large limits, the longest registered interval was 85 minutes, but even longer ones are not excluded.

This sudden transition from the low-current discharge mode to the strong-current one is very similar to the Thichel pulse formation in air. The light pulse which corresponds to this transition does not differ from that of the Thichel pulse in air. Furthermore, during the first tens of nanoseconds there is no difference between the spatio-temporal distribution of light [15] and that of a negative corona pulse in air [14]. Also there is no remarkable difference between the corresponding current pulses, but in pure nitrogen the transition is finished by the establishment of a steady-state discharge controlled by circuitry resistance while the duration of the Thichel pulse current is detectable only during some hundreds of nanoseconds.

2.2. Experiment B: nitrogen

After a 0.5 h pumping, the pressure attained in the discharge chamber was $< 10^{-5}$ Torr; the chamber was then filled with the same nitrogen as in experiment A. No additional efforts were made to achieve purer conditions.

2.2.1. Experiment B1. Point electrodes made of different materials were prepared as in experiment A and they were used for only a short time: if small craters or other changes were observed on the surface of the electrode, the point was replaced by a new one. Discharge was studied in the pressure range of 50–760 Torr. When the voltage supply was switched on at onset potential ($U_0 \approx 9\text{ kV}$ at atmospheric pressure) a strong-current steady-state discharge was established. As a small external resistor $R_T = 10\text{ k}\Omega$ was used, it was only possible to register that part of a strong-current $I-U$ curve that had a positive slope (curve E'F' in figure 1). Point

Figure 3. Typical current pulse in nitrogen: I_0 , value of the step current; I_{max} , value of the current peak.

U' corresponds to the onset potential U_0 of the discharge, point E' to the extinction potential. Comparing curve E'F' with EF, we can see that E'F' is shifted towards higher voltages, i.e. at every current a higher energy input is needed. Furthermore, curve E'F' changes over the course of time: at any $U = \text{constant}$ the current diminishes if running time of discharge increases. Simultaneously, the extinction potential rises too, but regardless of the value of the extinction potential the corresponding minimum current is always the same. If the extinction potential is equal to the onset potential U_0 , the steady-state discharge is replaced by a pulse discharge; to achieve the steady-state discharge higher voltages are needed. After refilling the chamber with fresh gas a steady-state discharge is established again at the onset potential U_0 .

In such a medium, repetitive corona pulses were investigated near the onset potential [17]. A typical current pulse is presented in figure 3; its duration diminishes while the time of discharge burning is prolonged. A coaxial design of the point electrode connection like that in figure 4 and a 350 MHz bandwidth oscilloscope were used to investigate the leading edge of the current pulse. Whether the step is observable or not depends on point properties and gas pressure. In the case of a new ('unconditioned') oxidized Al point a stable step is recorded at pressures $p < 500$ Torr. When the discharge has been running for some time the step disappears. In the case of a graphite point the step exists for all pressures under observation, but its height i_s and duration vary from pulse to pulse.

2.2.2. Experiment B2. Measurements were made at a pressure of 760 Torr in the same medium as in experiment B1. Corona pulses were initiated by an excimer laser beam ($\lambda = 308$ nm, pulse duration is 50 ns, maximum of the beam intensity is $I_0 = 5 \times 10^7$ W cm⁻²/s directed along the gap axis like the x-ray beam in figure 4 [18, 19] and focused at a distance of some millimetres from the point tip. Initiation was caused mainly by heating the point surface and not by a photoeffect. This was proved by measurements at low voltages ($U = 5.6$ kV) where the current was mainly caused by emission from the point: the current did not follow the waveform of the laser pulse but rose gradually during the laser pulse. As estimated, the excimer laser pulse heats the Pt point to more than 1000 K. If the intensity is approximately 10^7 W cm⁻², a laser pulse initiates a corona pulse with a delay of 5 ns from the beginning of the laser pulse.

Figure 4. Experimental set-up in air: X-ray, x-ray pulse generator; EM, electrometer; $R_0 = 10$ k Ω ; $C = 1$ nF; R_L disc-like low inductance 50 Ω resistor.

With the intensity decrease, delay time increases, but stable initiation is possible even when the laser pulse intensity is $I_0/32$. The waveform of the corona current pulse which is initiated two kilovolts below the onset potential of non-initiated (spontaneous) pulses does not differ from the typical corona pulse shape (figure 3), but the peak value i_{max} of the current pulse depends both on the voltage U and intensity I of the laser beam.

2.3. Experiment C: ambient air

Experiments were carried out in ambient air at atmospheric pressure. Different samples of Al and Pt points were used. The experimental set-up is presented in figure 4. An x-ray pulse generator was used for corona initiation. The mean quantum energy of the x-ray beam is 5 keV, the pulse duration is 140 ns (its shape is presented in A of figure 5). A single x-ray pulse produces 10^7 cm⁻³ charged particles as measured by an ionization chamber. A more detailed description of the x-ray pulse generator is presented in [20]. Discharge light was detected by an image intensifier.

Previously the parameters of discharge were measured without x-ray initiation. As in experiment A, a low current $I-U$ curve was registered. The $I-U$ curve depends strongly on the material of the point and its prehistory. Typical $I = f(U)$ dependences for Al and Pt points are presented in figure 1. The $I-U$ curve for Pt is similar to that in pure nitrogen, but in the case of an Al point a remarkable increase in current is registered only near the onset potential of corona pulses U_0 . In the case of a Pt point, diffuse light is already visible 1 kV below the onset potential, but is absent for an Al point. The onset potential of spontaneous corona pulses varies within wide limits ($U_0 = 7.5-7.9$ kV) and depends on the point material as well as on the prehistory of the point. The current pulse has a rise time < 2 ns; its peak value near U_0 is practically the same for all points.

To study the initiation of corona pulses by x-ray radiation, the time interval between the beginning of the x-ray pulse and the corona pulse (delay time t_d) was measured for different points and voltages. Since at any voltages under observation there was also a chance of a spontaneous pulse arising, the mean number of spontaneous pulses per second (PPS) \bar{n}_1 was determined at every voltage as well as the mean number of PPS in the presence of x-ray radiation \bar{n}_2 . The repetition rate of corona pulses was 10 PPS. The number of corona pulses per second (figure 5) was determined by pulse counting

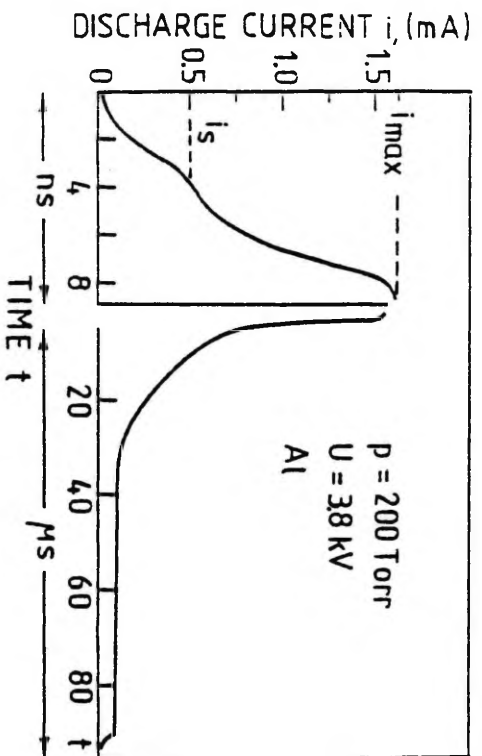


FIGURE 3

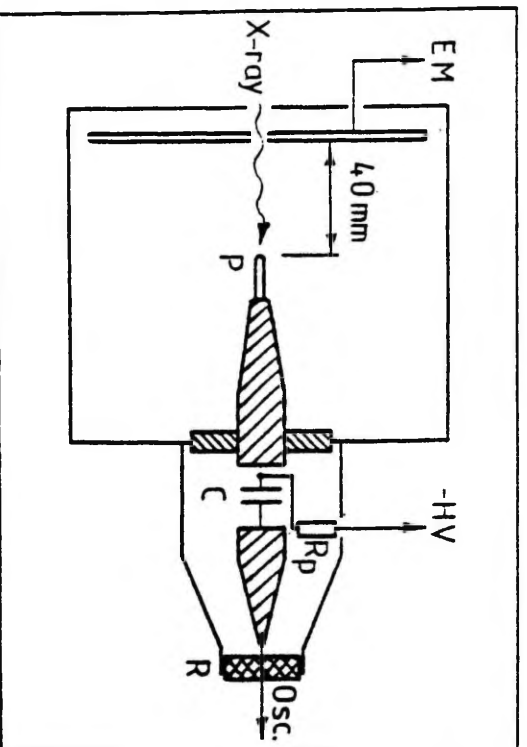


FIGURE 4

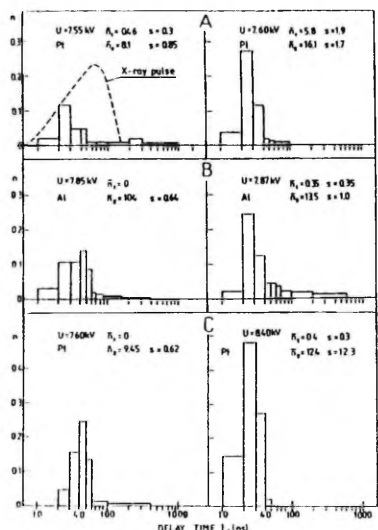


Figure 5. Delay time t_d distribution for different point electrodes: A, Pt point, $U_0 = 7.2$ kV; B, Al point, $U_0 = 7.67$ kV; C, oil-coated Pt point. Broken curve, shape of x-ray pulse; n , relative number of initiated pulses; \bar{n}_1 , mean number of spontaneous pulses per second; \bar{n}_2 , mean number of pulses in the presence of x-radiation; s_1, s_2 , standard deviations of \bar{n}_1 and \bar{n}_2 respectively.

using a 10 s time interval. The presented mean values are the results of at least ten measurements.

In the case of a Pt point (A in figure 5) it is not possible to initiate a corona pulse by our x-ray pulse at voltages below $U_0 = 7.55$ kV. Near the onset U_0 where spontaneous corona pulses are almost absent ($\bar{n}_1 = 0.46$) not every x-ray pulse initiates a corona pulse ($\bar{n}_2 = 8.1$) and t_d is distributed over a large interval. At $U = 7.60$ kV each x-ray pulse already initiates a corona pulse ($\bar{n}_1 = 5.8$, $\bar{n}_2 = 16.1$) and 30% of pulses have t_d less than 30 ns. At more than 500 V above U_0 spontaneous pulses prevail and it is difficult to determine the influence of x-radiation.

In the case of an Al point (B in figure 5) x-ray initiation is more efficient. A corona pulse can be created below the onset $U_0 = 7.7$ kV, and at $U = 7.85$ kV each x-ray pulse initiates a corona pulse ($\bar{n}_1 = 0$, $\bar{n}_2 = 10.4$). At a 20 V higher voltage a single x-ray pulse creates even more than one corona pulse ($\bar{n}_2 = 13.5$). Delay time t_d distribution is presented only for the first corona pulse.

Strong effects are observed when a Pt point is coated with a thin layer of transformer oil. The low current mode of discharge is practically absent (the current is

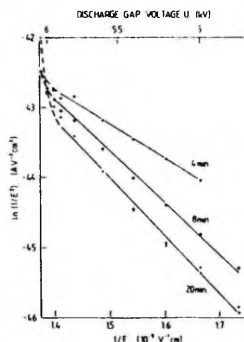


Figure 6. Fowler-Nordheim plot of $\ln(I/E^2) = f(1/E)$ for pure nitrogen. Parameters: time from the moment that the voltage supply is switched on; I , current; E , field strength.

at least two orders of magnitude less than in the case of an uncoated point). The onset potential of spontaneous pulses rises remarkably; in some experiments (it depends on the thickness of the oil layer) it rises by more than 3 kV, but initiated pulses start at nearly the same voltage as in the case of an uncovered point, and initiation is effective ($\bar{n}_1 = 0$, $\bar{n}_2 = 9.45$; C in figure 5). At higher voltages ($U = 8.4$ kV) a single x-ray pulse initiates a series of corona pulses ($\bar{n}_2 = 12.4$).

Beyond this, the following trends were observed: in the case of Pt points, the onset potential was systematically lower than that for Al points, and a new oxidized Al point had a higher onset potential than a used one.

3. Discussion

The registered $I-U$ curve in pure nitrogen (ABCDEF, figure 1) is very similar to that of low-pressure discharge (LPD) in a homogeneous field, but due to discharge gap geometry the range of characteristic parts is modified. The most striking difference in this $I-U$ curve, compared with the LPD one, is in part AB: in the case of LPD there is a plateau, i.e. the current is independent of voltage and its value is determined by external ionization; in our case current strongly depends on voltage. Calculations of the ionization integral $\int \alpha dx$ show that its value is too low to explain the self-sustaining of discharge by the Townsend mechanism (e.g. for $U = 4.6$ kV $\int \alpha dx = 1.8$ [15]). Assuming that the low current discharge is determined by field emission, the dependence of $I = f(U)$ is presented using Fowler-Nordheim (FN) plots in figure 6. As the current I depends on time (figure 2), each plotted curve corresponds to time $t = \text{constant}$ from the moment of raising the voltage. We can see that the FN plot is quite a good fit of experimental results. $I-U$ dependence for a Pt point in air (A'B', figure 1) also follows the FN plot, but has another slope.

Field emission (FE) is possible if there are sites (micropoints, microinclusions of foreign materials) on the electrode surface which have enhanced emissivity [8, 21, 22]. In gases, large areas of electrode are usually covered by oxide (or other insulator) layers; their emissivity depends on oxide type and its thickness [22, 23]. If we treat an emission site simply as a micropoint some doubts arise:

(i) at lower pressures the onset potential (in nitrogen for $p = 150$ Torr, $U_0 \approx 3$ kV) is too low for effective FE from micropoints;

(ii) in the case of an Al point in air the region of low current does not exist (figure 1).

Detailed studies of the characteristics of electrode emissivity have been made for prebreakdown currents in vacuum [8]. The modern model of emission site assumes a metal-insulator emission regime, i.e. the presence of foreign insulator inclusions on the electrode surface. Several investigators [9-11, 21] have proved that prebreakdown phenomena in vacuum as well as in high-pressure gases are similar: the values of field strengths are close, current follows the FN type of dependence, emission sites on electrodes in vacuum and gases are spatially correlated. The presence of gas poisons the formed emissive sites causing the diminishing of emissivity [8]. The poisoning tends to saturate in time. This tendency is noticeable in figure 2 (curves 5.00 and 5.60 kV), but is clearly stated by prolonging the registration time up to one hour.

The strong-current discharge in gas is triggered by the breakdown of the insulator ('a dielectric switching mechanism') due to its charging by positive ions and/or liberation of electrons by UV-light from the discharge gap. As a result, a conducting channel is formed in the insulator and a large burst of electrons (duration of burst is < 10 ns) is injected into the discharge gap [22]. This process is often called explosive-like emission [21].

Applying the above we can interpret our experimental results as follows. The low-current discharge is sustained by field emission and the recorded temporal decrease in low currents is caused by the loss of emissivity of emission sites due to poisoning. Different $I-U$ dependences for a Pt point in air and pure nitrogen are explainable by different gas compositions and point surface conditions. The difference between the low-current parts of $I-U$ curves in air for Pt and Al points is also understandable: an Al point is covered with a homogeneous and comparatively thick oxide layer; it suppresses the emission over a large range of voltage and the current increase is observable only near the corona pulse onset (see curve A''B'' in figure 1).

In the following let us consider the transition to strong-current discharge on the basis of the dielectric switching mechanism. As we see in pure nitrogen, the gas ionization begins to contribute to the low-current growth at voltages $U \geq 6$ kV and systematic deviation from the FN plot occurs (figure 6). A sudden increase in current magnitude at $U = \text{constant}$ (figure 1, point B, and figure 2, 6.05 kV curve) is triggered by the

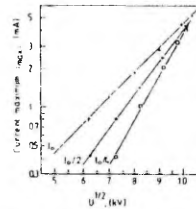


Figure 7. Peak current value dependence on voltage in $I_{\text{max}} = f(\sqrt{U})$ for different laser intensities; $I_0 \approx 5 \times 10^7 \text{ W cm}^{-2}$.

breakdown of the insulator layer and formation of a conducting channel in it due to the charging of layers by positive ions (a consequence of gas ionization). The charging counteracts the poisoning if the voltage is sufficient and leads to the breakdown of the layers.

Experiments B and C confirm the proposed mechanism from another viewpoint. In [8] the effect of temperature and uv radiation on emissivity is described. An increase of temperature by 200 K causes the five-fold increase in electron emission, but the effect of uv radiation on emissivity is less pronounced:

(i) The initiation of discharge with laser pulse in experiment B2 shows the peak current i_{max} dependence on the temperature ($T \sim I$) of the point surface. The amplitude of the initiated pulse i_{max} may be considered to be proportional to the quantity of emitted electrons at voltages below the onset of corona pulses. The linear dependence $\ln i_{\text{max}} = f(\sqrt{U})$ (figure 7) really indicates [24] that the height of the initiated corona pulse is correlated with the emissive site temperature, thus being caused by field-assisted thermionic emission.

(ii) In the case of x-ray initiation (experiment C) the charging of an insulator on the point electrode surface is caused by photoeffect. Its efficiency is different for different points (figure 5): charging of large oxide layers on an Al point is more effective than that of microinclusions on a Pt point. An oil layer on a Pt point plays a similar role to an oxide layer on Al: it suppresses the low-current region. X-radiation charges the layer to high densities of positive ions, causing the lowering of corona pulse onset potential.

So we can assume the following evolution of discharge: a low-current discharge determined by a FN type of emission precedes the corona pulse in an electronegative gas as well as the transition to a strong-current discharge in pure nitrogen; the corona pulse and the transition are both triggered by an electron emission due to the breakdown of the dielectric layer; in the later stages the discharge is sustained mainly by the γ secondary mechanism.

The dielectric switching mechanism is supported by correlation between the step and point properties demonstrated in experiment B1: a new Al point is covered with a homogeneous oxide layer and there is

a stable step on the leading edge of the corona pulse; after the layer has been destroyed by discharge the step is not observable. The homogeneous layer is charged to high density by positive ions, and intensive injection of electrons into the gap after the layer breakdown causes the initial fast rise of current, or step.

The proposed emission mechanism is substantiated by the electrode sputtering because of the formation of a conducting channel through the insulating layer [23]. In the case of a negative corona sputtering is observed [25, 26], but the correlation between the moment of sputtering and corona pulse evolution is not specially investigated. So the determination of the moment of sputtering should support or go against the dielectric switching mechanism.

4. Conclusion

In negative corona studies the importance of point surface properties (presence of foreign inclusions, 'conditioning' procedure) is always stressed. But usually it is assumed that the role of different inclusions is to create the first electron. In contrast to this, the present treatment indicates that for a corona pulse formation a large number of electrons must be emitted from the point that is substantiated by the breakdown of the dielectric layer.

References

- [1] Loeb L B, Kip A F, Hudson G G and Bennett W H 1941 Pulses in negative point-to-plane corona *Phys. Rev.* **60** 714–22
- [2] Weissler B I. 1943 Positive and negative point-to-plane corona in pure and impure hydrogen, nitrogen and argon *Phys. Rev.* **63** 96–107
- [3] Zentner R 1970 Über die Anstiegszeiten der negativen Koronaentladungsimpulse *Z. Angew. (Math.) Phys.* **29** 294–301
- [4] Zentner R 1970 Stufenimpulse der negativen Koronaentladung *Elektrotechn. Z.* **91** 303–5
- [5] Morrow R 1985 Theory of stepped pulses in negative corona discharges *Phys. Rev. A* **32** 3821–4
- [6] Černák M and Hosokawa T 1988 Initial phases of negative point-to-plane breakdown in N_2 and $N_2 + 10\%$ CH_4 : verification of Morrow's theory *Japan. J. Appl. Phys.* **27** 1005–9
- [7] Černák M and Hosokawa T 1991 Complex form of current pulses in negative corona discharges *Phys. Rev. A* **43** 1107–9
- [8] Latham R V 1988 High-voltage insulation. New Horizons *IEEE Trans. Electr. Insul.* **23** 881–93
- [9] Latham R V, Bayliss K H and Cox B M 1986 Spatially correlated breakdown events initiated by field electron emission in vacuum and high-pressure SF_6 *J. Phys. D: Appl. Phys.* **19** 219–31
- [10] Heylen A 1991 Similarities between high electric field electron emission and consequent breakdown processes in compressed gases and vacuum *Gaseous Dielectrics* (New York and London: Plenum) pp 151–8
- [11] Guile A E, Latham R V and Heylen A E D 1988 Similarities between electron emission and consequent breakdown process in high-pressure gases and in vacuum *IEEE Proc. A* **133** 280–3
- [12] Černák M and Hosokawa T 1989 Secondary electron emission in the course of the first Trichel-like pulse development in $N_2 + SF_6$ mixtures *IEEE Trans. Electr. Insul.* **24** 699–708
- [13] Černák M, Kaneda T and Hosokawa T 1989 First negative corona pulses in 70% $N_2 + 30\%$ SF_6 mixture *Japan. J. Appl. Phys.* **28** 1989–96
- [14] Korge H, Kudu K and Laan M 1977 Development of DC corona pulses at atmospheric pressure *Proc. 13th Int. Conf. on Phenomena in Ionized Gases (Berlin)* (Berlin: Physical Society of the GDR) pp 451–2
- [15] Korge H 1992 Investigation of negative point discharge in pure nitrogen at atmospheric pressure *Dissert. Physicae Univ. Tartuensis* **9** 35
- [16] Korge H, Kudu K and Laan M 1979 The discharge in pure nitrogen at atmospheric pressure in point-to-plane discharge gap *3rd Int. Symp. on High Voltage Engineering (Milan)* paper 31.04
- [17] Laan M and Pereygin V 1991 The dependence of negative corona on electrode surface properties *Proc. 20th Int. Conf. on Phenomena in Ionized Gases (Pisa)* vol 4 pp 929–30
- [18] Laan M, Paris P and Pereygin V 1991 Negative corona pulse initiation *Proc. 5th Soviet Union Conf. on Gas Discharges (Omsk)* part 1 pp 191–2
- [19] Laan M, Paris P and Pereygin V 1991 Laser action on corona pulses *Acta Phys. Slov.* **42** 91–7
- [20] Laan M and Paris P 1992 Streamer initiation by x-ray pulse *Acta et Comment. Univ. Tartuensis: Methods of Study of Electrical Processes in Gases and Aerosols* **950** 14–22
- [21] Korolyev Yu D and Mesyats G A 1982 *Avtoemissionnye i vzryvnye processy v gazovom razryade* (Novosibirsk: Nauka) (in Russian)
- [22] Guile A E, Dinoff K and Vijn A K 1983 Transient low-current arc having a very thin oxide film in air at atmospheric pressure *IEEE Proc. A* **130** 379–86
- [23] Guile A E and Hitchcock A H 1975 Oxide films on arc cathode and their emission and erosion *J. Phys. D: Appl. Phys.* **8** 663–9
- [24] Chatterton P A 1978 Vacuum breakdown *Electrical Breakdown of Gases* ed J M Meek and J D Graggs (New York: Wiley)
- [25] Buchet G, Goldman M and Takiris-Zeitaan A 1962 Arrachement de métal aux électrodes dans la décharge couronnée autonome *C. R. Acad. Sci., Paris* **255** 79–91
- [26] Buchet G and Goldman A 1970 Effects of the negative corona discharge on the electrode surface *Int. Conf. on Gas Discharges (London)* (London: IEE) pp 459–62

Tartu Ülikooli Kirjastuse trükikoda
Tiigi 78, EE2400 Tartu
Tellimus nr. 165. Trükiarv 180.